MINISTRY OF EDUCATION

THE ANNALS OF "DUNAREA DE JOS" UNIVERSITY OF GALATI

Fascicle IX
METALLURGY AND MATERIALS SCIENCE

YEAR XXXIX (XLIV)
December 2021, no. 4

ISSN 2668-4748; e-ISSN 2668-4756

2021
GALATI UNIVERSITY PRESS

EDITORIAL BOARD

EDITOR-IN-CHIEF

Assist. Prof. Marius BODOR – "Dunarea de Jos" University of Galati, Romania

SCIENTIFIC ADVISORY COMMITTEE

Assist. Prof. Dragos-Cristian ACHITEI – "Gheorghe Asachi" Technical University Iasi, Romania
Assoc. Prof. Stefan BALTA – "Dunarea de Jos" University of Galati, Romania
Assist. Prof. Chenna Rao BORRA – Indian Institute of Technology, Republic of India
Prof. Acad. Ion BOSTAN – Technical University of Moldova, the Republic of Moldova
Researcher Mihai BOTAN – The National Institute of Aerospace Research, Romania
Prof. Vasile BRATU – Valahia University of Targoviste, Romania
Prof. Francisco Manuel BRAZ FERNANDES – New University of Lisbon Caparica, Portugal
Prof. Bart Van der BRUGGEN – Katholieke Universiteit Leuven, Belgium
Prof. Acad. Valeriu CANTSER – Academy of the Republic of Moldova
Assoc. Prof. Viorel DRAGAN – "Dunarea de Jos" University of Galati, Romania
Prof. Valeriu DULGHERU – Technical University of Moldova, the Republic of Moldova
Prof. Gheorghe GURAU – "Dunarea de Jos" University of Galati, Romania
Assist. Prof. Gina Genoveva ISTRATE – "Dunarea de Jos" University of Galati, Romania
Assist. Prof. Nora JULLOK – Universiti Malaysia Perlis, Malaysia
Prof. Rodrigo MARTINS – NOVA University of Lisbon, Portugal
Prof. Strul MOISA – Ben Gurion University of the Negev, Israel
Assist. Prof. Priyanka MONDAL – CSIR-Central Glass and Ceramic Research Institute, India
Prof. Daniel MUNTEANU – "Transilvania" University of Brasov, Romania
Assist. Prof. Alina MURESAN – "Dunarea de Jos" University of Galati, Romania
Prof. Maria NICOLAE – Politehnica University Bucuresti, Romania
Assist. Prof. Manuela-Cristina PERJU – "Gheorghe Asachi" Technical University Iasi, Romania
Prof. Cristian PREDESCU – Politehnica University of Bucuresti, Romania
Prof. Iulian RIPOSAN – Politehnica University of Bucuresti, Romania
Prof. Antonio de SAJA – University of Valladolid, Spain
Assist. Prof. Rafael M. SANTOS – University of Guelph, Canada
Prof. Ion SANDU – "Al. I. Cuza" University of Iasi, Romania
Prof. Mircea Horia TIEREAN – "Transilvania" University of Brasov, Romania
Prof. Ioan VIDA-SIMITI – Technical University of Cluj Napoca, Romania
Assoc. Prof. Petrica VIZUREANU – "Gheorghe Asachi" Technical University Iasi, Romania

EDITING SECRETARY

Assist. Prof. Marius BODOR – "Dunarea de Jos" University of Galati, Romania
Assist. Nicoleta BOGATU – "Dunarea de Jos" University of Galati, Romania
Assist. Prof. Eliza DANAILA – "Dunarea de Jos" University of Galati, Romania
Assist. Prof. Florin Bogdan MARIN – "Dunarea de Jos" University of Galati, Romania
Assist. Prof. Mihaela MARIN – "Dunarea de Jos" University of Galati, Romania

THE ANNALS OF "DUNAREA DE JOS" UNIVERSITY OF GALATI
FASCICLE IX. METALLURGY AND MATERIALS SCIENCE
Nº. 4 - 2021, ISSN 2668-4748; e-ISSN 2668-4756
Volume DOI: https://doi.org/10.35219/mms.2021.4

Table of Contents

1. Adrian LEOPA, Daniela TRIFAN, Valentin BARDAHAN, Niculai HAUK - Digitalization of Agriculture in Northern Baragan, by Using Drones, for the Purpose of Monitoring Crops, to Increases the Efficiency of Agricultural Technologies 5

2. Cristian Ștefan DUMITRIU - On the Corrosion of Two Types of Bronzes Under Cavitation 12

3. Alina BĂRBULESCU, Cristian Ștefan DUMITRIU - RBF Model for the Mass Loss of a Brass in Cavitation Field 17

4. Romică CREȚU - Research on Some Freshwater Fish Catalase Activity - As a Potential Biomarker for Environmental Pollution 22

5. Carmelia Mariana DRAGOMIR BĂLĂNICĂ, Adrian LEOPA - Current Challenges and Prospective Benefits of Using UAVs 30

6. Florin-Bogdan MARIN, Mihaela MARIN - Drone Detection Using Image Processing Based on Deep Learning 36

7. Mihaela MARIN, Florin-Bogdan MARIN - Determination of Porosity in Fluidized-Bed Carburized P/M Compacts Using an Image Software Analysis 40

8. Florin-Bogdan MARIN, Mihaela MARIN - CFD Modeling of Aerodynamic Car Brake Cooling System 44

9. Bogdan Manolin JURCHIȘ - The Impact of Various Fuels on Particulate Emissions for a Compression Ignition Engine Equipped with a Diesel Particulate Filter 48

10. Bogdan Manolin JURCHIȘ - Researches on Soot Filtration Process by Comparing Simulation and Experimental Tests 54

11. Beatrice Daniela TUDOR, Bianca Teodora BUCEVSCHI - Analysis of the Influence of Pesticides on the Soil in an Agricultural Area 60

12. Andrei-Constantin SOFIAN, Mădălin-Florin POPA, Bogdan Manolin JURCHIȘ - NO_x and CO Emission Analysis Using Oxygenated Fuels for a Diesel Engine Equipped with Diesel Particulate Filter 67

13. Mădălin-Florin POPA, Bogdan Manolin JURCHIȘ - Analysis of the Wear Process of the Elements in the Braking System of Heavy Trucks 72

14. Andrei-Constantin SOFIAN, Bogdan Manolin JURCHIȘ, Mădălin-Florin POPA - Rack and Pinion Steering System Design for a Passenger Car 79

15. Florin-Bogdan MARIN, Mihaela MARIN - CFD Modeling and Simulation of an Industrial Hall 86

THE ANNALS OF "DUNAREA DE JOS" UNIVERSITY OF GALATI
FASCICLE IX. METALLURGY AND MATERIALS SCIENCE
Nº. 4 - 2021, ISSN 2668-4748; e-ISSN 2668-4756
Volume DOI: https://doi.org/10.35219/mms.2021.4

THE ANNALS OF "DUNAREA DE JOS" UNIVERSITY OF GALATI
FASCICLE IX. METALLURGY AND MATERIALS SCIENCE
N°. 4 - 2021, ISSN 2668-4748; e-ISSN 2668-4756
Article DOI: https://doi.org/10.35219/mms.2021.4.01

DIGITALIZATION OF AGRICULTURE IN NORTHERN BARAGAN, BY USING DRONES, FOR THE PURPOSE OF MONITORING CROPS, TO INCREASES THE EFFICIENCY OF AGRICULTURAL TECHNOLOGIES

[1]Adrian LEOPA, [2]Daniela TRIFAN, [1]Valentin BARDAHAN, [1]Niculai HAUK

[1]"Dunarea de Jos" University of Galati, Romania
[2]SCDA Braila Romania
e-mail: adrian.leopa@ugal.ro

ABSTRACT

With the increase of the population appeared the need to increase the agricultural production. However, this desideratum comes with a series of requirements that are somewhat contradictory:

- reducing the use of pesticides;
- reducing the quantities of agricultural fertilizers by optimizing their use;
- the use of more environmentally friendly technologies;
- cost reduction.

Thus appeared the concept of "precision agriculture" that meets the requirements listed. This concept involves processing a large volume of digitized data. The data must be purchased with appropriate means, processed with specialized software and interpreted by qualified specialists.

The software also generates the data necessary for the practical application, on farms, of the measures necessary to achieve a precision agriculture.

KEYWORDS: drones, precision agriculture, digitalization

1. Introduction

In order to obtain data regarding the state of the crops at a given moment, photographs of the area of interest are taken. The photos are taken in digital format. The height from which the photos are taken considers:

- the cameras resolution;
- the minimum resolution necessary to highlight significant details;
- the type of culture analysed;
- expected economic efficiency.

There are the following data acquisition options:

- Acquisition of data using specialized satellites. It depends on the moment of the satellite passing over the observed area, on the level of cloudiness at the time of taking the photos and on the resolution of the cameras used. Given the high height from which the shooting is taken, large areas with a low resolution are framed;

- Data acquisition using specially equipped aircraft, ensures good resolutions but requires large areas, specially arranged, from where the aircraft can make take-offs and landings;

- Acquisition of data using drones. It is expanding, especially in the case of medium and small surfaces analysed. It can be achieved when the atmospheric conditions are acceptable, from a relatively low altitude. The resolutions obtained allow the highlighting of significant details. The increase of the storage and data processing capacities, together with the improvement of the software, allowed the imposition of this solution, especially in small and medium farms. Another advantage comes from the existence of a significant number of companies specialized in making specialized equipment and software.

This paper analyses some aspects related to the use of drones in precision agriculture.

Both flying wing drones and multicopter drones are used. The former is used for medium to large areas and the multicopter are used for small and medium areas.

Multispectral cameras are used for data acquisition. Practically, several images in different

THE ANNALS OF "DUNAREA DE JOS" UNIVERSITY OF GALATI
FASCICLE IX. METALLURGY AND MATERIALS SCIENCE
N°. 4 - 2021, ISSN 2668-4748; e-ISSN 2668-4756
Article DOI: https://doi.org/10.35219/mms.2021.4.01

spectra are made from the same point. Based on previous research, certain relationships have been established, at the level of a combination of pixels from different spectra, which allow:

- establishing the health level of the culture at a given time;
- soil moisture level;
- the level of useful substances in the soil;
- the presence of weeds in different areas;
- a possible attack of some pests;
- the existence of natural or artificial obstacles that can affect the work of agricultural equipment;
- vegetation level at the time of data acquisition.

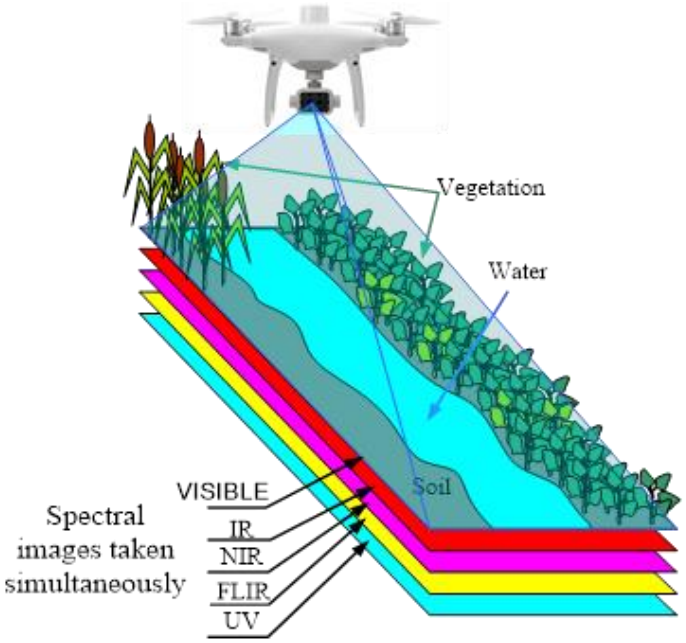

Fig. 1. *The multispectral data acquisition*

In Fig. 1 presents the principle according to which multispectral analysis works. The camera takes several images, from the same place, on a single surface. Each image is made in a different spectrum. The spectral components are emitted depending on the condition of the plants and the soil.

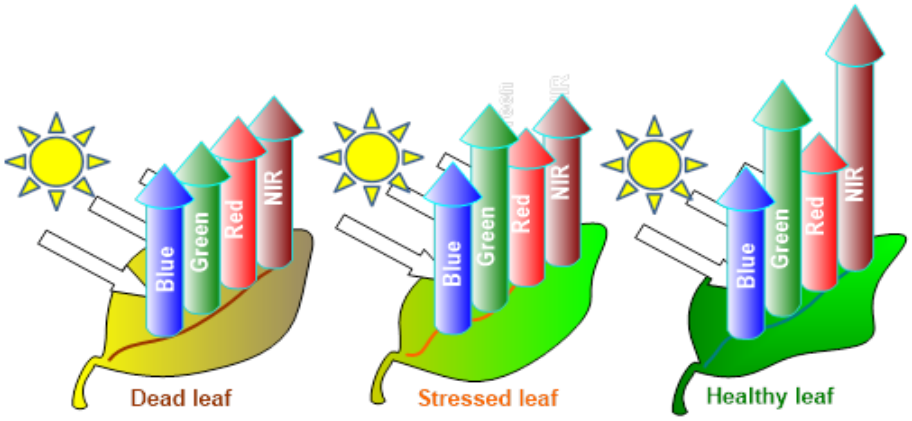

Fig. 2. *The way the light is reflected by the vegetation in different biological stages*

Figure 2 highlights aspects of how light is reflected by the leaves of plants in different vegetation situations. This different way of reflection is the basis of the analyses that are made starting from the multispectral images.

The images thus made are processed with specialized software, obtaining useful information about the respective agricultural crop.

THE ANNALS OF "DUNAREA DE JOS" UNIVERSITY OF GALATI
FASCICLE IX. METALLURGY AND MATERIALS SCIENCE
Nº. 4 - 2021, ISSN 2668-4748; e-ISSN 2668-4756
Article DOI: https://doi.org/10.35219/mms.2021.4.01

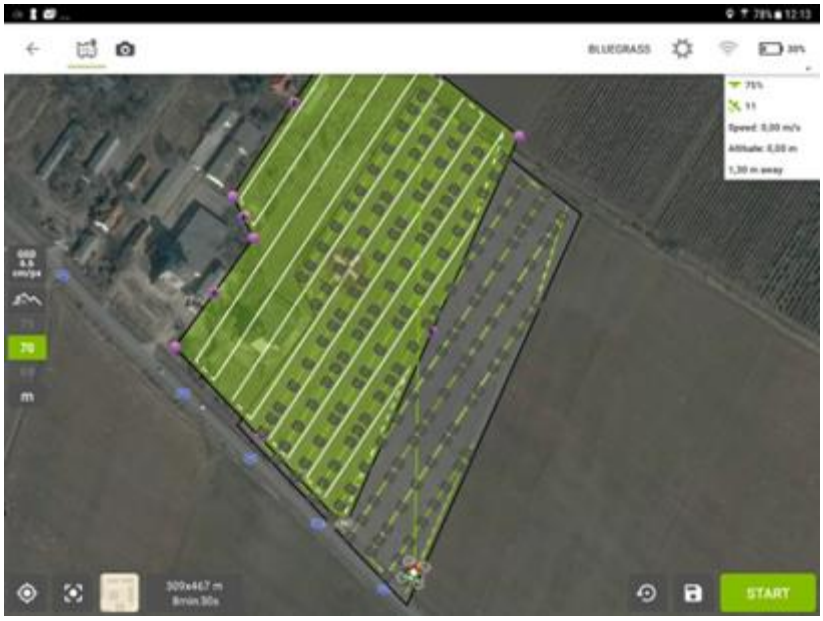

Fig. 3. *Image capture with flight plane and multispectral shooting*

Because the drones fly at low altitudes (maximum 120 m, according to aviation regulations), the overall picture is obtained from several photos of the area. These are done with a precise planning of the flight route, so that there are sufficient side overlays of the images for assembling the images with specialized software. Figure 3 shows a screenshot that shows the flight plan of a drone over an area of SCDA Braila. The points where the multispectral photos will be taken are highlighted.

2. Data processing

The realization of multispectral images consists in the simultaneous performance, from the same point of the drone's trajectory, of several images in different spectra. The images are digital and have entered, among other data, the GPS coordinates of the point from which they were taken.

After downloading the information, they are processed with specialized software.

The first stage consists in obtaining the overall image of the analysed area, on each spectrum (orthophotoplans). These are 3D images.

Based on these images, is calculated, at the pixel level, and are represented in the form of maps, the so-called vegetation indices.

The vegetation index is an indicator that is calculated as a result of operations with different spectral ranges of remote sensing data and is related to vegetation parameters. The calculation of most vegetation indices is based on two sections, the most stable, of the spectral reflectance of plants.

The most widely used vegetation index is the NDVI, Normalized Difference Vegetation Index. It characterizes the health of vegetation and allows farmers to assess germination, growth, the presence of weeds or diseases, and to predict field productivity. The values of the indices are generated starting from the green mass, which absorbs the electromagnetic waves in the visible red range and reflects them in the near infrared range. The red region of the spectrum (0.62-0.75 μm) represents the maximum absorption of solar radiation by chlorophyll, and the near infrared area (0.75-1.3 μm) and has the maximum energy reflection by the leaf cell structure. Thus, high photosynthetic activity leads to lower values of reflection coefficients in the red region of the spectrum and high values in the near infrared region of the spectrum.

The NVDI index is calculated with relation 1.

$$NVDI = \frac{NIR - Red}{NIR + Red} \quad (1)$$

There are other vegetation indices, each with applicability for various requirements, each with specific calculation relationships.

Figure 4 shows an example of spectral analysis, with the generation of a zoned map, starting from the spectral images of the analysed area. It is observed that the NDVI analysis highlighted areas with different characteristics, impossible to see in the visible spectrum.

THE ANNALS OF "DUNAREA DE JOS" UNIVERSITY OF GALATI
FASCICLE IX. METALLURGY AND MATERIALS SCIENCE
N°. 4 - 2021, ISSN 2668-4748; e-ISSN 2668-4756
Article DOI: https://doi.org/10.35219/mms.2021.4.01

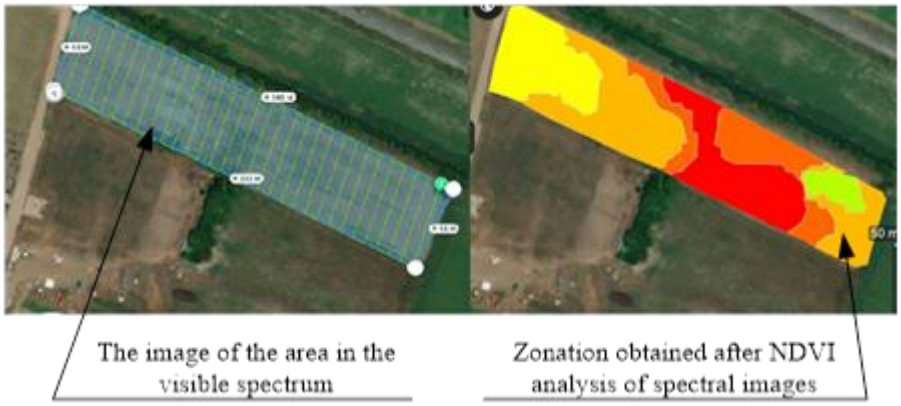

Fig. 4. *Comparison between the image obtained in the visible spectrum and the zoning obtained from the NDVI analysis*

3. Use of results

3.1. Using the MyJohnDeere platform for variable rate applications

John Deere machines benefit from the possibility of using the computer platform dedicated to them, which allows continuous communication between the machine working in the field and the agronomist. Through the MyJohnDeere platform, agronomic decisions can be easily transmitted to the machine and operator, and the execution of the work is reported in real time. The Operations Center application can be used for the remote transmission, to the machines equipped with intelligent John Deere displays and the JDLink system, of the maps for the application of dispersions with variable rate, these being able to be used in few moments from the transmission. Figure 5 shows a screenshot of the application during the file transfer.

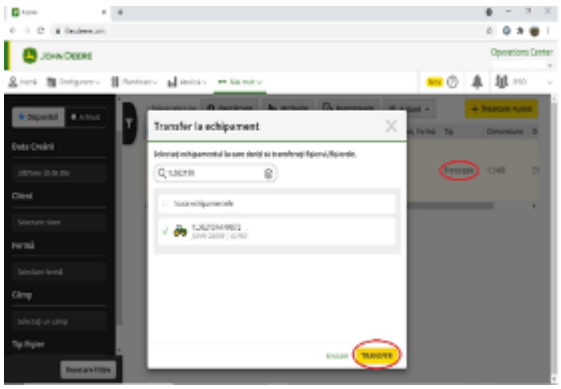

Fig. 5. *Transfer of the prescription file, from the Operations Centre application, to the variable rate spreading machine*

The application commands are sent to the implementation system through the ISOBUS system, which connects the machine and the implementation. After starting the machine-implementation system and starting the application, the implementation in the plot of the proposed rate can be watched in real time on the display.

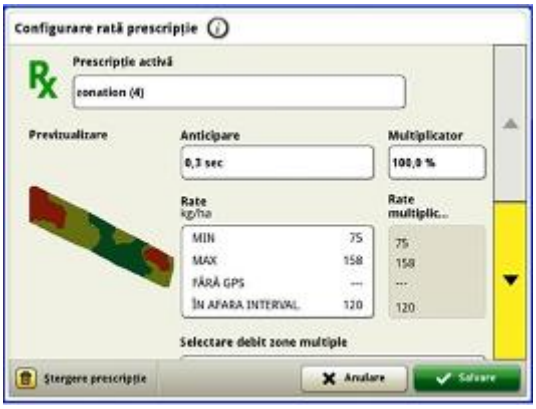

Fig. 6. *View of information received on the John Deere smart display*

Fig. 7. *Automatic transfer of the application command to the implementation system*

THE ANNALS OF "DUNAREA DE JOS" UNIVERSITY OF GALATI
FASCICLE IX. METALLURGY AND MATERIALS SCIENCE
No. 4 - 2021, ISSN 2668-4748; e-ISSN 2668-4756
Article DOI: https://doi.org/10.35219/mms.2021.4.01

Fig. 8. *Visualization of the application of dispersions, on the machine display, in real time*

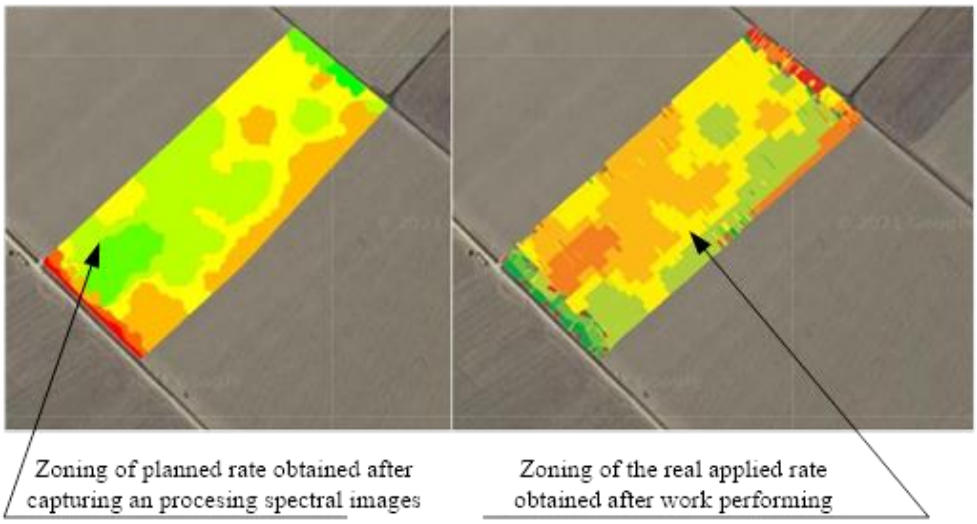

Fig. 9. *Comparative analysis, taken from the Operations Centre, between the planned rate and the applied rate*

At the same time, the data of the performed work are transmitted through the JDLink system to the Operations Centre application, where they can be compared: Planned Rate vs. Applied Rate

3.2. The need for agrochemical study

Precision agriculture is based on the extensive use of flight systems, which can provide essential data on crops, but for a limited time. Flying over agricultural crops with flight systems, equipped with different sensors, is an essential component on which precision agriculture is based. In this way, certain deficiencies can be detected in real time and can be corrected to avoid a possible decrease in the expected harvest.

For the efficient application of precision agriculture, it is necessary to know in advance the physico-chemical parameters of the soil in order to establish the fertilization plan for the cultivated areas, according to the scheduled crop and the expected harvests.

Therefore, in the current context, the realization of a precise agrochemical study can no longer be optional, it becomes mandatory in order to obtain an expected harvest by the farmer.

In order to carry out an agrochemical study, the well-known steps must be completed, namely:

THE ANNALS OF "DUNAREA DE JOS" UNIVERSITY OF GALATI
FASCICLE IX. METALLURGY AND MATERIALS SCIENCE
Nº. 4 - 2021, ISSN 2668-4748; e-ISSN 2668-4756
Article DOI: https://doi.org/10.35219/mms.2021.4.01

- the field phase, consists in taking soil samples based on a previously established model;

- the laboratory phase, consists in the analysis of the soil samples taken previously to know the physico-chemical properties;

- the office phase, consists of the analysis of the limiting factors of the agricultural production, the realization of the cartographic materials, of the interpretative tables and of the fertilization plans, depending on the crop structure desired by the beneficiary and the expected productions.

In order to prepare cartographic materials, a mathematical apparatus integrated in a software can be used. Therefore, using the calculation technique, cartograms with chemical fertility indices can be obtained, their degree of fidelity being in close correlation with the location of the points from which the soil samples are collected. Obtaining maps as accurate as possible requires taking soil samples from points at equidistant distances from each other. In other words, the refinement of the cartograms is possible by approximating the agricultural area with a matrix, and the soil samples are taken from points corresponding to its elements.

For example, the following is a mapping carried out in the research project, PN-III-P2-2.1-PTE-2019-0085, in which a series of maps with chemical fertility indices for different agricultural areas were made.

The presented mapping had as objective the determination of the supply state with mobile potassium, its novelty degree consisting in the fact that for its elaboration the MATLAB program was used, Fig. 10 [1-3].

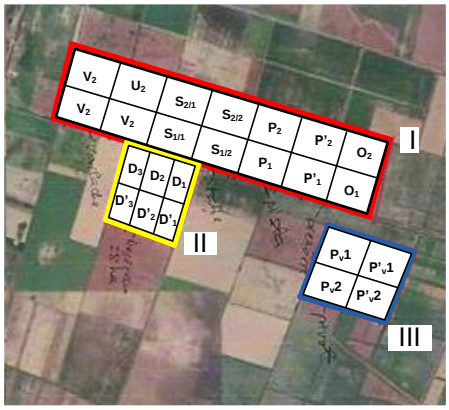

a. Map of the areas for which the state of supply of mobile potassium was represented

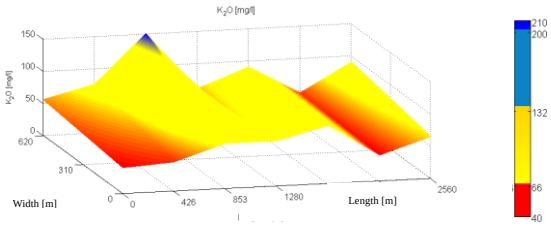

b. 3D map for experimentally determined CTSS values, field I

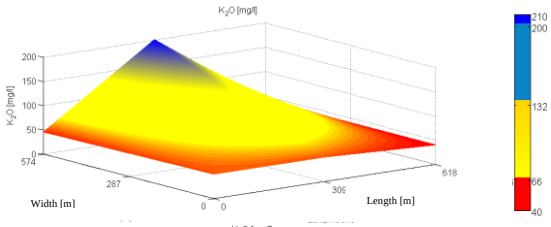

c. 3D map for experimentally determined CTSS values, field II

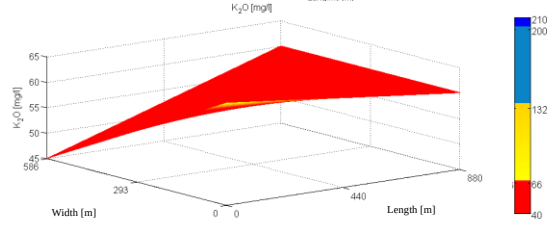

d. 3D map for experimentally determined CTSS values, field III

Fig. 10. *3D maps for the state of supply of mobile potassium*

4. Conclusion

The trend of population growth on a global level and implicitly of the need for food, forces current generations to identify viable solutions to increase agricultural production, but in full agreement with the commitments arising from Romania's adoption of the principle of sustainable development.

Therefore, agriculture has an obligation to ensure a growing production, but without affecting the chances of future generations to meet their own needs. As presented in this paper, one of the possibilities for achieving this goal is precision agriculture. Compared to classical agriculture, precision agriculture, as the name suggests, uses modern means that allow real-time monitoring of crops, which allows a reduced reaction time. A suitable reaction time does nothing but stagnate the decrease in production in some cases, and in others lead to an increase in it. The use of the calculation technique in the agrochemical study represents a substantial advantage in the accurate evaluation of soil nutrients. The correlation of the maps thus obtained over several years, represents a modern method by which it can appreciate the tendency of qualitative parameters of the analysed soil.

Also, flying over crops with the help of aerial drones at certain intervals, provides in addition to an effective reaction time in certain situations, but helps to accurately dose fertilizers.

Proper dosing of these chemicals significantly and long-term reduces soil pollution.

Even if the adoption of precision agriculture by farmers generates additional costs, it is estimated that these costs will be amortized by the crop increase obtained in these conditions.

Acknowledgements

This work was supported by a grant of the Romanian National Authority for Scientific Research and Innovation, CNCS/CCCDI – UEFISCDI, project number PN-III-P2-2.1-PTE-2019-0085, within PNCDI III.

References

[1]. ***, *Raport tehnic, etapa I*, proiectul PN-III-P2-2.1-PTE-2019-0085.

[2]. Marin Ghinea, Virgiliu Fireteanu, *Matlab - Calcul numeric, grafică, aplicații*, Ed. Teora.

[3]. Leopa A., Trifan D., *Quantification of Atmospheric Pollution by Qualitative Analysis of Precipitation as Snow*, The Annals of „Dunărea de Jos" University of Galați, Fascicle IX Metallurgy and Materials Science, Galati University Press, special issue - 2013, p. 197-203, ISSN 1453-083X, 2013.

THE ANNALS OF "DUNAREA DE JOS" UNIVERSITY OF GALATI
FASCICLE IX. METALLURGY AND MATERIALS SCIENCE
N°. 4 - 2021, ISSN 2668-4748; e-ISSN 2668-4756
Article DOI: https://doi.org/10.35219/mms.2021.4.02

ON THE CORROSION OF TWO TYPES OF BRONZES UNDER CAVITATION

Cristian Ștefan DUMITRIU
Transilvania University of Brasov, Romania
e-mail: cristian.dumitriu@unitbv.ro

ABSTRACT

This article contains the results of the experiments concerning the mass loss of two types of bronze in seawater in the cavitation produced by ultrasound generated by a high-frequency generator. The mass loss models are presented for the experimental conditions when the generator worked at different powers - 80 W, 120 W, and 180 W. In all scenarios, the results show that the bronze with Sn has the highest mass loss in the cavitation field.

KEYWORDS: cavitation, bronze, mass loss, gravimetric index

1. Introduction

The phenomena related to the mechanical erosion of materials in the cavitation field are of major importance for selecting the alloys used in the naval industry. Some are copper alloys employed for building propellers, bilge systems, ballast installation, and other connection pieces that work in cavitation conditions. Due to the necessity of materials with high resistance to corrosion in this industry, different authors analysed the behavior of some copper alloys in seawater [1-3], while only a few investigated their behavior under cavitation and studied the corrosion type [4-5]. Ivanov [6] showed that some bronzes with Sn have gravimetric index 0.004 -0.015 g/m^2h^{-1} at a concentration of 0.19% (at 15 °C) and have high corrosion resistance in seawater vapors at high pressure. The same study [6] emphasized that the resistance of bronzes with Al and Ni can be nine times bigger than that of the bronzes with Sn, depending on the percentages of Al and Ni. Adding Ni in a bronze containing Al and Fe increases its mechanical resistance, resistance to cavitation, and corrosion in conditions of fatigue stress is four times greater than for the bronzes with Mn.

In this article, we present the results of the experiments concerning the mass loss of two types of bronzes in seawater under cavitation, using an experimental setup built by us [7]. The equations of the mass loss in time are determined, and the gravimetric indices are provided for comparing the materials' resistance to corrosion.

2. Materials and methods

The studied materials are two bronzes, with the following composition:

- A bronze with 83.09% Cu, 6.4% Sn, 4.40% Pb, 4.07% Zn, called in the following Bronze 1;
- A bronze with 80.54% Cu, 9.85% Al, 4.59% Fe, 4.40% Ni, called in the following Bronze 2.

These materials have been chosen because they are used for elements of ships working under pressure and cavitation, as pipes, fittings, joining components, and propellers.

Bronze 1 belongs to the class of the bronzes with Sn, Zn, and Pb, while Bronze 2 is a bronze with Al and Ni.

The composition of the seawater used for all the experiments is the following: salinity: 22.17 g/L NaCl, 0.31 g/L, pH = 7, 6.27 meq/L - total water hardness, 0.051 mg/L Fe, 0.0033 mg/L Ni.

The experimental setup used for studying the mass loss in the cavitation field is presented in Fig.1 [7-10]. It is mainly formed by the tank where the studied liquid is introduced (1); the high frequency (20 Hz) generator (8); a ceramic transducer (7) that is excited by the generator; a pair of copper electrodes (13), with the role of collecting the electrical signals produced during the periods when the generator works; a cooling fan (11) utilized for preserving a constant temperature (in this case 20 °C) of the liquid during the experiment (given that the cavitation is an exogenous process); the command block (12) used for selecting different powers for the generator regime (80 W, 120 W, or 180 W).

The samples were kept in saline water under cavitation produced by ultrasound for a total of 1320

THE ANNALS OF "DUNAREA DE JOS" UNIVERSITY OF GALATI
FASCICLE IX. METALLURGY AND MATERIALS SCIENCE
N°. 4 - 2021, ISSN 2668-4748; e-ISSN 2668-4756
Article DOI: https://doi.org/10.35219/mms.2021.4.02

minutes (380 minutes at 80 W, 480 minutes at 120 W, and 480 minutes at 180 W of the generator power) and weighted every 20 minutes.

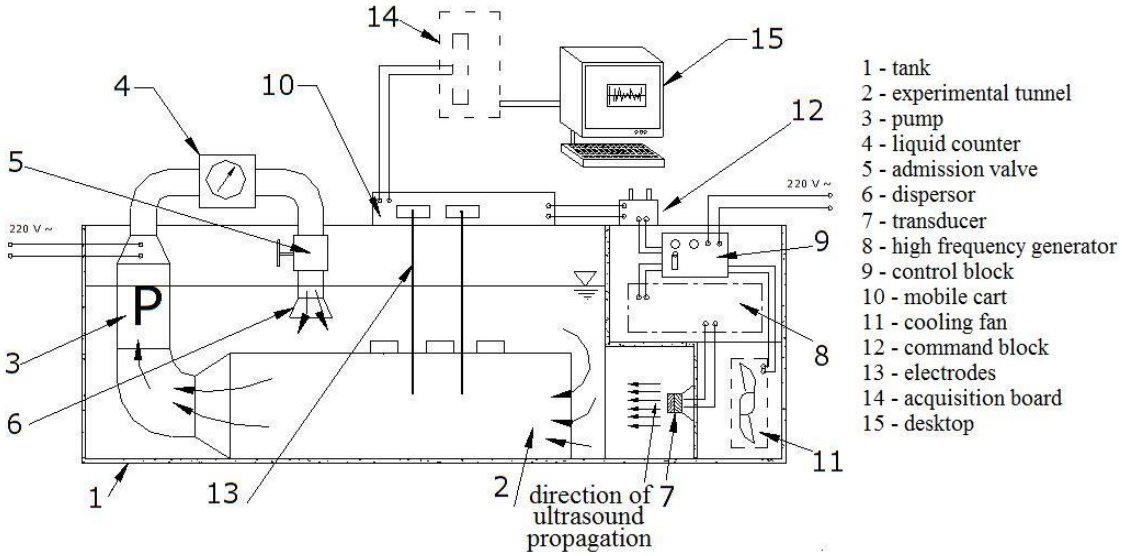

Fig. 1. *The experimental setup*

The mass loss trend of each material at each power level has been determined and validated by statistical methods. The determination coefficients (R^2) and the residuals' standard deviation (s) are reported. An R^2 close to 1 and a residual standard deviation close to zero indicate a good fit.

The Kolmogorov-Smirnov, the portmanteau, and the Levene tests [11] have been performed for testing that the residual forms a Gaussian white noise. The tests have been performed at a significance level of 5%.

To determine if the mass loss series at the three-power level come from the same distribution, the Kruskal-Wallis test [12] has been performed. If the null hypothesis was rejected, the non-parametric Wilconxon test [13] has been performed to test the same hypothesis for pairs of series.

To quantitatively appreciate the corrosion-erosion, the absolute mass variation on the surface (S) and the gravimetric indexes (mass loss in time and per surface) have been determined.

3. Results and discussion

Let us denote by:

- t - the time,
- m_t - the sample mass at the moment t,
- R^2 - the determination coefficient,
- s - the residual standard deviation,
- S - the total surface of a sample.

Figures 2 (a)-(c) (Figure 3 (a)-(c)) show the mass evolution of the sample of Bronze 1 (Bronze 2) at each power level of the generator. Figure 2 (d) (Figure 3 (d)) shows the overall evolution of the mass of the same sample.

For Bronze 1, the equations of the mass variation are polynomial of the second degree, when the generator worked at 80 W and 120 W, while when working at 180 W is, the polynomial is of the third order. In all cases, R^2 (Fig. 2 (a)-(c)) is above 0.92, and the residual standard deviations are lower than 0.0002, indicating a good fit of the recorded values. Residuals' analysis shows all the residuals in the models form a white noise.

Kruskal - Wallis and the Wilconxon tests rejected the null hypotheses, so one cannot find enough evidence that there is no difference between the time series. Hence, the corrosion trend depends on the generator's power.

For Bronze 2, the mass loss is described by third-degree polynomials at 80 W and 180 W and a second-degree polynomial at 120 W. The corresponding R^2 are higher for Bronze 2 than for Bronze 1, with the residuals standard deviations less than 0.00007. The residuals in the models form white noises. Again, the null hypotheses have been rejected by Kruskal - Wallis and the Wilconxon tests, confirming that the generator's power influences the mass loss.

The studied samples mass variation during the experiments is:

- for Bronze 1:

THE ANNALS OF "DUNAREA DE JOS" UNIVERSITY OF GALATI
FASCICLE IX. METALLURGY AND MATERIALS SCIENCE
N°. 4 - 2021, ISSN 2668-4748; e-ISSN 2668-4756
Article DOI: https://doi.org/10.35219/mms.2021.4.02

$$m_t = 17.244908 - 5.075136 \cdot 10^{-6} t + 1.887143 \cdot 10^{-10} t^2, \quad (1)$$

with a standard deviation s s =0.00019783 and R^2 = 0.9911;

- for Bronze 2:

$$m_t = 23.445849 - 8.922002 \cdot 10^{-6} t + 2.798266 \cdot 10^{-10} t^2, \quad (2)$$

with s = 0.000228 and R^2 = 0.9904.

To determine the material with the best behavior in cavitation conditions, the absolute mass variation per surface [in g/m^2] has been computed, using the formula:

$$\Delta m_t / S = (m_1 - m_t) / S \quad (3)$$

where S is the surface of the sample, m_1 is the sample mass at the beginning of the experiment, and m_t is the mass of the sample at the moment t.

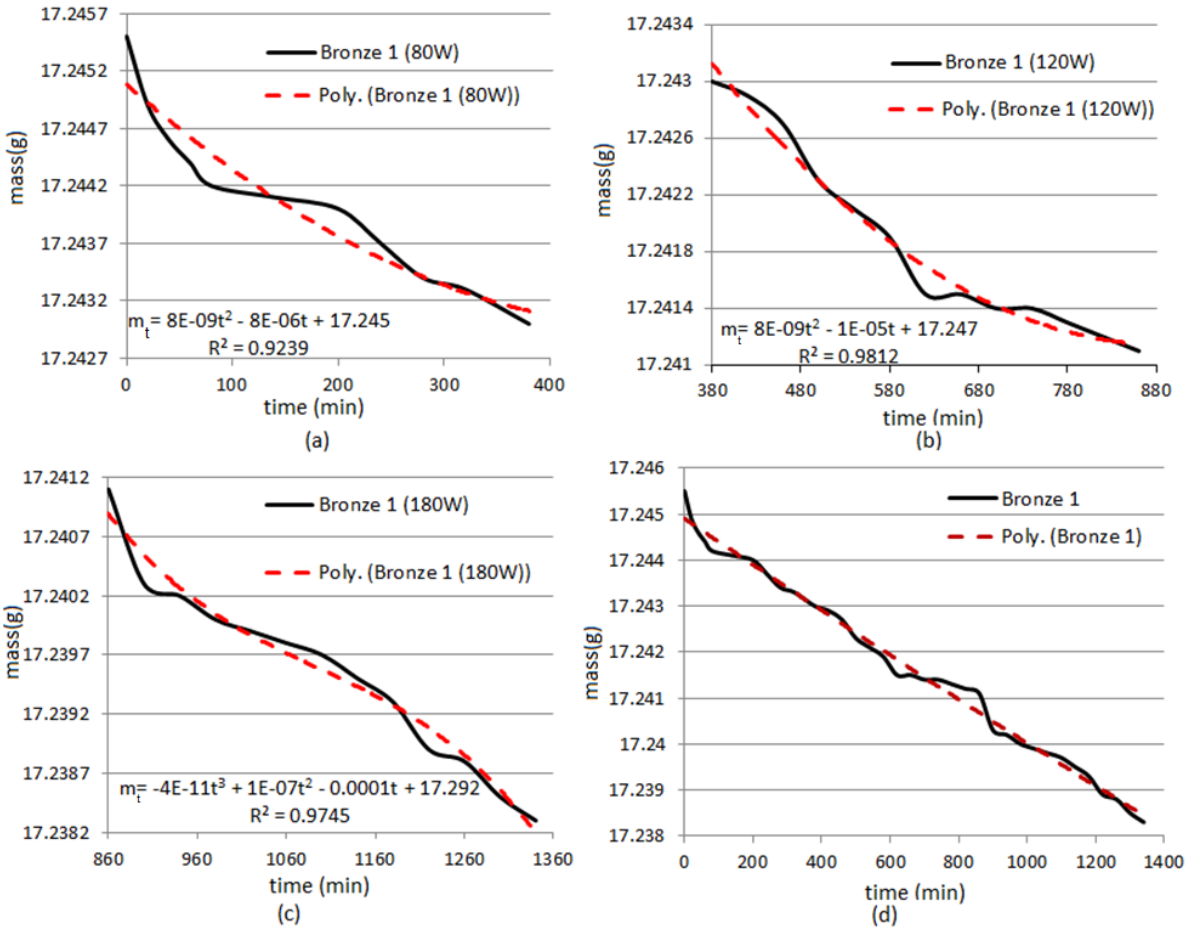

Fig. 2. *The mass variation of Bronze 1: (a) at 80 W, (b) at 120 W, (c) at 180 W, (d) during the entire experiment. The continuous line represents the recorded data, and the dotted ones the fitted trend*

The charts of mass variation per surface for both materials are presented in Fig. 4. The continuous curves represent the data series, whereas the dotted ones are the fitted trends. Remark that Bronze 2 experiences the highest values compared to Bronze 2, significantly higher at the third power level. All the models fitted for the series trends have R^2 greater than 0.97.

The trend equations for the total variation of the mass in time per surface are respectively:

- for Bronze 1:

$$\Delta m_t / S = 0.0758 + 0.1237t - 0.0003t^2, \quad (4)$$

THE ANNALS OF "DUNAREA DE JOS" UNIVERSITY OF GALATI
FASCICLE IX. METALLURGY AND MATERIALS SCIENCE
N°. 4 - 2021, ISSN 2668-4748; e-ISSN 2668-4756
Article DOI: https://doi.org/10.35219/mms.2021.4.02

with s = 0.11308 and R^2= 0.9933, and

- for Bronze 2:

$$\Delta m_t/S = 0.1609 + 0.1513t - 0.0019t^2, \quad (5)$$

with: s = 0.0894 and R^2 = 0.9908.

Finally, the gravimetric indices have been computed in all scenarios, based on the data from Fig. 4. They are presented in Table 1.

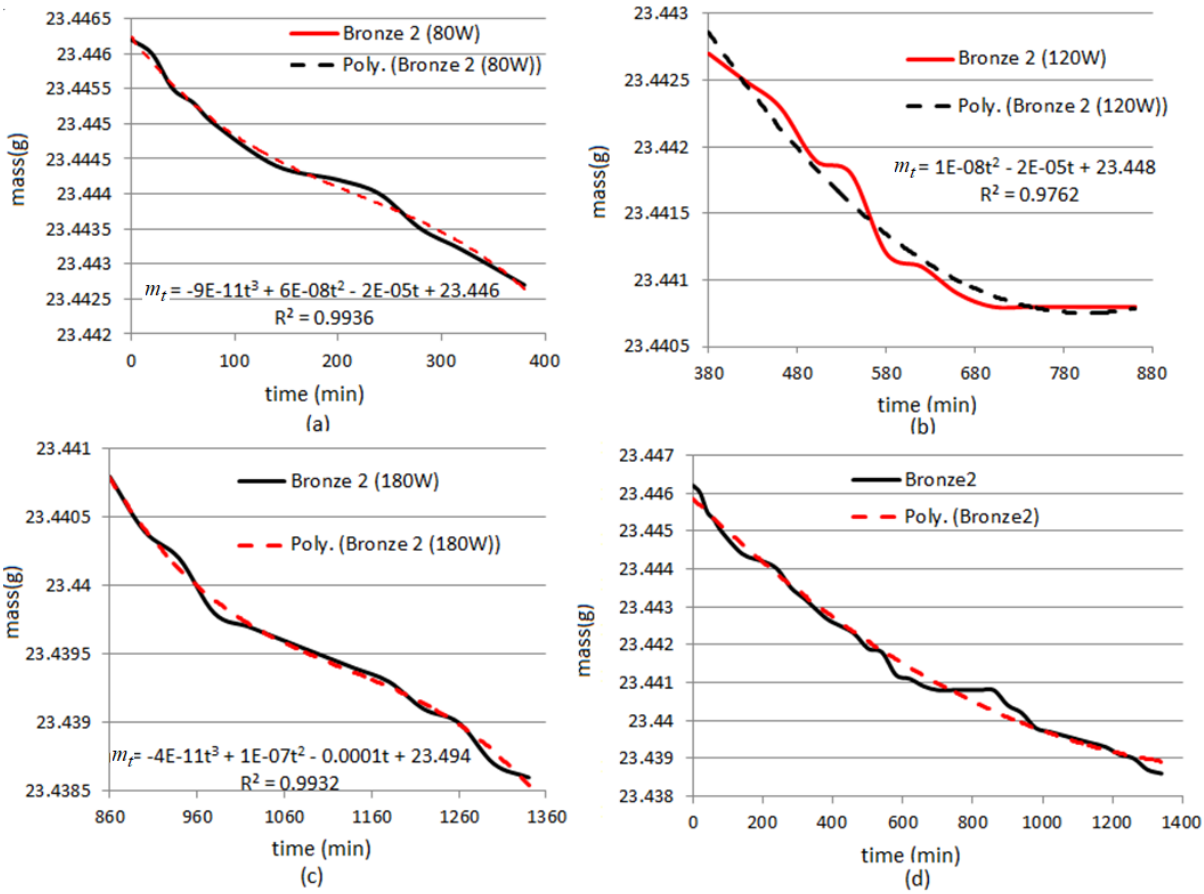

Fig. 3. *The mass variation of Bronze 2: (a) at 80 W, (b) at 120 W, (c) at 180 W, (d) during the entire experiment. The continuous line represents the recorded data, and the dotted ones, the fitted trend*

Table 1. *The gravimetric indices [g/m²h]*

Power [W]	Bronze 1	Bronze 2
80	0.2256	0.2166
120	0.1357	0.0931
180	0.2000	0.1078

The highest gravimetric index is that of Bronze 1, in the first scenario, while the lowest is that of Bronze 2, at 120 W. Unexpectedly, the highest gravimetric index was obtained at 80 W for both bronzes and the lowest for the second one.

THE ANNALS OF "DUNAREA DE JOS" UNIVERSITY OF GALATI
FASCICLE IX. METALLURGY AND MATERIALS SCIENCE
N°. 4 - 2021, ISSN 2668-4748; e-ISSN 2668-4756
Article DOI: https://doi.org/10.35219/mms.2021.4.02

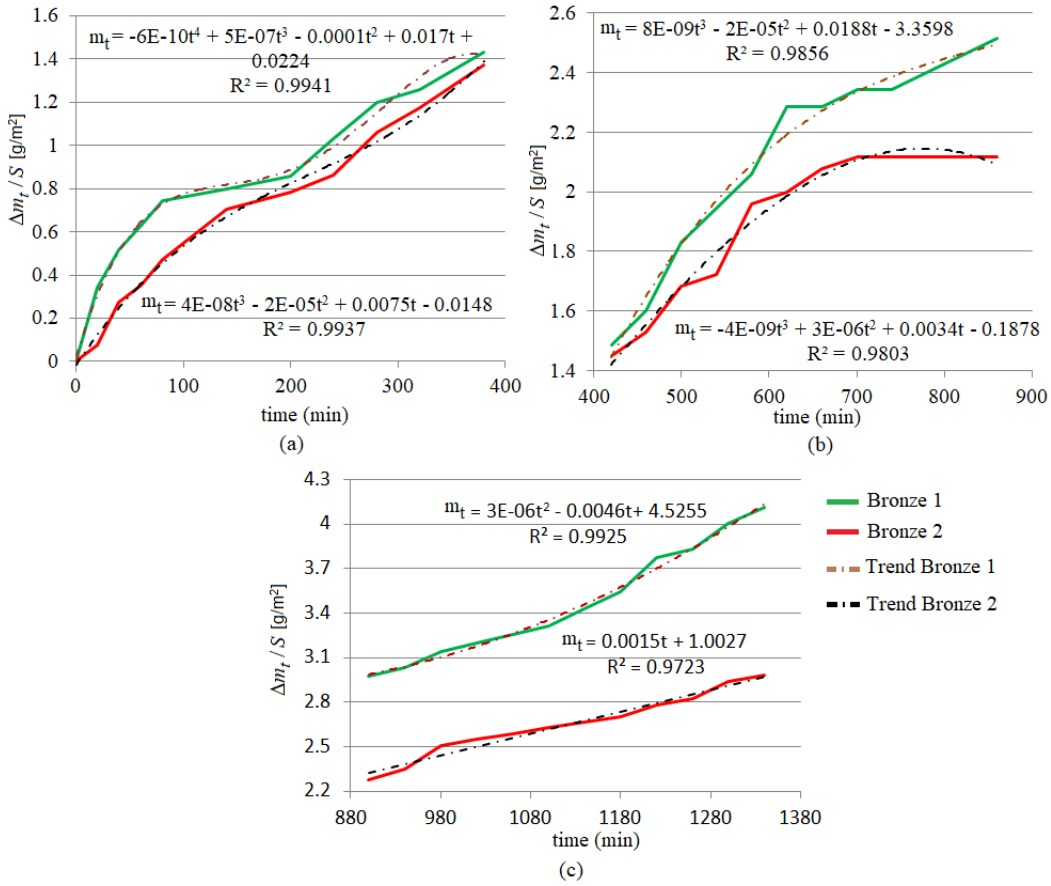

Fig. 4. *The variations in time of absolute mass per surface at: (a) 80 W, (b) 120 W and (c) 180 W*

4. Conclusion

The experiments of mass loss in ultrasound cavitation field proved that bronze with Sn has a lower resistance than that with Al. The gravimetric indices show the highest mass loss at the first stage of the generator. The study show that the corrosion speed is higher than in freshwater [10] due to the accentuated chemical corrosion that appears due to the salt content.

For future, it would be interesting to study the mass loss of the same materials in circulating liquids given the importance of these materials for the naval constructions.

References

[1]. Schüssler A., Exner H. E., *The corrosion of nickel-aluminium bronzes in seawater - I. Protective layer formation and the passivation mechanism*, Corros. Sci., 3(11), p. 1793-1802, 1993.
[2]. Wharton J. A., *et al.*, *The corrosion of nickel-aluminium bronze in seawater*, Corros. Sci., 47(12), p. 3336-3367, 2005.
[3]. Basumatary J., Nie M., Wood J. K., *The synergistic effects of cavitation erosion-corrosion in ship propeller materials*, J. Bio-Tribo-corros., 1, p. 1-12, 2015.
[4]. Wharton J. A., Stokes K. R., *The influence of nickel–aluminium bronze microstructure and crevice solution on the initiation of crevice corrosion*, Electrochim. Acta, 53 (5), p. 2463-2473, 2008.
[5]. Basumatary J., Wood R. J. K., *Synergistic effects of cavitation erosion and corrosion for nickel aluminium bronze with oxide film in 3.5% NaCl solution*, Wear, 376-377, p. 1286-1297, 2017.
[6]. Ivanov I. V., *Corrosion resistant materials in food industry*, Editura Agro-Silvica Bucuresti, Romania, 1959.
[7]. Bărbulescu A., Marza V., Dumitriu C. S., *Patent no RO 123086-B1 (30.09.2010) Installation and method for measuring and determining the effects produced by cavitation in ultrasound field in stationary and circulating media*, 2010.
[8]. Bărbulescu A., *Models of the voltage induced by cavitation in hydrocarbons*, Acta Phys. Pol. B, vol. 37 (10), p. 2919-2931, 2006.
[9]. Bărbulescu A., Dumitriu C. S., *Mathematical aspects of the study of the cavitation in liquids, in Mathematical Modelling of Environmental and Life Sciences*, S. Ion, G. Marinoschi and C. Popa, Eds. București: Editura Academiei Române, p. 7-14, 2006.
[10]. Dumitriu C. S., Bărbulescu A., *Studies about the copper base alloys used in naval constructions – modeling the loss mass in different media*, Sitech, Craiova, 2007.
[11]. Bărbulescu A., *Studies on time series. Applications in Environmental Sciences*, Springer, 2016.
[12]. Kruskal W. H., Wallis W. A., *Use of ranks in one-criterion variance analysis*, J. Am. Stat. Assoc., vol. 47 (260), p. 583-621, 1952.
[13]. Mann H. B., Whitney D. R., *On a Test of Whether one of Two Random Variables is Stochastically Larger than the Other*, Ann. Math. Stat., 18 (1), p. 50-60, 1947.

THE ANNALS OF "DUNAREA DE JOS" UNIVERSITY OF GALATI
FASCICLE IX. METALLURGY AND MATERIALS SCIENCE
Nº. 4 - 2021, ISSN 2668-4748; e-ISSN 2668-4756
Article DOI: https://doi.org/10.35219/mms.2021.4.03

RBF MODEL FOR THE MASS LOSS OF A BRASS IN CAVITATION FIELD

Alina BĂRBULESCU, Cristian Ștefan DUMITRIU
Transilvania University of Brasov, Romania
e-mail: alina.barbulescu@unitbv.ro, cristian.dumitriu@unitbv.ro

ABSTRACT

This article aims at presenting the model of the mass loss of a brass sample in ultrasonic cavitation field in saline water. The experiments done for data collecting was performed in three scenarios. In the first one, the high frequency generator worked at three power levels - 80 W, at the second one - at 120 W, and in the third one - at 180 W. The Model has been built using the series of the mass loss on surface.

KEYWORDS: brass, cavitation, mass loss, mathematical model

1. Introduction

Ultrasound cavitation is the process of formation, growth, and collapse of vapors bubbles inside a liquid traversed by an ultrasonic field [1]. High energies appear during this process, resulting in vibrations, noise, erosion-corrosion, unpassivation, sonoluminescence, emulsification etc. [2-3]. The phenomenon is characterized by the liquid discontinuity state when the pressure drop happens under critical values [4]. The cycle collapse/rebound induces a voltage at the cavitation zone boundaries [5-7].

Due to the practical implications of the negative effect of cavitation on the machines and their components working in such conditions, the attach type on materials with different compositions and the mass loss process became a topic of interest for scientists [8-14]. For example, Basumatary *et al.* [8] analysed the erosion-corrosion mechanism of ships propellers. Petkovsek and Dular [9] observed the cavitation erosion and structures. Wharton and Stokes investigated the corrosion mechanism of some Nickel-Aluminum bronzes, whereas Schüssler and Exner [11] studied the mass loss of the same type of materials in seawater. Other authors [12-14] modelled electrical signals that appeared in the cavitation field in different liquids and the mass loss of different materials in such conditions.

The present article is in line with the previous research investigating the mass loss of copper-based alloys in seawater and modelled the trend of this process [13-14]. The novelty consists of proposing an RBF model that fits the mass loss of a brass (utilized in the shipbuilding industry) in the ultrasound cavitation field.

2. Materials and methods

The studied material is a brass, with 57.95% Cu, 38.45% Zn, and 2.75% Pb.

The of the seawater composition used for all the experiments is the following: salinity: 22.17 g/L NaCl, 0.31 g/L SO_4^{2-}, pH = 7, 6.27 meq/L - total water hardness, 0.051 mg/L Fe, 0.0033 mg/L Ni.

The setup utilized for the experiment is shown in Fig. 1 [5, 14]. Its main parts are:

The tank containing the liquid (1);

- The high-frequency generator, working at 20 kHz (8)
- The ceramic transducer (7) that is excited by the generator (8);
- A cooling fan (11) utilized for keeping the liquid's temperature constant. The experiment has been performed at 20 ºC;
- The command block (12) used for selecting different powers for the generator regime (80 W, 120 W, or 180 W).

The samples were kept in saline water under cavitation produced by ultrasound for a total of 1320 minutes (380 minutes at 80 W, 480 minutes at 120 W, and 480 minutes at 180 W) and weighted every 20 minutes.

Based on the measured mass loss values, the variations of the ratios between the absolute mass loss (i.e., the difference between the mass at the moment t and the mass at the beginning of the experiment) on surface have been computed. To test if these values

THE ANNALS OF "DUNAREA DE JOS" UNIVERSITY OF GALATI
FASCICLE IX. METALLURGY AND MATERIALS SCIENCE
Nº. 4 - 2021, ISSN 2668-4748; e-ISSN 2668-4756
Article DOI: https://doi.org/10.35219/mms.2021.4.03

come from the same distribution, the Kruskal-Wallis test [15] was performed at the significance level of 0.05.

The last step was to put together the three data series and determine a Radial Basis Function (RBF) model of the mass loss per surface.

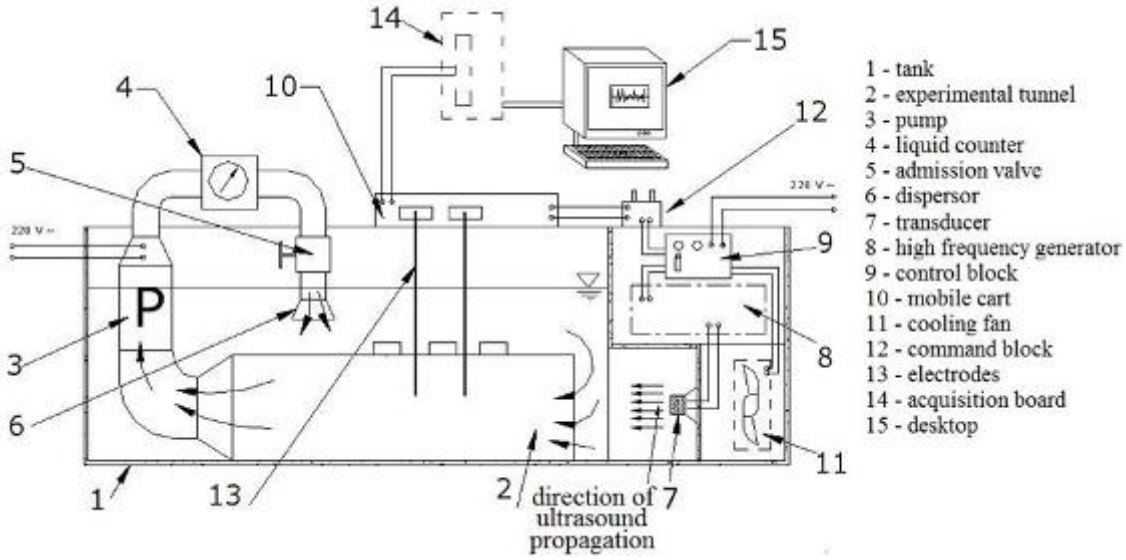

Fig. 1. *The experimental setup*

Artificial Neural Networks (ANNs) were firstly introduced for modelling the human brain structure and have been developed to understand the brain functioning (direction 1) and to the concept adaptation for using the computational capabilities in solving practical problems (direction 2) [16].

Nowadays, ANNs are widely used for modelling data from various domains where classical modelling methods do not provide satisfactory results, data series present high variability, or do not satisfy the hypotheses necessary to apply classical methods. ANNs have proved to have good approximation capabilities [17], thus they are employed to find answers to various classification, regression, and forecasting problems [18-24].

An ANNs is built of interconnected layers formed by neurons connected each to the others. There is an input layer, one or many hidden layers, and an output layer. Two classes of ANNs are known recurrent and feed-forward neural networks [25]. RBF networks (RBFNs) belong to the last class and have only a hidden layer.

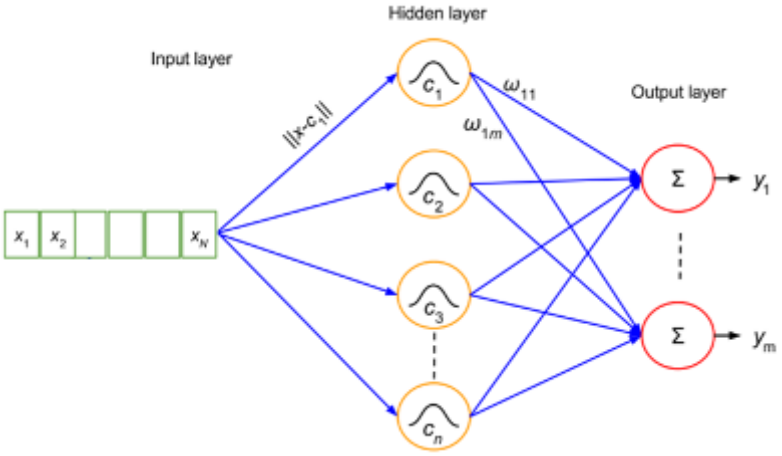

Fig. 2. *RBF neural network* [26]

ANNs are formed by artificial neurons that process the information that enters the network applying an activation function. The result is then transferred to the next layer.

THE ANNALS OF "DUNAREA DE JOS" UNIVERSITY OF GALATI
FASCICLE IX. METALLURGY AND MATERIALS SCIENCE
N°. 4 - 2021, ISSN 2668-4748; e-ISSN 2668-4756
Article DOI: https://doi.org/10.35219/mms.2021.4.03

The nodes in RBF network's hidden layer transform the input variables, using a radial basis function. The most used is the Gaussian function since no significant improvement of the modelling results was reported when employing other functions. The last layer acts as a summation unit.

The typical structure of an RBF neural network can be seen in Fig. 2.

The output of a hidden unit is $e^{-(\|x-c_i\|/b_i)^2}$ in case of a Gaussian kernel function, where $\|x - c_i\|$ is the Euclidian distance between *x* (the input vector) and the RBF's centroid, c_i, and b_i is the kernel width.

The hidden layer's output, o_i, are given by:

$$y_i = \sum_j w_{ij} o_j(x),$$

where w_{ij} are the weights of the links of the hidden layer *j* and the output layer, *i*.

At the network initialization, the centroid positions are chosen, whereas the weights and widths result from the network training (which is done by back-propagation).

In this case, the k-means clustering is employed to determine the centroids. An evolutionary algorithm [27] is utilized for selecting the optimum centroids and spread for each neuron and the moment when enough neurons are added to the network (based on the Leave-one-out procedure). The weights optimization is realized by ridge regression, and for minimizing the generalized cross-validation (GCV) error, the algorithm proposed by Orr [28] is utilized.

For details on this kind of network, the readers may see [29-30].

The following settings have been used in our study: the maximum number of neurons -100; population size – 200, the maximum number of generations – 20, maximum generations flat – 5, absolute tolerance – 10E-6, minimum radius – 0.01, maximum radius – 400. The optimal regularization Lambda parameter [28] varies between 0.001, and 10.

To validate the modeling results, the proportion of variance explained by model (R^2), the mean absolute error (MAE), the mean standard error (MSE), mean absolute percentage error (MAPE), the correlation between the actual and predicted values (r_{ap}) were employed.

3. Results and discussion

Let us denote by:
- *t* - the time,
- m_t - the sample mass at the moment *t*,
- R^2 - the determination coefficient,
- *s* - the standard deviation of the residuals in the linear models,
- *S* - the sample's surface.

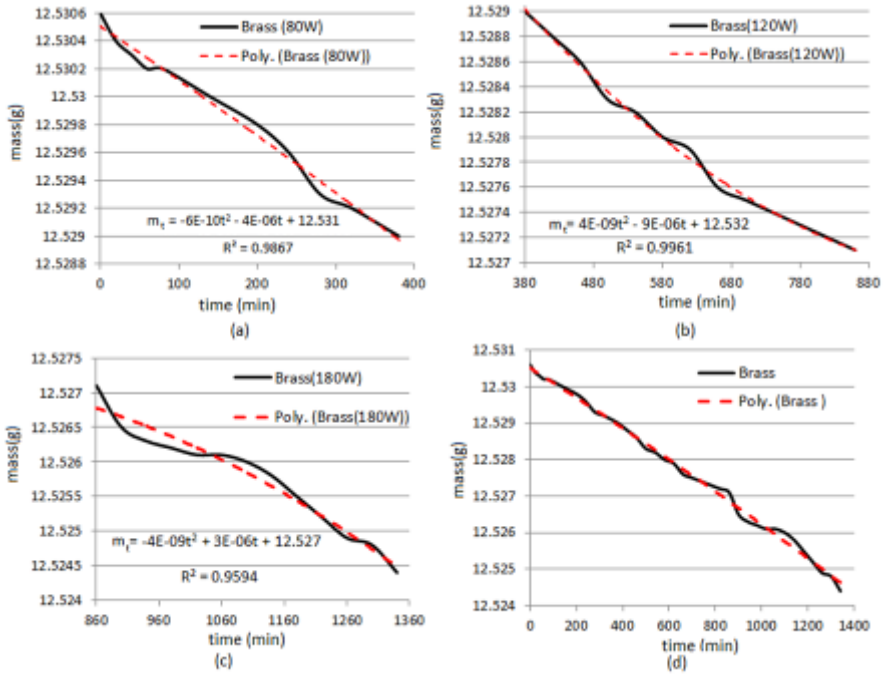

Fig. 3. *The brass mass variation: (a) at 80 W, (b) at 120 W, (c) at 180 W, (d) during the entire experiment. The continuous line represents the recorded data and the dotted ones the fitted trend*

THE ANNALS OF "DUNAREA DE JOS" UNIVERSITY OF GALATI
FASCICLE IX. METALLURGY AND MATERIALS SCIENCE
Nº. 4 - 2021, ISSN 2668-4748; e-ISSN 2668-4756
Article DOI: https://doi.org/10.35219/mms.2021.4.03

Figures 3 (a)-(c) show the evolution of the sample mass in time and the fitted trends, which are second-degree polynomials. Figure 3 (d) presents the overall evolution of the sample's mass in time. In all cases, R^2 is above 0.95, and the residual standard deviations are lower than 0.0001, emphasizing a good data fit.

The evolution of the absolute mass loss per surface at all the power stages is represented in Fig. 4, where the vertical lines delimitate the stages (I-80 W, II-120 W, III-180 W).

The Kruskal - Wallis did not reject the null hypotheses therefore, we built the RBF network. Two-third of the data has been used for training, and for the test, the last third. The parameters found after running the algorithm are:

- Number of neurons = 4
- Minimum radius = 0.01
- Maximum radius = 5.88084
- Minimum Lambda = 0.83554
- Maximum Lambda = 5.66617
- Regularization Lambda for final weights = 2.4643e-003 after 7 iterations.

The goodness of fit indicators is presented in Table 1, showing an excellent fit of the data series. The chart of actual versus predicted values confirms this assertion (Fig. 5).

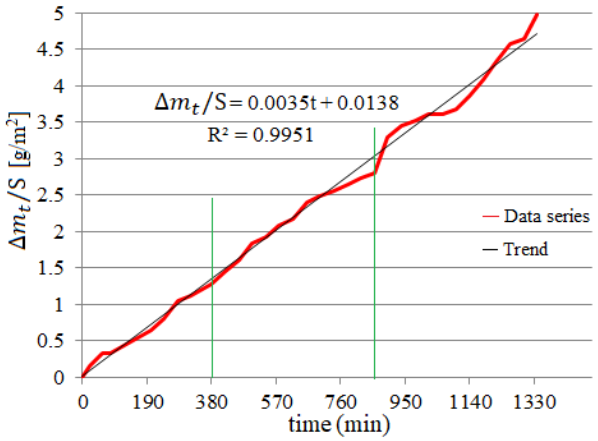

Fig. 4. *The absolute mass variation per surface. The vertical lines delimitate the stages (I-80 W, II-120 W, III-180 W)*

Table 1. *Goodness of fit indicators*

	Training	Test
R^2(%)	99.463	94.898
MSE	0.0047	0.0125
MAE	0.0582	0.0943
MAPE	9.1388	2.3057
r_{ap}	0.9973	0.9799

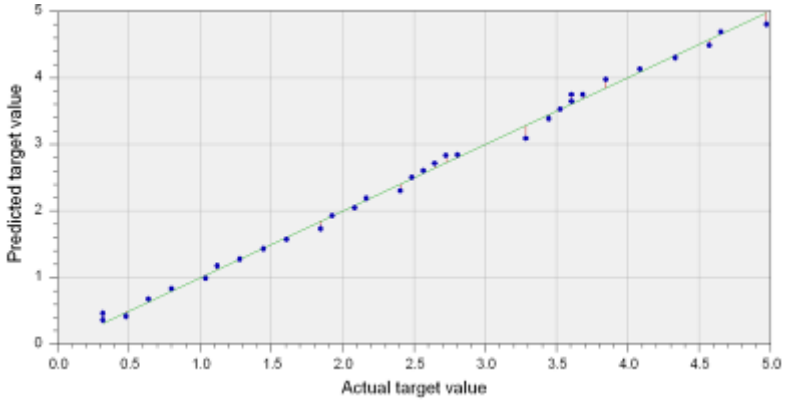

Fig. 5. *The predicted values versus the actual target values*

THE ANNALS OF "DUNAREA DE JOS" UNIVERSITY OF GALATI
FASCICLE IX. METALLURGY AND MATERIALS SCIENCE
No. 4 - 2021, ISSN 2668-4748; e-ISSN 2668-4756
Article DOI: https://doi.org/10.35219/mms.2021.4.03

4. Conclusion

This article presented the results of mass loss of a brass in ultrasound cavitation field in seawater. The main result is modeling the mass variation per surface in time. The estimation of the RBF model built has been done using five indicators. On both training and test set, R^2, and r_{ap} are very close to 1, showing a good fit of the initial series. MSE and MAPE are smaller on the training set, meaning that the algorithm performs the best on this set. Point of view of MAPE, the best performance is that obtained on the test set.

Overall, the model describes very well the process evolution.

References

[1]. Flynn H. G., *Physics of acoustic cavitation in liquids*, Physical Acoustics, vol. 1, Part B, W. P. Mason, Ed. New York: Academic Press, p. 57-172, 1964.
[2]. Young F. E., *Cavitation*, Mac Graw-Hill, Maidenhead, UK, New York, 1989.
[3]. Rooney J. A., *Ultrasound: its Chemical, Physical and Biological Effects*, Suslick, VCH, New York, USA 1988.
[4]. Bai L., Yan J., Zeng Z., Ma Y., *Cavitation in thin liquid layer: A review*, Ultrason. Sonochem., vol. 66, 105092, 2020.
[5]. Bărbulescu A., Marza V., Dumitriu C. S., *Patent no RO 123086-B1 (30.09.2010) Installation and method for measuring and determining the effects produced by cavitation in ultrasound field in stationary and circulating media*, 2010.
[6]. Bărbulescu A., *Models of the voltage induced by cavitation in hydrocarbons*, Acta Phys. Pol. B, vol. 37 (10), p. 2919-2931, 2006.
[7]. Bărbulescu A., Dumitriu C. S., *Mathematical aspects of the study of the cavitation in liquids*, Mathematical Modelling of Environmental and Life Sciences, S. Ion, G. Marinoschi and C. Popa, Eds. București: Editura Academiei Române, p. 7-14, 2006.
[8]. Basumatary J., Nie M., Wood J. K., *The synergistic effects of cavitation erosion-corrosion in ship propeller materials*, J. Bio-Tribo-corros., 1, p. 1-12, 2015.
[9]. Petkovsek M., Dular M., *Simultaneous observation of cavitation structures and cavitation erosion*, Wear, vol. 300, p. 55-64, 2013.
[10]. Wharton J. A., Stokes K. R., *The influence of nickel-aluminium bronze microstructure and crevice solution on the initiation of crevice corrosion*, Electrochim. Acta, 53 (5), p. 2463-2473, 2008.
[11]. Schüssler A., Exner H. E., *The corrosion of nickel-aluminium bronzes in seawater-I. Protective layer formation and the passivation mechanism*, Corros. Sci., 3 (11), p. 1793-1802, 1993.
[12]. Fortes-Patella R., Choffat T., Reboud J. L., Archer A., *Mass loss simulation in cavitation erosion: fatigue criterion approach*, Wear, vol. 300, p. 205-215, 2013.
[13]. Bărbulescu A., Dumitriu C. S., *Models of the mass loss of some copper alloys*, Chem. Bull. Politehnica University (Timișoara), vol. 52 (66), 1-2, p. 120-123, 2007.
[14]. Dumitriu C. S., Bărbulescu A., *Studies about the copper base alloys used in naval constructions – modeling the loss mass in different media*, Sitech, Craiova, 2007.
[15]. Kruskal W. H., Wallis W. A., *Use of ranks in one-criterion variance analysis*, J. Am. Stat. Assoc., vol. 47 (260), p. 583-621, 1952.
[16]. Vandeginste B. G. M., Massart D. L., Buydens L. M. C., De Jong S., Lewi P. J., Smeyers-Verbeke J., *Artificial Neural Networks. Handbook of Chemometrics and Qualimetrics: Part B*, p. 649–699, doi:10.1016/s0922-3487(98)80054-3, 1998.
[17]. Hornik K., Stinchcombe M., White H., *Multilayer feedforward networks are universal approximators. Neural Networ*, vol. 2 (5), p. 359-366, 1989.
[18]. Bărbulescu A., Dani A., *Statistical analysis and classification of the water parameters of Beas River (India)*, Rom. Rep. Phys., vol. 71, no. 4, art.716, 2019.
[19]. Bărbulescu A., Dumitriu C. S., *On the Connection between the GEP Performances and the Time Series Properties*, Mathematics, 9 (16), 1853, 2021.
[20]. Bărbulescu A., Dumitriu C. S., *Artificial intelligence models for financial time series*, Ovidius University Annals, Economic Sciences Series, vol. XXI, Issue 1, p. 685-690, 2021.
[21]. Bărbulescu A., Șerban C., Caramihai S., *Assessing the soil pollution using a genetic algorithm*, Rom. J. Phys., vol. 66 (3-4), 80, 2021.
[22]. Jia W., Zhao Ding D. L., *An optimized RBF neural network algorithm based on partial least squares and genetic algorithm for classification of small sample*, Appl. Soft Comput., vol. 48, p. 373-384, 2016.
[23]. Meng K., Dong Z. Y. Wang D. H., Wong K. P., *A self-adaptive RBF neural network classifier for transformer fault analysis*, IEEE Trans. Power Syst., vol. 25 (3), p. 1350-1360, 2010.
[24]. Sheta A. F., De Jong K., *Time-series forecasting using GA-tuned radial basis functions*, Inform. Sci., vol. 133 (3), p. 221-228, 2001.
[25]. Al-Mahasneh A. J., Anavatti S., Garratt M., Pratama M., *Applications of General Regression Neural Networks*, Dynamic Systems, Digital Systems, Asadpour, V. Ed., IntechOpen, DOI: 10.5772/intechopen.80258, 2018.
[26]. Faris H., Aljarah I., Mirjalili S., *Evolving Radial Basis Function Networks using moth-flame optimizer*, Handbook of Neural Computation, p. 537-550, 2017.
[27]. Chen S., Hong X., Harris C. J., *Orthogonal Forward Selection for Constructing the Radial Basis Function Network with Tunable Nodes*, Available at: https://eprints.soton.ac.uk/261028/1/36440777.pdf, 2005.
[28]. Orr M. J. L., *Optimizing the widths of radial basis functions*, Proceedings of the 5th Brazilian Symposium on Neural Networks (Cat. No.98EX209), p. 26-29, doi: 10.1109/SBRN. 1998.730989, 1998.
[29]. Park J., Sandberg I. W., *Universal approximation using radial basis function networks*, Neural Comput., vol.3, p. 246-257, 1991.
[30]. Moody J., Darken C. J., *Fast learning in networks of locally-tuned processing units*, Neural Comput., vol. 1, p. 281-294, 1989.

THE ANNALS OF "DUNAREA DE JOS" UNIVERSITY OF GALATI
FASCICLE IX. METALLURGY AND MATERIALS SCIENCE
Nº. 4 - 2021, ISSN 2668-4748; e-ISSN 2668-4756
Article DOI: https://doi.org/10.35219/mms.2021.4.04

RESEARCH ON SOME FRESHWATER FISH CATALASE ACTIVITY - AS A POTENTIAL BIOMARKER FOR ENVIRONMENTAL POLLUTION

Romică CREȚU
"Dunarea de Jos" University of Galati, Romania
e-mail: romica.cretu@ugal.ro

ABSTRACT

In the last decade studies show that water pollution is a very serious problem, especially since the degree of water pollution plays a key role in the growth and fish multiplication. As a biomarker of environmental pollution, antioxidant enzymes such as catalase (CAT; EC 1.11.1.6) play an essential role in preventing the harmful effects of heavy metals in the tissues of fish. These researches were carried out to investigate the effect of various environment conditions and some pollutant agents on oxidative stress in some aquatic organisms. The enzymatic assay of CAT (in fish organs, e.g., liver, kidney, gill, intestine and brain, as well as in mixture of these organs) was carried out according to standard enzyme assay protocol.

The results showed decrease of CAT activity: the enzymatic activity was 35.89 ± 1.02 µmol H_2O_2/min/mg protein to pH 7 and 6.59 ± 0.47 µmol H_2O_2/min/mg protein to pH 12. More, the enzymatic activity was 38.1 ± 0.3 µmol H_2O_2/min/mg protein to pH 3. Also, the catalase activity increased with 23 enzymatic units to a less dissolved oxygen concentration (6.2877 mg/L).

Furthermore, this study indicated that heavy metals, such as Cr, Cu and Zn can inhibit biochemical reactions in various organs of fish. During exposure duration of the fish to a mixture of metal ions the catalase activity decreases from 35.89 ± 1.02 µmol H_2O_2/min/mg protein to 23.51 ± 2.85 µmol H_2O_2/min/mg protein. On the other hand, as a result of the response of the enzyme system, the catalase activity increases to 36.25 ± 3.22 µmol H_2O_2/min/mg protein.

KEYWORDS: metallurgy, heavy metals mixture, freshwater fish organs, catalase activity, dissolved oxygen

1. Introduction

In the last years, the aquatic organisms are exposed to significant amounts of pollutants from industrial technological processes in various fields and agriculture, another factor being the anthropogenic activities [1-6]. Many of the industrial activities and many of the industrial products serve as sources of heavy metals [7].

In this context, both surface water and groundwater can be contaminated with heavy metals such as Cu, Zn and Cr. The accumulation of Cu in river water, for example, is largely the result of the metallurgical industry's impact on environmental pollution [8].

Since two decades ago Rashed [9] shows that heavy metals such as cadmium and lead present in the tissues of some fish, e.g. *Tilapia*, can be used as indicators to identify water pollution. Tilapia fish is currently very studied, on the one hand the high growth and on the other hand, adaptability to a wide range of environmental conditions. It also shows a great capacity for growth and breeding [10].

Heavy metals even though play an important role in metabolic processes they may inhibit biochemical reactions when is an increase in their concentration [11].

Moreover, specialized studies [12] showed that the most common heavy metals found in the fish body (cadmium, lead, mercury, zinc, copper, nickel, cobalt, molybdenum, chromium, and tin) may be aquatic pollutants, some of them (cadmium, mercury and lead) even at very low concentrations, through the accumulation in tissues. According to the same study, the fish absorb heavy metals through gills and digestive tract and, in a small measure, through the skin.

THE ANNALS OF "DUNAREA DE JOS" UNIVERSITY OF GALATI
FASCICLE IX. METALLURGY AND MATERIALS SCIENCE
N°. 4 - 2021, ISSN 2668-4748; e-ISSN 2668-4756
Article DOI: https://doi.org/10.35219/mms.2021.4.04

In this context, previous studies [13] demonstrate that antioxidant enzymes such as catalase (CAT) play an essential role in preventing the harmful effects of heavy metals in the tissues of fish. CAT (Figure 1) is an enzyme found in a wide range of plants and animals, but also in aerobic and anaerobic microorganisms.

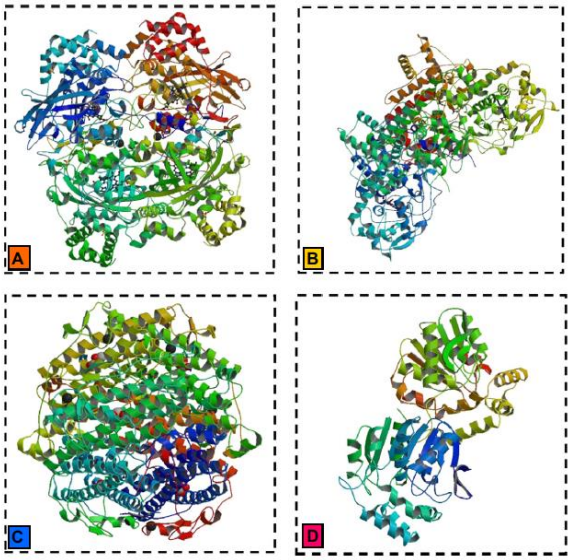

Fig. 1. *Different types of catalase: typical catalase (A), atypical catalase (B), Pseudocatalases (C) and Chloroperoxidase (D). All the figures have been reproduced after* [14]

Atli *et al.* [15] show that this enzyme can be used to determine enzyme activity as identifying indicator for aquatic environment pollution. On the other hand, studies on the internal organs of fish *Oreochromis niloticus*, such as the liver, kidneys, gills, intestines, and brain, the CAT activity showed response to the action of heavy metals depends on the tissue, metals and their concentration. However, there is no information's about completely activity changes. Furthermore, although in the scientific literature exist studies about the impact of heavy metals on enzyme activity in various organs of fish [16-19] the best of our knowledge there is no article about cumulative and induced enzymatic activity changes for all fish organs.

So, this study shows the results of various environment conditions effect and some pollutant agents on oxidative stress in *Oreochromis niloticus* fish. Another specific objective of this study is to compare the heavy metals cumulative impact on CAT activity changes in the case of some organs and organs mixture of the *Oreochromis niloticus* fish.

2. Materials and methods

Experimental protocol was realized according to Atli *et al.* [15] with some modifications. The *Oreochromis niloticus* fish were obtained from the Department of Food Science, Food Engineering, Biotechnology and Aquaculture of "Dunarea de Jos" University of Galati. These were transferred in safety conditions to the laboratory in a glass aquarium with four compartments containing water for contaminated test solution or controls (25 × 25 × 40 cm each), where they were acclimatized to 20 °C ± 1 °C.

The aquarium was aerated with air pump so that the dissolved oxygen concentration was 7.033 ± 0.16 mg O_2/L. The dissolved oxygen was daily measured with Hannah HI 98186 oximeter and pH was determined by electrical method involving the use of a pH-meter (HI 255 Combined Meter pH/mV and EC/TDS/NaCl LV2, HANNA equipped with pH electrode (HI1131B), EC probe (HI 76310) and temperature probe (HI 7662).

The dechlorinated water used in this study for control had a pH value of 7.47 ± 0.16 and conductivity of 602.4 ± 5.6 µS/cm. During experiments the laboratory was illuminated using as a light source a fluorescent lamp (daylight 65/80 W).

Fish were exposed to a mixture of different concentrations of heavy metals for some individual organs such as the liver, kidney, gills, intestines and brain (Cu, 0.2 to 1 mg/L, Zn from 0.2 to 1 mg/L, and Cr from 0.8 to 1.5 mg/L) for 96 hours. For this purpose, $CuCl_2 \cdot 2H_2O$, $K_2Cr_2O_7$ and $ZnCl_2$ salts (Sigma or Merck AG, Germany) were used as metal sources.

All fish were euthanized after they were placed in the freezer [20], anesthetized with 2-phenoxyethanol and by transaction of the spinal cord according to Atli and Canli [18] at the end of the exposure period. To extract the catalase, an amount of 0.5 g of fish tissue is homogenized with quartz sand and 5 mL of a 100 mM solution of disodium phosphate. After 30 minutes conventional extraction and 10 minutes ultrasound extraction (water bath, 35 kHz) the homogenate was centrifuged at 10,000 g (Hettich Universal) for 15 min (+4 °C). Separate supernatant was served as a source of catalase. The method for enzyme activity evaluation is based on the fact that catalase is allowed to act on the hydrogen peroxide for a fixed period of time. Then the catalase is inactivated by the addition of a mixture of high purity potassium dichromate - glacial acetic acid.

The amount of hydrogen peroxide decomposing remained after stopping the action of catalase, reduces in acidic medium the potassium dichromate to chromic acetate, which can be determined by spectrophotometry. The CAT activity was measured at 570 nm. Because $K_2Cr_2O_7$ does not absorb at this

THE ANNALS OF "DUNAREA DE JOS" UNIVERSITY OF GALATI
FASCICLE IX. METALLURGY AND MATERIALS SCIENCE
Nº. 4 - 2021, ISSN 2668-4748; e-ISSN 2668-4756
Article DOI: https://doi.org/10.35219/mms.2021.4.04

wavelength, his presence in the reaction medium does not interfere with the chromic acetate spectrophotometric determination.

The total protein concentration from supernatants of fish tissue was determined according to the method of Lowry *et al.* [21] with bovine serum albumin (BSA) as standard.

There was no significant difference in weight (19.157 ± 3.77 g) between the fish under study, both for control samples and in that of fish exposed to experimental conditions.

Statistical Analysis of data was carried out using SPSS for Windows (standard version 10) statistical package software. The experiment was performed in triplicate.

3. Results and discussion

Although it is difficult to collect samples for several internal organs of fish *Oreochromis niloticus*, the obtained results in this paper suggest that catalase activity measurement can provide important information about environmental pollution. At the same time, measurement of catalase activity can be an alternative to the physico-chemical methods for the detection of pollutants.

The present research shows that under the action of important factors such as pH and heavy metals, there are changes in CAT activity in all the studied organs. The results of this study are mostly comparable to those that were elaborated by Atli *et al.* [15] who conducted comparative studies on various internal organs.

3.1. Studies on the dissolved oxygen concentration

One of the first objectives was to establish the relationship between the dissolved oxygen content in aquarium water and enzymatic activity during the monitoring of fish activity.

In this case, Figure 2 shows that the low dissolved oxygen exerts severe pressure on catalase activity. Enzymatic activity increases in general as a result of the stress to which the fish are subjected under these experimental conditions.

As can be seen from the analysis of data shown in Figure 2 the catalase activity increased with 23 enzymatic units (EU) approximately (from 47.1899 to 70.0821 µmol H_2O_2/min/mg protein) to a less dissolved oxygen concentration (6.287 mg/L) compared to a higher dissolved oxygen (10.898 mg/L). This increase is justified by the fact that probably the fish has made an extra effort in an environment with less oxygen. At the same time, catalase activity remains almost constant when dissolved oxygen has values: 7.033, 9.417 and 10.898 (mg/L) respectively. For maintaining normal behavior of aquarium fish studies and optimal conditions for development and breeding research conducted, it preferred to adjust the air flow rate to maintain dissolved oxygen around 7 mg/L (7.033 mg O_2/L).

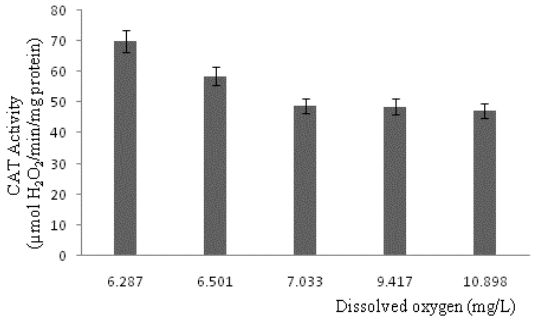

Fig. 2. *Catalase activity of* Oreochromis niloticus *depending on the dissolved oxygen. Vertical bars represent standard deviation of the mean (n = 3)*

3.2. Analysis of the pH effect

Initially, pH was ranged from 7 (control) to 12. According to experimental observations, at extreme pH (pH = 12), immediately after exposure, the fish activity was relatively low. Also, the gills have become black. Thus, the exposure of the *Oreochromis niloticus* fish at a highly basic environment for about 1 hour leads to inhibition of catalase activity (Figure 3). Experimental results show that after exposure in a strongly basic environment, internal organs of the *Oreochromis niloticus* tracked in the study are soft, indistinguishable and pungent odor (the results are not shown). These results suggest the high sensitivity of this antioxidant enzyme exposure in highly alkaline conditions. Moreover, the initial pH was varied to pH 3 (Figure 3). No case of mortality was found in this exposure. In the first hours of exposure, no visible differences in the appearance of the fish were observed. Instead, his behavior was completely changed: his activity was completely reduced and his appetite was low. After 24 hours, there was a slight activity, the appetite being just as low. After exposing the fish to acidic medium for 96 h, the appearance of the fish changed, having a much lighter colour than the initial one. Also, as in the case of exposure of fish in conditions of extreme basic pH (pH = 12), their dissection was difficult, their skin becoming very hard. The internal organs have visibly changed, being soft, difficult to differentiate and with a bad smell (the results are not shown).

THE ANNALS OF "DUNAREA DE JOS" UNIVERSITY OF GALATI
FASCICLE IX. METALLURGY AND MATERIALS SCIENCE
No. 4 - 2021, ISSN 2668-4748; e-ISSN 2668-4756
Article DOI: https://doi.org/10.35219/mms.2021.4.04

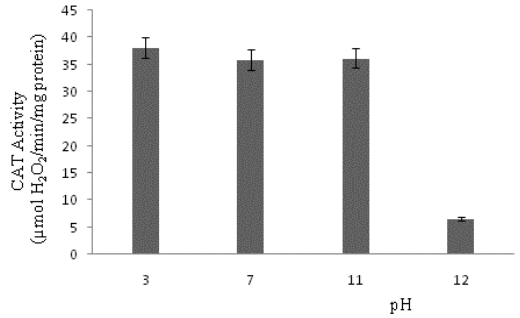

Fig. 3. *The effects of pH on CAT activity in some organ's mixture (liver, kidney, gill, intestine and brain) of* Oreochromis niloticus. *The pH values correspond to inflection points*

Figure 3 show that the enzymatic activity, evaluated in the case of a mixture of internal organs of the studied fish, is influenced by pH variation.

In this context, there are variations in catalase activity corresponding to the inflection points of the pH values: 38.1 ± 0.3 µmol H_2O_2/min/mg protein (pH = 3), 35.89 ± 1.02 µmol H_2O_2/min/mg protein (pH = 7), 36.14 ± 0.29 µmol H_2O_2/min/mg protein (pH = 11) and 6.59 ± 0.47 µmol H_2O_2/min/mg protein (pH = 12).

According to the results shown in Figure 3, regarding the evolution of enzymatic activity under the impact of sub-lethal (pH = 11) and lethal (pH = 12) pH, the alarming decrease in catalase activity by approximately 82% suggests severe enzyme inhibition.

Also, these results indicate a decrease with 6% in terms of catalase inactivation under extreme conditions, at pH = 2. In this case the enzymatic activity was 35.82 ± 0.53 µmol H_2O_2/min/mg protein (the results are not show in Figure 3). However, this situation corresponds to the death condition, according to the obtained results. Consequently, *Oreochromis niloticus* fish have a much better resistance in an acidic environment compared to a basic one. Because the fish exposed in a basic environment (pH = 11) managed to survive, it can be concluded that *Oreochromis niloticus* fish have a good resistance.

However, it can be considered that the results in terms of catalase activity, on exposure to basic medium, cannot be conclusive, the difference between the enzymatic activities corresponding to the sub-lethal and lethal basic pH being about 30 EU. In contrast, there is a difference of less than 3 EU between the enzymatic activities corresponding to neutral and acidic (not lethal) pH. This suggests that although catalase activity is also slightly inhibited in this unfavourable living environment due to metabolic disturbance, the impact in this case is ten times lower than in the basic environment.

Therefore, in order to prevent the toxic effect associated with the variation of fish habitat, expressed in terms of pH, it can be monitored by determining the enzymatic activity. As a result, more detailed monitoring of this parameter is desirable.

3.3. Effects of some metal ions on the antioxidant enzyme activities of Oreochromis niloticus *intern organs*

Some metals, although toxic at certain concentrations, may act as catalysts in the oxidative reactions of biological macromolecules. Some metals, such as copper and chromium, undergo redox cycles, and others, such as cadmium, deplete antioxidants in cells. Such metals, whose action is pursued in the present study, can cause oxidative stress and therefore lead to dysfunctional abnormalities in various biomolecules such as lipids, proteins and DNA [22].

According to the results of this paper, heavy metals can alter metabolism, activating or inhibiting catalase, and these changes in enzymatic activity can cause metabolic changes and cellular destruction of internal organs. Experimental research has suggested that measuring enzymatic activity may be an effective biomarker of chemical pollution, in line with other recent scientific findings in the literature [23].

The highlighting of the impact produced by some heavy metals on the enzymatic activity followed in this study is presented in Figure 4.

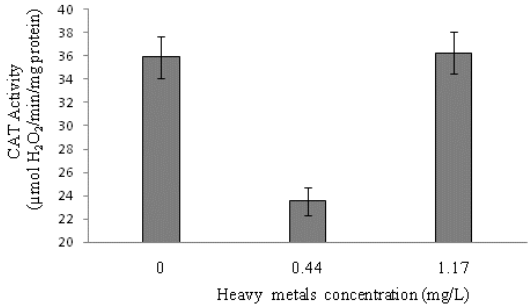

Fig. 4. *CAT activities in the mixture of some organs (intestine, liver, kidney, gill and brain) of* O. niloticus *after* Cu^{2+}, Zn^{2+} *and* Cr^{6+} *mixture (1:1:1) exposures*

Figure 4 shows the results obtained on the exposure of fish to concentrations of heavy metals similar to those reported in the research of other specialized works in which the enzymatic activity is minimal and maximum, respectively [10], but using a mixture of these metals. According to the data in Figure 4, there are visible differences in the case of

THE ANNALS OF "DUNAREA DE JOS" UNIVERSITY OF GALATI
FASCICLE IX. METALLURGY AND MATERIALS SCIENCE
Nº. 4 - 2021, ISSN 2668-4748; e-ISSN 2668-4756
Article DOI: https://doi.org/10.35219/mms.2021.4.04

exposure to the minimum concentration studied (0.44 mg/L), the catalase activity decreasing by approximately 12 EU from 35.89 ± 1.02 µmol H_2O_2/min/mg protein to (control sample value) to 23.51 ± 2.85 µmol H_2O_2/min/mg protein. More so, as a result of the response of the enzyme system, when the concentration of the heavy metal mixture increases, there is an intensification of the enzyme activity with 1% approximately compared to the value of the control sample. Thus, exposure of fish to a mixture of 1.17 mg/L Cu^{2+}, Zn^{2+} and Cr^{6+} has as a result in a slight increase in catalase activity.

The increase in catalase activity after exposure of fish to the studied metal ion mixture from 0.44 mg/L to 1.17 mg/L may be associated with increased oxidative stress [24] due to the presence of heavy metals in aquarium water.

Therefore, CAT inhibition in the presence of the metal ion mixture can be attributed to the direct effect of metal exposure due to the formation of direct bonds of metal ions to the catalase molecule. In this context, finally there is an increase in hydrogen peroxide radicals. Thus, the experimental results of this study on the total impact of heavy metals, at sub-lethal concentrations, on some organs of *Oreochromis niloticus* fish showed that the catalase activity can be used as a biomarker in terms of environmental pollution.

Research has been extended to fish exposed to lethal concentrations (LC) of heavy metals, when the catalase activity is 15.946±5.46 µmol H_2O_2/min/mg protein (Figure 5).

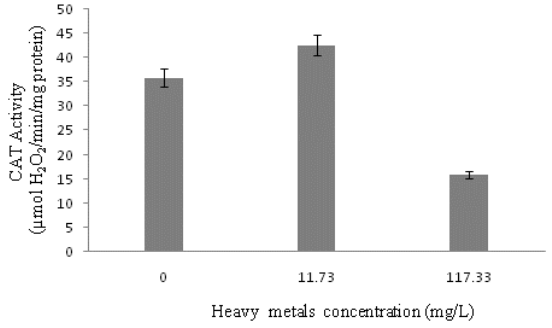

Fig. 5. *CAT activities in some organs mixture (liver, kidney, gill, intestine, and brain) of* Oreochromis niloticus *after higher concentrations of Cu^{2+}, Zn^{2+} and Cr^{6+} mixture exposures (as explained in Figure 4)*

The data presented in Figure 5 highlight the increase in catalase activity of approximately 6.74 EU at exposure to a mixture of heavy metals at a concentration ten times higher than the highest concentration in the initial study, which demonstrates catalase activation under these conditions. However, catalase activity decreased dramatically by approximately 20 EU in case of exposure to a concentration (LC) 100 times higher than the maximum shown in Figure 4, when the death of the fish was ascertained. The concomitant presence of heavy metals Cu, Zn and Cr in water eventually leads to a decrease in the activity of antioxidant enzymes, such as catalase, due to its inhibitory effect on it. Therefore, a significant decrease in the enzymatic activity of catalase in *Oreochromis niloticus* is an indicator of short-, medium- and long-term environmental pollution.

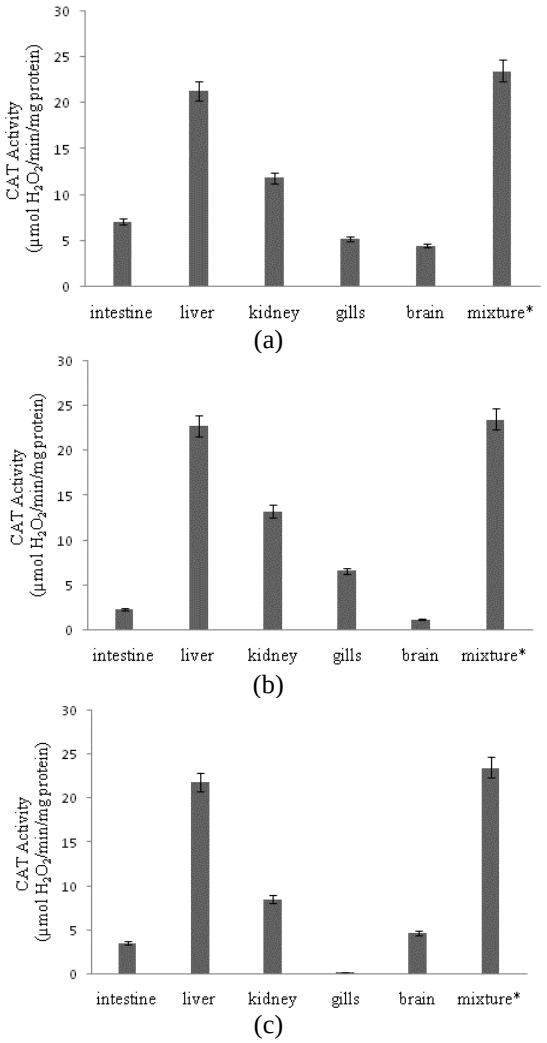

Fig. 6. *Comparative evaluation of the CAT activity in some organs and their mixtures (see Figures 4 and 5 for details) of* Oreochromis niloticus *after lower concentrations (0.44 mg/L) of Cu^{2+} (a), Zn^{2+} (b) and Cr^{6+} (c) exposures*
**organs mixture to the lower sub-lethal concentrations of the heavy metals*

THE ANNALS OF "DUNAREA DE JOS" UNIVERSITY OF GALATI
FASCICLE IX. METALLURGY AND MATERIALS SCIENCE
Nº. 4 - 2021, ISSN 2668-4748; e-ISSN 2668-4756
Article DOI: https://doi.org/10.35219/mms.2021.4.04

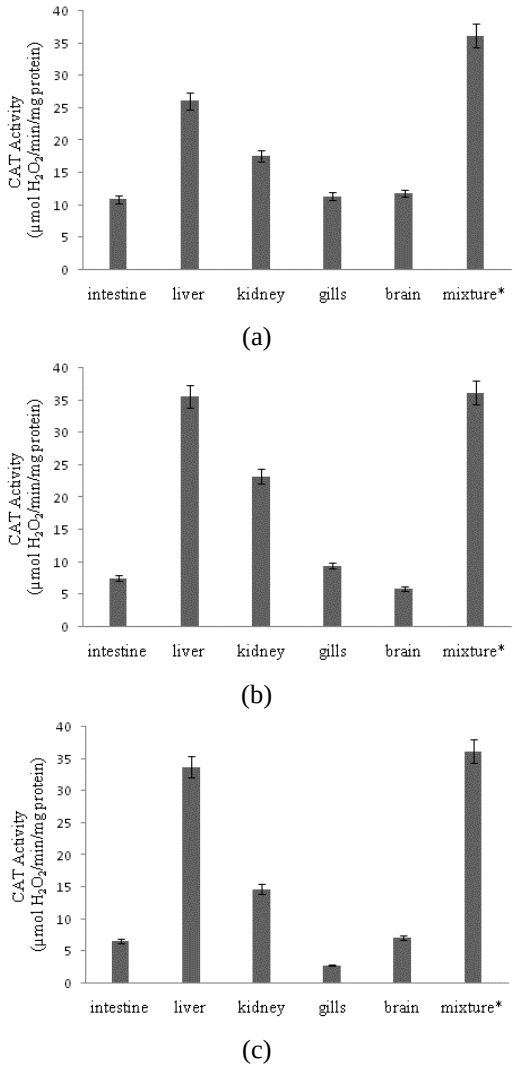

Fig. 7. *Comparative evaluation of the CAT activities in some organs and their mixtures (see Figures 4 and 5 for details) of* Oreochromis niloticus *after the highest concentrations (mean of the concentrations: 11.73 mg/L) of Cu^{2+} (a), Zn^{2+} (b) and Cr^{6+} (c) exposures.*
**organs mixture to the highest sub-lethal concentrations of the heavy metals*

Results regarding the effect of some heavy metals (Cu^{2+}, Zn^{2+} and Cr^{6+}) on some organs of *Oreochromis niloticus* fish, compared to the cumulative effect of these metals on the mixtures of some organs (intestines, liver, kidney, gill and brain) are reported in Figures 6 and 7. The research was performed using some concentrations, considered inflection points in the variation of the enzymatic response.

As shown in Figure 7 the differences are often remarkable. The enzymatic response to the action of the pollutant depends primarily on its type and concentration, but also on the type of organ affected. It seems that the contribution of the liver is the largest of all the organs studied to the response of the enzymatic system of the *Oreochromis niloticus* fish organism to the cumulative action of heavy metals.

This variation in the impact of heavy metals on the internal organs of *Oreochromis niloticus* fish, for example, brain, kidneys, gills and intestines, shown in Figure 7, indicates a more aggressive action and, consequently, a more negative impact on fish when in water are present simultaneously some heavy metals, such as Cu, Zn and Cr.

Moreover, the correlation coefficients between the CAT activity values for all types of organs studied (Table 1) showed that there are significant correlations between certain organs depending on the concentration of heavy metals to which they are exposed.

These results suggest that the study of the cumulative action of heavy metals on *Oreochromis niloticus* fish by using advanced methods of statistical analysis of enzymatic activity is effective and allows the optimal evaluation of their response to the action of heavy metals.

As shown in Table 1 in the cases of catalase activity in kidney (CAT-K) and catalase activity in gill (CAT-G) the relationships were significant between these parameters depending on the concentration of heavy metals. Furthermore, CAT-G values correlated positively with catalase activity in intestine (CAT-I) only when the concentration of heavy metals increases significantly. Also, the data in Table 1 suggests that CAT-I showed there were significant positive correlations with catalase activity in gill (CAT-G) and catalase activity in brain (CAT-B), but also significant negative correlations with catalase activity in liver (CAT-L). Furthermore, significant negative correlations and moderate positive correlations between CAT-L and CAT-B were determined in the case of both concentrations of heavy metals analysed.

THE ANNALS OF "DUNAREA DE JOS" UNIVERSITY OF GALATI
FASCICLE IX. METALLURGY AND MATERIALS SCIENCE
Nº. 4 - 2021, ISSN 2668-4748; e-ISSN 2668-4756
Article DOI: https://doi.org/10.35219/mms.2021.4.04

Table 1. *Pearson linear correlation coefficients between the values of CAT in the case of the heavy metals (Cu^{2+}, Zn^{2+} and Cr^{6+}) mixture* [a, b]

	CAT-I	CAT-L	CAT-K	CAT-G	CAT-B
[a] lower concentration (0.44 mg/L)					
CAT-I	1.000				
CAT-L	-0.891	1.000			
CAT-K	-0.016	0.468	1.000		
CAT-G	0.068	0.392	0.997	1.000	
CAT-B	0.649	-0.924	-0.771	-0.715	1.000
[b] highest concentrations (11.73 mg/L)					
CAT-I	1.000				
CAT-L	-0.920	1.000			
CAT-K	0.023	0.371	1.000		
CAT-G	0.813	-0.520	0.600	1.000	
CAT-B	0.920	-0.998	-0.371	0.520	1.000

Abbreviations: CAT-I, catalase activity in intestine; CAT-L, catalase activity in liver; CAT-K, catalase activity in kidney; CAT-G, catalase activity in gill; CAT-B, catalase activity in brain. Marked correlations are significant at $p < 0.05$

4. Conclusions and future perspectives

These results indicate that catalase activity plays an important role in the body's defense against oxidative stress induced by extreme variations of the air flow, pH and concentration of heavy metals.

Accumulation of heavy metals in fish from contaminated water is an important aspect in terms of environmental awareness, this action leading to damage to all products from the food chain of fish, including fish. This study emphasized that the catalase is very sensitive to the action of some metals e.g., Cu, Zn, Cr on the all-intern organs of the fish when these heavy metals concentration exceeds some limits. Also, low and especially high pH values exposure strong affects CAT activity. The duration of the exposure time also plays an important role.

Given the fact that aquatic organisms are very sensitive to metal exposure, I had the opportunity to highlight as much information related to oxidative stress induction and other adverse effects of pollution. According to obtained experimental results, when heavy metals are present concurrently, the effect on the internal organs of the fish indicates a negative impact and therefore more aggressive action.

Although this study made reference to cumulative catalase activity changes induced in fish organs (liver, kidney, gills, intestines and brain) of *Oreochromis niloticus* species by exposing them to the variation of two of the most important water physical-chemical parameters, future research consists in a study on the impact of heavy metals on the specific enzymatic activity of various organs on other categories of fish.

The results obtained in this paper can contribute to the establishment of a database for monitoring the impact of pollutants on the environment through biochemical analyses.

Acknowledgements

I would like to thank the Department of Food Science, Food Engineering, Biotechnology and Aquaculture of "Dunarea de Jos" University of Galati for providing necessary *Oreochromis niloticus* fish.

References

[1]. Demirak A., Yilmaz F., Tuna L. A., Ozdemir N., *Heavy metals in water, sediment and tissues of Leuciscus cephalus from a stream in southwestern Turkey*, Chemosphere, 63, p. 1451-8, 2006.

[2]. Ivanciuc T., Ivanciuc O., Klein D. J., *Modelling the bioconcentration factors and bioaccumulation factors of polychlorinated byphenils with posetic quantitative super-structure/activity relationships (QSSAR)*, Mol Divers, 10, p. 133-45, 2006.

[3]. Agah H., Leemakers M., Elskens M., Fatemi S. M. R., Baeyens W., *Accumulation of trace metals in the muscles and liver tissues of five fish species from the Persian Gulf*, Environ Monit Assess, 157, p. 499-514, 2009.

[4]. Uysal K., Köse E., Bülbül M., Dönmez M., Erdogan Y., Koyun M., *The comparison of heavy metal accumulation ratios of some fish species in Enne Dame Lake (Kütahya/Turkey)*, Environ Monit Assess, 157, p. 355-362, 2009.

[5]. Bereswill R., Streloke M., Schulz R., *Current-use pesticides in stream water and suspended particles following runoff: exposure, effects, and mitigation requirements*, Environ Toxicol Chem, 32 (6), p. 1254-1263, 2013.

[6]. Jinling L., Xiangrong X., Shen Y., Hefa C., Yiguo H., Xinbin F., *Mercury pollutionin fish from South China Sea: Levels, species-specific accumulation, and possible sources*, Environmental Research, 131, p. 160-164, 2014.

[7]. Demaku S., Jusufi K., Kastrati G., *Contamination of Environment with the Heavy Metals Emitted from a Cement*

Factory, Kosovo, Journal of Ecological Engineering, 21 (8), p. 75-83, 2020.

[8]. Kumari S., Mishra A., *Heavy Metal Contamination*, In: Marcelo L. Larramendy, Sonia Soloneski (Eds.), Soil Contamination - Threats and Sustainable Solutions, https://doi.org/10.5772/intechopen.93412, 2021.

[9]. Rashed M. N., *Cadmium and Lead levels in fish (*Tilapia nilotica*) tissues as biological indicator for lake water pollution*, Environmental Monitoring and Assessment, 68, p. 75-89, 2001.

[10]. Zvavahera C., Hamandishe V., Saidi P., Imbayarwo-Chikosi V., Nhiwatiwa T., *Growth Performance, Survival and Breeding of* Oreochromis Niloticus *and* Oreochromis Macrochir *Reared Under Greenhouse Conditions*, Aquatic Research, 1 (1), p. 1-11., 2018.

[11]. Kojadinovic J., Potier M., Le Corre M., Cosson R. P., Bustamante P., *Bioaccumulation of trace elements in pelagic fish from the Western Indian Ocean*, Environ Pollut., 146, p. 548-66, 2007.

[12]. Sfakianakis D. G., Koumoundouros G., Divanach P., Kentouri M., *Osteological development of the vertebral column and of the fins in* Pagellus erythrinus, 1758, 2004.

[13]. Gül S., Belge-Kurutaş E., Yildiz E., Sahan A., Doran F., *Pollution correlated modifications of liver antioxidant systems and histopathology of fish (*Cyprinidae*) living in Seyhan Dam Lake, Turkey*, Environment international, 30 (5), p. 605-609, 2004.

[14]. Balwinder S., Baljinder S. K., Munish P., *Recent insights into microbial catalases: Isolation, production and purification*, Biotechnology Advances, 32, p. 1429-1447, 2014.

[15]. Atli G., Alptekin O., Tukel S., Canli M., *Response of catalase activity to* Ag^{+}, Cd^{2+}, Cr^{6+}, Cu^{2+} *and* Zn^{2+} *in five tissues of fresh water fish* Oreochromis niloticus, Comp. Biochem. Physiol, 143, p. 218-224, 2006.

[16]. Canli M., Atli G., *The relationships between heavy metal (Cd, Cr, Cu, Fe, Pb, Zn) levels and the size of six Mediterranean fish species*, Environ Pollut, 121, p. 129-136, 2003.

[17]. Birungi Z., Masola B., Zaranyika M. F., Naigaga I., Marshall B., *Active biomonitoring of trace heavy metals using fish (*Oreochromis niloticus*) as bioindicator species. The case of Nakivubo wetland along Lake Victoria*, Physics and Chemistry of the Earth, 32, p. 1350-1358, 2007.

[18]. Atli G., Canli M., *Response of antioxidant system of freshwater fish* Oreochromis niloticus *to acute and chronic metal (Cd, Cu, Cr, Zn, Fe) exposures*, Ecotoxicology and environmental safety, 73 (8), p. 1884-1889, 2010.

[19]. Abdel-Baki A. S., Dkhil M. A., Al-Quraishy S., *Bioaccumulation of some heavy metals in tilapia fish relevant to their concentration in water and sediment of Wadi Hanifah*, Saudi Arabia. Afr. J. Biotechnol., 10, p. 2541-2547, 2011.

[20]. Aladesanmi O. T., Agboola F. K., Okonji R. E., *Enzymes as Biomarkers of Environmental Stress in African Catfish (*Clarias gariepinus*) in Osun State*, Nigeria. Journal of health and pollution, 7 (14), p. 71-83, 2017.

[21]. Lowry O. H., Rosebrough N. J., Farr A. L., Randall R. J., *Protein measurement with the Folin phenol reagent*, The Journal of biological chemistry, 193 (1), p. 265-275, 1951.

[22]. Pinto E., Sigaud-Kutner T. C. S., Leitao M. A. S., Okamoto O. K., Morse D., Colepicolo P., *Heavy metal-induced oxidative stress in algae*, J. Phycol., 39, p. 1008-1018, 2003.

[23]. Olena Yu. V., Olga I. K., Kenneth B. S., Volodymyr I. L., *Catalase activity as a potential vital biomarker of fish intoxication by the herbicide aminotriazole*, Pesticide Biochemistry and Physiology, 101, p. 1-5, 2011.

[24]. Ercal N., Gurer-Orhan H., Aykin-Burns N., *Toxic metals and oxidative stress part I: mechanisms involved in induced oxidative damage*, Curr. Top. Med. Chem., 1, p. 529-539, 2001.

THE ANNALS OF "DUNAREA DE JOS" UNIVERSITY OF GALATI
FASCICLE IX. METALLURGY AND MATERIALS SCIENCE
Nº. 4 - 2021, ISSN 2668-4748; e-ISSN 2668-4756
Article DOI: https://doi.org/10.35219/mms.2021.4.05

CURRENT CHALLENGES AND PROSPECTIVE BENEFITS OF USING UAVs

Carmelia Mariana DRAGOMIR BĂLĂNICĂ, Adrian LEOPA
"Dunarea de Jos" University of Galati, Romania
e-mail: cdragomir@ugal.ro

ABSTRACT

The modern economy completely changed by offering to industry groups the capability to reorganize their operating processes. Nowadays we become observers of similar in scale revolutionary transformations: technologies for the use of unmanned aerial vehicles substantially modified business models and new operating conditions have been developed in various sectors from industries, agriculture to the emergency, parcel delivery or movie industry. In the very near future, clients' enterprises from multiple sectors of the economy will recognize the first effect of the use of unmanned aerial vehicles (UAVs) in diverse fields - from commercial sectors to examining and exploring the environment or to reduce the impacts of unexpected disasters. The aim of the present review paper is to analyse the opportunities and advantages of using the application of UAVs technologies. On the other hand, not only the devices (drones) themselves are of importance, but also their wider utilization to acquire extraordinary volumes of data.

KEYWORDS: UAV; unmanned aerial vehicle; data acquisition

1. Introduction

Presently the progress of small UAVs is of great interest of numerous researchers trying to identify the indefinite application sectors. Starting with 1980s in Japan were used unmanned aerial vehicles in the treatment of rice fields with pesticides. Progress continued, new technologies were perfected, the legislative and administrative framework developed and funds were allocated [1]. Numerous stakeholders and companies, including governmental administration, commercial entrepreneurs, scientific establishments, take the advantages of UAVs as an inexpensive data acquisition instrument: facilitating the cartography at temporal and spatial scales in clearly superior conditions than using the conventional remote sensing bases [2].

The variety of utilization starting from multiple civil requests, involving high-accuracy terrestrial rehabilitation in the geosciences [3], agriculture and forest monitoring [4-6], assistance for disastrous events management (hurricanes, earthquake, fire detection and tsunami) [7-12], land administration [13, 14], flora and fauna monitoring [15], geodesy and cartography [16], risk assessments [17-19], medical intervention [20-22].

First of all, drone should be used firstly for those industries where you need both mobility and excellent information. In particular, companies that manage goods located in large territories, for a long-time confront with difficulties and challenges that may be solved using drone technology [23]. Integration of such devices into the daily operating process will help to create considerable advantages in implementation of large-scale capital construction projects, in infrastructure management, transport industry, agriculture and emergency interventions regardless of whether they are natural or anthropogenic disasters. Recent research and investment have resulted in a substantial number of new applications for drone devices, especially in agriculture, infrastructure, security, transportation, media and entertainment, telecommunications, studying and protecting the natural and cultural area [24, 25].

Taking into account the general area of feasible applications for unmanned aerial vehicles, it is extremely important to understand which exactly the international market for solutions using unmanned aerial vehicles will evolute in the future [26]. Although when consider the continuous emergence of new uses for unmanned aerial vehicles, it is crucial to examine regulatory and technological issues.

Staring with April 2021 the European Commission adopted the U-space package

THE ANNALS OF "DUNAREA DE JOS" UNIVERSITY OF GALATI
FASCICLE IX. METALLURGY AND MATERIALS SCIENCE
N°. 4 - 2021, ISSN 2668-4748; e-ISSN 2668-4756
Article DOI: https://doi.org/10.35219/mms.2021.4.05

establishing the appropriate conditions for both drones and manned aircraft to operate without risk (below 120 m). Institutions that control the country's airspace should approach the daunting challenge of how to guarantee the safety of citizens and privacy, while not restraining innovative development and progress [27].

2. Main areas of using UAVs

Knowledge and experience of international experts and equally important, a major interest in learning innovative methods the use of new technologies, in order to collect and analyse data for solving different types of problems. Unmanned devices equipped with cameras and sensors are used more and more throughout world to provide more global and comprehensive information.

Initially, drones have delivered such products to remote, inaccessible locations that receive food from other areas such as research stations, oil rigs or isolated islands. Gradually, drones start to be used to accomplish similar tasks in residential areas, thereby reducing delivery times and increasing the efficiency of the entire transport chain.

2.1. Infrastructure and construction

Unmanned aerial vehicles offer new perspectives and have only recently begun to be utilised to support in the management of several infrastructure facilities. Sectors like: energy, road, railways, and oil and gas can be easily and accurately monitored particularly in these industries where companies manage complex resources disperse over vast areas, providing geotechnical and hydrological data, assist in the design of haul roads, dumps and open pits, display steep, inaccessible slopes, and monitor surface stability. The principal utilization for drones in the infrastructure industry are investment control, maintenance and asset inventory. By using these technologies, both dangerous work and the facilitation and access to various data sets can be performed, ensuring high accuracy and minimal cost of information.

One sector with tremendous untapped potential for drone use is the mining industry. The potential for commercial use of drones in mining is not so obvious at first glance, and yet unmanned aerial vehicles can replace manual labour in dangerous and repetitive operations. UAVs are more versatile and cost effective than helicopters, they are also faster, easier to operate, and emit less emissions than mining equipment. Drones are now being tested and implemented mainly in open pit mining, where they replace labour-intensive surveying, site survey and geological surveying. At the same time can be equipped with additional equipment for delivering spare parts or taking soil samples for field analysis Drones can be used to quickly create an overview map of the work site, optimize travel routes and provide control information. Several applications in exploration work range from providing data to calculate mineral resources, compiling an overview map of the mining area. By creating a digital model of the current status of an open pit mine and identifying changes in mine structure (collapses, infrastructure damage), mine owners can improve safety and reduce control costs. Early detection of abnormalities and correct pit appraisal ensure quick response and more efficient job planning. In addition, it will facilitate the automation of the entire process of extracting minerals from the subsoil, which will lead to a decrease in mining costs.

Unmanned aerial vehicles can operate with video files and high-resolution photos, which allows you to do 3D modelling and provide investors and property owners with information about the initial state of the site even before work begins and more than that can be used in the development of digital terrain models and for a more accurately evaluation. Real-time information and data accuracy have permanently been a challenge on construction sites. During the pre-construction level, drones can generate higher quality data, consequently considerable increasing the speed and quality of design. During the construction phase for various objectives of major interest, drones are ideal for quick on-site surveys to collect accurate data for project progress reports. Investors will have no difficulty in monitoring progress by overlaying plans with photographs of actual construction status, to identify discrepancies up to 1 cm and for verification of information in the reports of contractors.

2.2. Transport and delivery

Lately, traffic supervision and monitoring has been one of the major tools for transport regulation as part of traffic management and control strategy. The transport industry has excellent prospects for the development of unmanned aerial vehicle technology, which is mainly associated with the upcoming improvements of technological solutions. Unmanned devices can play an important role in this technological shift. UAVs are now gaining ground in a wide variety of transportation activities, from online shopping and drug delivery to fleet management, spare parts supply and even delivery of food on the day of order. Drones will soon become an integral part of the transportation industry, both as a new delivery method and as a service accompanying transportation services. Industry companies will look

THE ANNALS OF "DUNAREA DE JOS" UNIVERSITY OF GALATI
FASCICLE IX. METALLURGY AND MATERIALS SCIENCE
N°. 4 - 2021, ISSN 2668-4748; e-ISSN 2668-4756
Article DOI: https://doi.org/10.35219/mms.2021.4.05

to drones because these can be more efficient than other ways of transport, and also tend to have lower operating costs. In the field of e-commerce, when choosing a courier service, delivery times are of crucial importance. UAVs ensure the delivery of goods in a short time to a specific, predetermined place and not requiring a large number of human actions. Thanks to the possibility of delivering parcels to the customer's door, the quality of customer service will increase. Several logistics companies are already using drones to get the job done. For example, the postal service has been delivering parcels using unmanned aerial vehicles, drones fly autonomously along predetermined routes. The routes are based on a cloud program that can deliver shipments weighing up few kilograms.

The crowded traffic evolves more and more space and time and we may try to predict and to the understand the frequent traffic conditions, the systematic management of pedestrian and vehicle traffic, in addition to the traffic and request a management under unpredicted transportation network circumstances (e.g. extreme traffic jam, unfavourable weather conditions, protests, terrorist attacks), that might critically deteriorate the efficiency of the transport networks and impact the security and safety of customers.

One of the most promising areas for the use of UAVs may be food delivery whether we're talking about the delivery of frozen food, ready-to-eat meals and even everyday groceries and dairy products. This way of delivering the products could be a significant current milestone in the expansion of the food industry and restaurant business.

An unmanned aerial vehicle delivered pharmaceuticals from the delivery point to a nearby clinic in some minutes. Delivering medical supplies to inaccessible rural areas is a major plus for using drones in the transportation industry. In addition, drones can be used as flying defibrillators for patients with signs of a heart attack, determining its location and identifying it, after which it will automatically defibrillate.

2.3. Agriculture

Agricultural production has grown significantly over the past few years. In order to meet the growing population demand, agricultural companies will need to make radical changes to their food production methods and considerably improve their efficiency. In addition, production must be environmentally sustainable and contribute to the prevention of environmental damage. Climate change and unforeseen natural disasters around the world are some of the obstacles that have to face the agriculture. Thus, in order to meet the global demand for food products, cooperation between representatives of government, technology and industrial sectors will expand.

Remote sensing is commonly assessed among the most significant applied science for accuracy agriculture and smart farming. Previously, remote sensing was frequently based upon satellite images or photographs obtained by using manned aircraft for the purpose of monitor vegetation condition at certain growth phases. Nevertheless, satellite imagery is usually not the best alternative due to the reduced spatial resolution of images acquired and the constrains of the temporal resolutions as satellites are not constantly accessible to capture the required photographs. Moreover, it is regularly required to wait long intervals between photography moment and obtaining of images. In certain cases, environmental conditions, such as clouds, frequently obstruct their reliable utilize.

UAVs are more and more frequently applied in remote sensing applications. Equipped with detectors of various types, UAVs can be operated to observe which areas of the crops necessitate distinct management. These facilities allow the farmers the capacity to react promptly in every problem observed. UAVs can be used in a multitude of distinct applications like health monitoring and disease identification, growth controlling and productivity assessment, etc.

Until now, the main agricultural problem has been the size of cultivated agricultural land and the low efficiency of crop monitoring. This problem is exacerbated by an increase in unpredictable weather events, which heightens the risks posed by agricultural activities and increases the cost of field repairs. Until recently, the most modern form of field monitoring was the use of satellite technology. The main limitations of this method were the need to order satellite images in advance, the ability to take images only once a day, and the lack of accuracy of such images. In addition, such services are very expensive and do not guarantee the quality of shooting, which can deteriorate sharply in case of strong clouds. Today, UAVs technologies offer a number of cheaper options for monitoring crops. Drones can be used in other stages of the crop life cycle, from soil analysis and planting to determining the optimal harvest time. Soil analysis is the first step in any agricultural cycle. Drones can create accurate 3D terrain models that allow for initial soil analysis. The results of this analysis can be used in planning a seed planting scheme. These systems drop seeds into the soil that are coated with a nutrient that provides the plant with all the nutrients it needs. In addition, this analysis provides data for the management of irrigation systems and nitrogen monitoring.

THE ANNALS OF "DUNAREA DE JOS" UNIVERSITY OF GALATI
FASCICLE IX. METALLURGY AND MATERIALS SCIENCE
Nº. 4 - 2021, ISSN 2668-4748; e-ISSN 2668-4756
Article DOI: https://doi.org/10.35219/mms.2021.4.05

UAVs equipped with hyperspectral, multispectral or thermal sensors are able to determine which part of the field needs additional watering or other activities. At later stages of the crop life cycle, the main task of agricultural workers is to prevent plant death and disease. This work requires constant monitoring of the fields. One of the new developments allows to assess the condition of plants and detect damage to trees by bacteria or fungi. Scanning plants using both the visible and near infrared ranges gives an idea of how much green and near infrared waves are reflected off the plants. Based on this data, multispectral near-infrared images are generated to detect changes in plant health. In addition, once a plant disease is detected, a more accurate decision can be made on its treatment and monitoring of the situation. UAVs can also be used for spraying plantations. The drones can scan the terrain and maintain a set distance from the top of the plants to spray the right amount of liquid, adjusting the sprinkler parameters in real time to ensure even planting. This not only improves spraying efficiency, but also reduces the amount of excess chemicals entering the soil.

According to experts, aerial spraying can be done up to five times faster than using traditional equipment such as tractors.

2.4. Environmental protection and risk monitoring

An excellent example of a drone application is the use of drones to monitor areas prone to natural disasters such as floods, droughts, volcanic eruptions or hurricanes. Unmanned aerial vehicles can detect erosion, track changes in plant cover and landscape changes, can monitor floods, landslides, and they can do this much easier and definitely faster than a person without the help of any technical means.

Economic growth and the increase in population density and the expansion of activities in high-risk areas are the main causes that have led to risks in areas prone to disasters. By monitoring areas located in high-risk areas, local and central public authorities can observe the risk and notify local residents about emergencies preventing accidents and serious damage. Monitoring systems should include drones and a ground data collection and analysis system. Such systems allow preventing or minimizing the negative economic consequences of natural disasters, which will have a positive impact on the development of the entire industry.

First-class biodiversity dataset on fauna and flora distributions and its integration with environmental factors are crucial for maintaining populations and to avoid the extinction of some species of major importance, tracking biodiversity changes, and preparing efficient conservation practices. Traditional field studies are exhausting, expensive and spending an enormous time and energy on the terrain. Remote sensing techniques are more and more being used to evaluate changes in forest while satellite and airborne sensors can be costly and unreachable for most scientists, necessitating compromise among resolution, scale, and frequency. UAVs are lightweight and are advantageous from the point of view of time and cost-effective monitoring of environmental changes.

In the last decade the world became oftentimes vulnerable to disastrous events that generate devastating repercussions for humanity. Unpredictable catastrophes namely seism and tsunami or hurricanes can be detected several days prior to their appearance. Considering the disastrous potential of hurricanes, it is an important responsibility to utilize this forecast data to manage the preparedness operations to reduce hurricane's impact and to strength the efficiency of the post-disaster assistance attempts.

In several countries, drones start to be used for environmental control (surveillance). As part of the fight against pollution, the authorities should use drones that track illegal emissions, illegal exploitation or hunting and fishing during the periods when these activities are prohibited.

2.5. Media and entertainment industry

The media and entertainment industry are one of the areas where drone solutions are most widely used. The main function of drones used in the media and entertainment industry is to provide photography and video filming for both commercials and feature films and on sports events. Another interesting area of their application is the production of documentaries about wildlife. They can also help improve the quality of film production and photographs, especially since the miniaturization of equipment allows them to be installed with high resolution cameras.

Thanks to their low noise, UAVs can take pictures from very close distances during sportive competitions without distracting them. In addition, they can be used to capture images that cannot be captured in any other way like to capture the behaviour of birds on the upper branches of trees for a documentary about wildlife.

2.6. Security sector

Technologies (the latest electronics, sensors and video equipment) have always served as a reliable support in the work of security services and security

THE ANNALS OF "DUNAREA DE JOS" UNIVERSITY OF GALATI
FASCICLE IX. METALLURGY AND MATERIALS SCIENCE
N°. 4 - 2021, ISSN 2668-4748; e-ISSN 2668-4756
Article DOI: https://doi.org/10.35219/mms.2021.4.05

agencies. But even today, many tasks still require a lot of manual labour. Due to their speed, size, agility and built-in technology, drones are changing the balance of power: they have proven to be an excellent aid for ground security forces who want to achieve greater agility and efficiency in monitoring operations.

Drones can quickly fly around large, hard-to-reach areas, reducing staffing and costs without requiring a lot of space for drone operators and more than that are reliable and be able to operate in all weather conditions and at night. The drone flight is controlled from small ground stations, so operators can be gathered in one place, for example, in a regular video monitoring centre.

There are two significant approaches: monitoring of linear zone and monitoring of areal objects. As part of the monitoring of linear zone, UAVs are used to monitor highways, coastlines and border protection. They are used to observe illegal border crossings, contraband and wildlife migration. As for the monitoring of areal objects, for these purposes, helicopter-type drones are more often used, since they have greater manoeuvrability and more easily make circles over the objects of observation. UAVs can be used for streaming data in real time, tracking objects or intruders from a safe distance and quickly flying around a large area, as well as for video recording that allows you to determine rapid an accident assessment in order to ensure the safety of the affected area for the operation of the operational services and provide an instant response to security alerts. Drones are capable of performing functions beyond simple monitoring, they can also be used to secure strategic facilities or infrastructure such as ports and airports. This information allows the port administration to more efficiently distribute tasks among employees. Unmanned aerial vehicles have found other uses in industrial facilities: along with monitoring and checking the quality of personnel, they help to reduce the costs associated with theft of assets.

3. Conclusions

A reliable control system cannot be created without the development of an integrated air traffic control system for unmanned aerial vehicles, designed to prevent drones from colliding with other flying objects. These systems should be designed to enable unmanned aerial vehicles to see and avoid collisions with other aircraft and potential obstacles, and to communicate with air traffic controllers controlling the movement of manned aircraft.

Photogrammetric and geospatial analysis gives access to valuable information about topography, hydrography, land cover, soil type, development level and other characteristics that can improve their efficiency. However, conventional aerial data is still quite expensive and does not necessarily provide the necessary detail, as the image quality is usually poor. Drones are more cost effective and guarantee better data quality.

Drones' business in the world is prospering. both the public and the private sector has invested massively in the business and certainly UAVs are the future not simply of the conflict, but their utilize in the non-military sector will also be unequalled.

Acknowledgements

This work was supported by a grant of the Ministry of Research, Innovation and Digitization, CNCS/CCCDI – UEFISCDI, project number 459 PED/2020, AWISEM, within PNCDI III.

References

[1]. Muhammad Nadeem Mirza, Irfan Qaisrani, Lubna Abid Ali, Ahmad Naqvi, *Unmanned Aerial Vehicles: A Revolution in the Making*, South Asian Studies - A Research Journal of South Asian Studies, Centre for South Asian Studies, University of the Punjab Lahore, 31 (2), p. 243-256, 2016.
[2]. Colomina I., Molina P., *Unmanned aerial systems for photogrammetry and remote sensing: A review*, ISPRS J. Photogramm. Remote Sens, 92, p. 79-97, 2014.
[3]. Harwin S., Lucieer A., *Assessing the accuracy of georeferenced point clouds produced via multi-view stereopsis from unmanned aerial vehicle (UAV) imagery*, Remote Sens, 4, p. 1573-1599, 2012.
[4]. Lindenmayer D. B., Likens G. E., Andersen A., Bowman D., Bull C. M., Burns E., Dickman C. R., Hoffmann A. A., Keith D. A., Liddell M. J., Lowe A. J., Metcalfe D. J., Phinn S. R., Russell-Smith J., Thurgate N., Wardle G. M., *Value of long-term ecological studies*, Austral Ecol., 37, p. 745-757, 2012.
[5]. Tsouros D. C., Bibi S., Sarigiannidis P. G., *A Review on UAV-Based Applications for Precision Agriculture*, Information, 10, 349, https://doi.org/10.3390/info10110349, 2019.
[6]. Jian Zhang, Jianbo Hu, Juyu Lian, Zongji Fan, Xuejun Ouyang, Wanhui Ye, *Seeing the forest from drones: Testing the potential of lightweight drones as a tool for long-term forest monitoring*, Biological Conservation, vol. 198, p. 60-69, ISSN 0006-3207, 2016.
[7]. Rawls C. G., Turnquist M. A., *Pre-positioning of emergency supplies for disaster response*, Transportation Research Part B, 44 (4), p. 521-534, doi: 10.1016/j.trb.2009.08.003, 2010.
[8]. Paul J. A., MacDonald L., *Location and capacity allocations decisions to mitigate the impacts of unexpected disasters*, European Journal of Operational Research, 251, p. 252-263, 2016.
[9]. Réstas A., *The regulation unmanned aerial vehicle of the Szendro fire department supporting fighting against forest fires 1st in the world*, For Ecol Manag 234S, 2006.
[10]. Zhang B., Peng J., Li S., *Covering location problem of emergency service facilities in an uncertain environment*, Applied Mathematical Modelling, 51, 2017.
[11]. Barnes G., Volkmann W., *High-resolution mapping with unmanned aerial systems*, Surv. Land Inf. Sci., 74, p. 5-13, 2015.
[12]. Martinez J. R., Merino L., Caballero F., Ollero A., Viegas D. X., *Experimental results of automatic fire detection and monitoring with UAVs*, For Ecol Manag, 234S(2006):S232, 2006.
[13]. Chou T.-Y., Yeh M.-L., Chen Y. C., Chen Y. H., *Disaster monitoring and management by the unmanned aerial vehicle*

technology, In: Int. Archives of Photogrammetry, Remote Sensing and Spatial Information Sciences, Vienna, Austria, 38(7B), p. 137-142, 2010.

[14]. Galindo G., Batta R., *Prepositioning of supplies in preparation for a hurricane under potential destruction of prepositioned supplies*, Socio Economic Planning Sciences, 47 (1), p. 20-37, 2013.

[15]. Bolten A., Bareth G., *Introducing a low-cost Mini-UAV for Thermal- and Multispectral-Imaging*, Int. Archives of Photogrammetry, Remote Sensing and Spatial Information Sciences, Melbourne (Australia), 39 (1), 2012.

[16]. Boonmee C., Arimura M., Asada T., *Facility location optimization model for emergency humanitarian logistics*, International Journal of Disaster Risk Reduction, 24, p. 485-498, 2017.

[17]. Burdakov O., Kvarnstrom J., Doherty P., *Optimal scheduling for replacing perimeter guarding unmanned aerial vehicles*, Annals of Operations Research, 249, p. 163-174, 2017.

[18]. Chang M. S., Tseng Y. L., Chen J. W., *A scenario planning approach for the flood emergency logistics preparation problem under uncertainty*, Transportation Research, Part E, 43, p. 737-754, 2007.

[19]. Goldberg J., Dietrich R., Chen J., Mitwasi G., Valenzuela T., Criss L., *Validating and applying a model for locating emergency medical vehicles in Tucson. Arizona*, European Journal of Operational Research, 49 (3), p. 308-324, 1990.

[20]. Humphreys T., *Statement on the Vulnerability of Civil Unmanned Aerial Vehicles and Other Systems to Civil GPS Spoofing*, University of Texas at Austin, July 18, 2012.

[21]. Koh L. P., Wich S. A., *Dawn of drone ecology: Low-cost autonomous aerial vehicles for conservation*, Trop. Conserv. Sci., 5, p. 121-132, 2012.

[22]. Remondino F., Barazzetti L., Nex F., Scaioni M., Sarazzi D., *UAV Photogrammetry for Mapping and 3D Modeling-Current Status and Future Perspectives*, Int. Arch. Photogramm. Remote Sens. Spat. Inf. Sci., XXXVIII, p. 14-16, 2011.

[23]. Evers L., Dollevoet T., Barros A. I., Monsuur H., *Robust UAV planning*, Annals of Operations Research, 222, p. 293-315, 2014.

[24]. Merwaday A., Guvenc I., *UAV assisted heterogeneous networks for public safety communications*, In Proceedings of 2015 IEEE wireless communications and networking conference workshops, WCNCW 2015, p. 329-334), New Orleans, United States, 2015.

[25]. Vu H., Keriven R., Labatut P., Pons J.-P., *Towards high-resolution large-scale multi-view stereo*, Proc. IEEE Conf. CVPR'09, p. 1430-1437, 2009.

[26]. Thamm H. P., Judex M., *The "Low-cost drone"-An interesting tool for process monitoring in a high spatial and temporal resolution*, Int. Archives of Photogrammetry, Remote Sensing and Spatial Information Sciences, Enschede, The Netherlands, 36 (7), 2006.

[27]. ***, Commission implementing regulation (EU) 2021/664 of 22 April 2021 on a regulatory framework for the U-space, European Commission.

THE ANNALS OF "DUNAREA DE JOS" UNIVERSITY OF GALATI
FASCICLE IX. METALLURGY AND MATERIALS SCIENCE
N°. 4 - 2021, ISSN 2668-4748; e-ISSN 2668-4756
Article DOI: https://doi.org/10.35219/mms.2021.4.06

DRONE DETECTION USING IMAGE PROCESSING BASED ON DEEP LEARNING

Florin-Bogdan MARIN, Mihaela MARIN
"Dunarea de Jos" University of Galati, Romania
e-mail: flmarin@ugal.ro

ABSTRACT

The objective of this experimental research is to identify solutions to detect drones using computer vision algorithm. Nowadays danger of drones operating near airports and other important sites is of utmost importance. The proposed techniques resolution pictures with a good rate of detection. The technique is using information concerning movement patterns of drones.

KEYWORDS: CFD, modelling, simulation, car brake, cooling

1. Introduction

The use of drones is becoming wide on different domains such as civil, commercial and military. With a huge number of applications, Unmanned Air Vehicles (UAVs) - also known as drones) pose a real safety issue concerning security that may lead to people live property but also cand produce catastrophes. Firstly, the danger source might be attackers who deliberately want to use drones, but also pilot lack of exercise might lead to severe consequences. Serious drones' incidents are very often. From drones having struck van in Scotland [1] to crashing drone to Pisa tower [2] the incidents produced by careless or inexperienced pilots are reported every week worldwide. The terrorist also used drones as the latest technology. The Iraq prime minister was attacked by a drone filled with explosive [3]. At the moment one of the most important threats is concerning disturbing traffic due to drone activity near airports. In 2018 hundreds of flights were cancelled at Gatwick Airport near London, England, because drones were reported close to the runway. On 14 September 2019, drones were used to attack oil processing facility in eastern Saudi Arabia.

Though authorities worldwide are imposing serious law by regulating drone operation careless drone operators' actions are causing serious problems for airports. Laws are discouraging using drones near airports but not address the criminal or terrorist activities [3]. The solution for avoiding tragic consequences is the use of technologies to detect and counter the drone operation in certain areas.

There are several solutions for detection of drones. One of the most used solution is detecting the Radio frequency (RF) [4]. Except autonomous ones most of the drones are navigating by communication between drone and the ground operator. This technique has very good results in case of civil drones that are operating at certain known frequency.

However, the main issue with this technology is that the drone may use peculiars frequency. With advanced RF scanner even, this issue can be solved but in the case the drone is autonomous or the drone has a pre-programmed flight path, it cannot be used at all [5].

Another solution is using acoustics analysis to detect drones [6,7]. Special software is using digital signal processing to identify specific sound of rotors. However, this solution cannot achieve good results for a greater than 200-400 m operational range.

Another technique used is the use of radar, but the small size and specific geometry means that are reflecting back to radar very limited electromagnetic signals. The use of the radar solution also provides high rate of false detection due to bird's activity [8].

Due to the latest development in computer vision and artificial intelligence algorithms a solution that provide good results might be used along other technical solution for drone detection. There are several computer visions approaches in order to detect drones. The "You Only Look Once" (YOLO) algorithm has enabled researchers to detect with high accuracy the drones [9, 10].

Deep learning is a latest algorithm developed that has shown very good results in computer vision. Convolutional neural networks (CNNs) can predict classes of objects by processing image features from a specific object. The training phase means providing several images sets with classes of objects to be detected. The deep learning is based on the idea that

THE ANNALS OF "DUNAREA DE JOS" UNIVERSITY OF GALATI
FASCICLE IX. METALLURGY AND MATERIALS SCIENCE
Nº. 4 - 2021, ISSN 2668-4748; e-ISSN 2668-4756
Article DOI: https://doi.org/10.35219/mms.2021.4.06

there is layer-based selection of features. For instance, first layer is collecting information concerning edges, the second level of layer extract colour information and the top lever layers define the object. CNNs are useful for performing identification of various objects such as humans, animals, types of plants and so on. The application varies from machine vision in industry for identification of defects, to security, and even detection of pedestrians used on ADAS (Advanced Drivers Assistance systems) onboard of the cars.

The frequency of incidents is also on the on airports worldwide which meant problems in operating air flights and serious disruptions because of drone presence and many scholars presented different approached and solutions. [11-13].

2. Experimental procedure

The detection system comprises of cameras arrays oriented to different positions towards the sky in order to identify drones. Video stream is processed by a computer running the proposed technique. In the first stage we prepare the image data sets for training. We have used 200 different images taken in different sky weather. Our object detection model uses deep learning to detect drones. A great challenge occurs in case of extreme foreground/background imbalance, such in cases when drones are black and the sky is also black.

To avoid false positive in case of presence of birds we used the information concerning relative speed of the object and also trajectory path. Birds are not usually performed close trajectory and also do not stop at a position as in fixed flight and then change the speed in an important amount. This basic path and speed analysis means that our technique significantly lowers the false positive cases. The confidence in predicting a drone class is of most important in order to develop such a detection to operate in real live conditions.

Using training only on images will not provide good results and thus the generated paths trajectory of real flights drones allows avoiding detection of birds. During detection process if the drone makes a small drift as well as stationary position, the algorithm increases chances of positive detection.

Accumulated drift analysis results in following the suspect object and its detection. To enhance algorithm feasibility, we also use speed evolution, as in case of birds there is no abrupt variation of speed. We analyse speed relative to camera position and thus we are using pixels per seconds as measurement unit. We measure different trajectories of drones and due to their technical specifications, are able to control to a complex flight's trajectories. As seen in Figure 1, we can identify and make selection between bird and drone path in case the drones are showing specific trajectory. However due to 3d spatial trajectory there are situations when trajectory is perpendicular to camera when the algorithm is not useful. This can be improved in case we will use matrix cameras from different angles of the same airspace.

Also, distinction between birds and drones can be easily done in some circumstances when analysing speed evolution. As seen in Figure 2, we analyse speed variation and we can also use the heuristic approach concerning the operating speed variation to avoid false positive identification of birds as drones. We stress that we consider bird species living in Romania climate able to fly at a maximum of 300 m altitude. The two conditions concerning speed variation and trajectories are introducing to the predictive model more information in case the drone is performing specific movement. The proposed algorithm is using deep learning algorithm for classification. The predictive model is also using movement pattern and speed pattern. The proposed technique is using deep learning Convolutional Neural Networks (CNNs). We used 200 pictures of own pictures of drones taken in different environment conditions and consequently sky colours. As stressed above, information concerning movement patter and speed pattern are used in predictive model to make distinction and eliminate in such a manner some false positive identification.

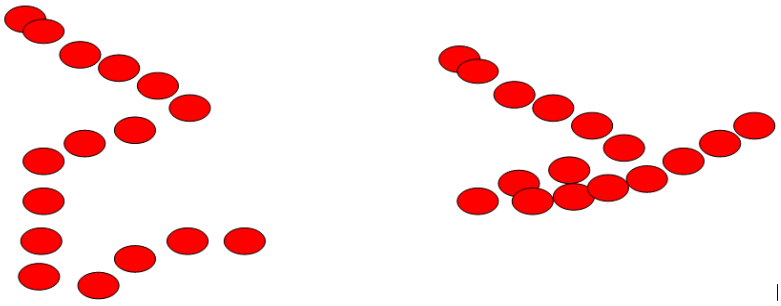

Fig. 1. *Drone path trajectory seen by a camera*

THE ANNALS OF "DUNAREA DE JOS" UNIVERSITY OF GALATI
FASCICLE IX. METALLURGY AND MATERIALS SCIENCE
N°. 4 - 2021, ISSN 2668-4748; e-ISSN 2668-4756
Article DOI: https://doi.org/10.35219/mms.2021.4.06

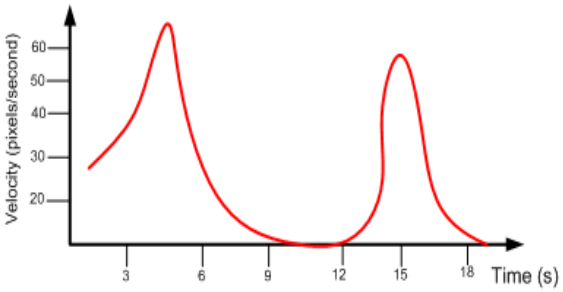

a)

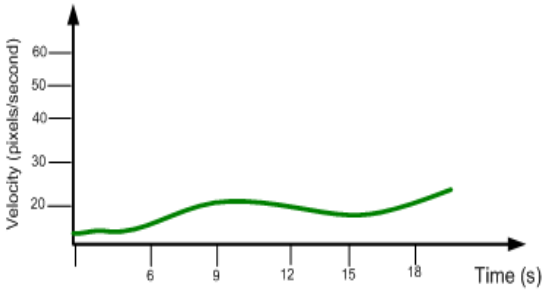

b)

Fig. 2. *Speed variation in case of a) drones b) birds*

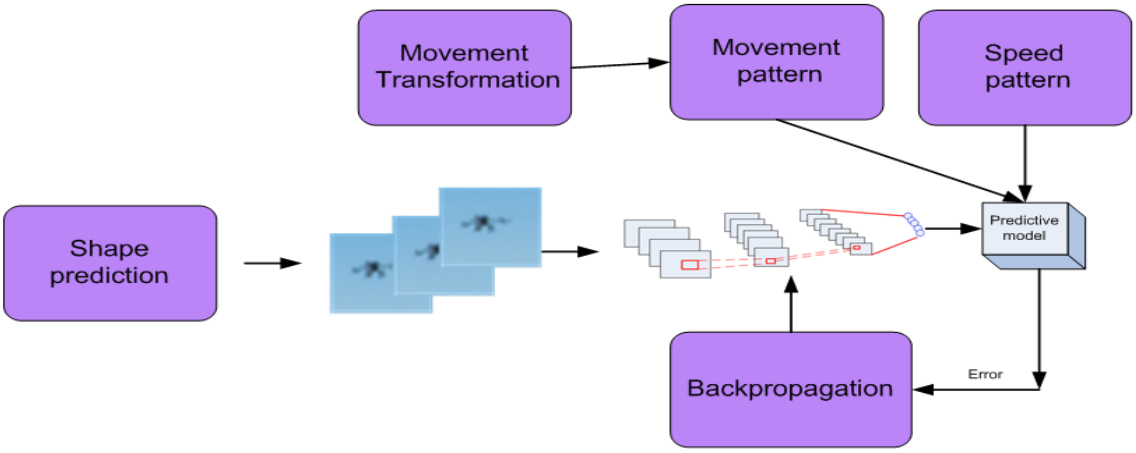

Fig. 3. *The proposed technique for drone detection*

3. Results and discussions

We used a web camera with good resolution but due to the distance to the drone, the drones need to be identified in low resolution pictures as the pixels representing the drones are in quite small amount. The dataset we use for experiment is not public data bases data set, because we need low resolution representation of our objects to be identified. Our data set contains different categories of objects: birds, airplanes. We converted the video sequences to images for CNN training and testing. We used a pc with AMD Ryzen™ 9 5900X. The application developed used 10 threads to process information in order to use processor multi-core capability better. Our case of multiple cameras processing such a platform can easily process 10 cameras in the same time without affecting speed of processing. We tested the application with 4 hours. The drone approaches the camera site every 3 minutes at different altitudes and movement patterns. The system is able to detect drone to a distance of maximum 200 meters. The

THE ANNALS OF "DUNAREA DE JOS" UNIVERSITY OF GALATI
FASCICLE IX. METALLURGY AND MATERIALS SCIENCE
N°. 4 - 2021, ISSN 2668-4748; e-ISSN 2668-4756
Article DOI: https://doi.org/10.35219/mms.2021.4.06

detection rate in videos is 89% percent of the frames where a human can identify drone. However, each approach of the drone has been detected. False positive consisted of 2 cases of birds identify as drone, but we need to stress that no consisted bird activity presence was in the area we tested. technique need low computational resources in respect to computational platform. The application is processing 16-23 frames per seconds to identify drones. That means real time processing for video streams. We consider that in good assessment concerning false positive reliability.

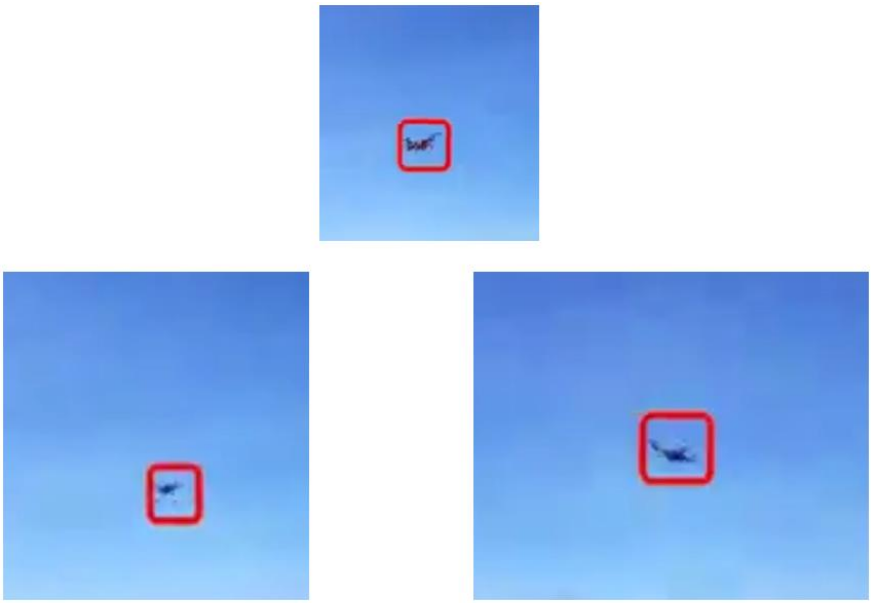

Fig. 4. *Drones' detection in low resolution pictures*

4. Conclusions

The main conclusions are the following:

- The proposed algorithm proved a good performance and can be used to a low-resolution picture.
- Low computational resources allows to implement on embedded devices as well and can be used to a matrix of cameras in order to detect drones.
- This algorithm can be used along radar detection technique.
- Further research should take into account using radar information, which are more accurate about 3d trajectory and speed in order to improve results.
- Further development need to consider better cameras or cameras with controlled zoom.
- The technique must be tested in areas with important bird presence.

References

[1]. Gabrielle Lea, *Drone Drops Leaflets over Football Stadiums, Raising Security Concerns*, Fox News, https://www.foxnews.com/tech/dronedrops-leaflets-over-football-stadiums-raising-security-concerns, November 27, 2017.
[2]. ***, https://news.in-24.com/news/186066.html, 2021.
[3]. ***, *Regierungschef übersteht Drohnenangriff*, https://www-tagesschau.de.
[4]. Krizhevsky A., Sutskever I., Hinton G. E., *Imagenet classification with deep convolutional neural networks*, Advances in neural information processing systems, p. 1097-1105, 2012.
[5]. Shengxiang Qi W. Z., *Detecting Consumer Drones from Static Infrared Images*, Proceedings of the 4th International Conference on Communication and Information Processing, p. 62-66, Qingdao, 2018.
[6]. Stokel-Walker Chris, *Why Drones Cause Airport Chaos*, New Scientist 241, no. 3213, 10, https://doi.org/10.1016/S0262-4079(19)30100-9, January 19, 2019.
[7]. Huang K., Wang H., *Combating the control signal spoofing attacking UAV systems*, IEEE Transactions on Vehicular Technology, vol. 67, no. 8, p. 7769-7773, Aug. 2018.
[8]. Zeitlin A. D., *Sense avoids capability development challenges*, IEEE Aerospace and Electronic Systems Magazine, vol. 25, no. 10, p. 27-32, Oct. 2010.
[9]. Nam H., Han B., *Learning multi-domain convolutional neural networks for visual tracking*, arXiv preprint arXiv:1510.07945, 2015.
[10]. Redmon J., Divvala S., Girshick R., Farhadi A., *You only look once: Unified, real-time object detection*, arXiv preprint arXiv:1506.02640, 2015.
[11]. Opromolla R., Fasano G., Accardo D., *Perspectives and sensing concepts for small uas sense and avoid*, IEEE/AIAA 37th Digital Avionics Systems Conference (DASC), p. 1-10, Sep. 2018.
[12]. Prats X., Delgado L., Ramirez J., Royo P., Pastor E., *Requirements, issues, and challenges for sense and avoid in unmanned aircraft systems*, Journal of Aircraft, vol. 49, no. 3, p. 677-687, 2012.
[13]. Yucong Lin, Saripalli S., *Sense and avoid for unmanned aerial vehicles using ads-b*, IEEE International Conference on Robotics and Automation (ICRA), p. 6402-6407, May 2015.

THE ANNALS OF "DUNAREA DE JOS" UNIVERSITY OF GALATI
FASCICLE IX. METALLURGY AND MATERIALS SCIENCE
Nº. 4 - 2021, ISSN 2668-4748; e-ISSN 2668-4756
Article DOI: https://doi.org/10.35219/mms.2021.4.07

DETERMINATION OF POROSITY IN FLUIDIZED - BED CARBURIZED P/M COMPACTS USING AN IMAGE SOFTWARE ANALYSIS

Mihaela MARIN, Florin-Bogdan MARIN
"Dunarea de Jos" University of Galati, Romania
e-mail: mihaela.marin@ugal.ro

ABSTRACT

The aim of this research was to study the porosity in carburizing in fluidized-bed on sintered alloys produced by powder metallurgy route using an image analysis software and to compare the obtained results with the conventional method for porosity measurements. Porosity is a measure of the void fraction in a material. The total porosity is defined by the ratio of the volume of void space to the total bulk volume of the material, expressed as a percentage. Development of digital images and computer software lead to a new and suitable method to determine the porosity of powder metallurgy materials.

KEYWORDS: powder metallurgy, sintering, fluidized bed carburizing, porosity, image software

1. Introduction

Powder metallurgy (P/M) is an important alternative technology of lower cost process. The main problem of P/M products is the presence of pores due to the fact the pores act as potential crack initiation sites and can also guide and propagate cracks through the material. The conventional P/M processing can produce iron-based P/M parts with a density less than 7.1 g/cm^3, so their mechanical properties are considerably less than their full density part obtained by classic metallurgy [1-3]. The properties of sintered P/M alloys can be improved by adding alloying elements [4-7]. The most commons alloying elements added in powder form are: copper, nickel, molybdenum, manganese and phosphorus. Cu increase the toughness and density by filling the pores due to melting during the sintering process (copper melts at 1083 °C) [8-11]. Nickel (Ni) increases the sintered density due to the formation of the Ni-rich areas during sintering in solid state which have a positive influence on hardness and strength by providing a local ductility [12, 13]. Molybdenum (Mo) has a good response in hardenability [14].

Another way to improve the properties of these alloys is by applying heat, thermochemical or mechanical treatments [15-22]. Fluidized bed carburizing is a thermochemical treatment that provides high heat and mass transfer.

The goal of this paper is to study the porosity in some fluidized bed carburizing sintered P/M materials by applying an image software tool and to compare the obtained results with the results obtained by the conventional method.

2. Experimental procedure

The specimens studied in this paper are represented by atomized iron powder and pre-alloyed iron base powder. The chemical composition of the powders, pure iron and iron-based pre-alloyed powder with Cu, Ni and Mo is presented in Table 1. The raw samples were mixed with 1% zinc stearate. The green compacts, obtained at 600 MPa pressure using a single die action, were sintered in a laboratory furnace at 1150 ºC for 60 minutes. The obtained disc specimens have the dimensions of ϕ8 X 6 mm. After cooling to room temperature, the samples were subjected to fluidized bed carburizing treatment at 900 °C during 60 minutes.

THE ANNALS OF "DUNAREA DE JOS" UNIVERSITY OF GALATI
FASCICLE IX. METALLURGY AND MATERIALS SCIENCE
Nº. 4 - 2021, ISSN 2668-4748; e-ISSN 2668-4756
Article DOI: https://doi.org/10.35219/mms.2021.4.07

Table 1. *Chemical composition of analysed powders*

Powder type	Cu	Mo	Ni	C
P_1	0.096	0.008	0.046	<0.01
P_2	1.50	0.50	1.75	<0.01

3. Results and discussions

3.1. Density results

The green, sintered and carburized in fluidized bed densities of the specimens were determined by using geometrical method, weight and dimensional measurements. The measurements result of the density in green state, sintered and carburized in fluidized bed, measured from by conventional technique are presented in Fig. 1.

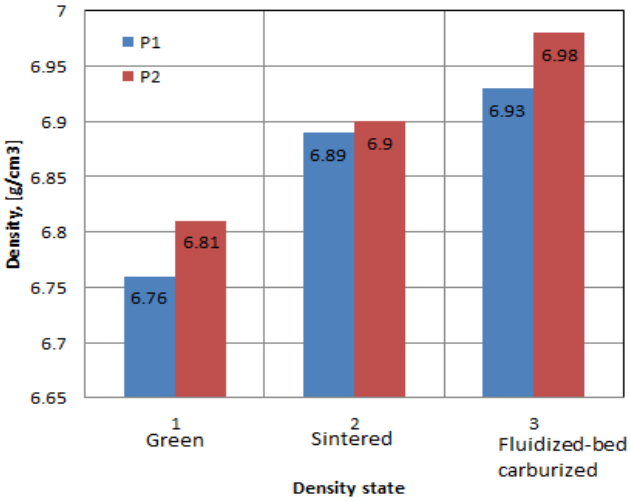

Fig. 1. *Green density, sintered and carburized in fluidized bed density for analysed specimens*

3.2. Microstructure analysis

The microstructures of fluidized bed carburized samples were observed by optical microscopy (Olympus BX 51M) at 100 X are presented in Figure 2. Examination of Figure 2 shows that the optical micrographs of the carburized in fluidized bed specimen P1 has the pores larges and irregulars than pores in the sample with the highest density, P2.

3.3. Porosity measurements

In Table 2 are presented the porosity measurements of P/M products calculated using the conventional method from density technique. Another method for porosity measurements was using an image processing software tool, Image J. Image J [23] is a free and useful image analysis software tool to analyse using filters, adjustments and Threshold binary function in detection the porosity. In [24-26], Image J was applied to study porosity in sintered P/M specimens. The images acquisition was carried out for non-etched samples using a digital camera coupled to optical microscope. By extrapolation the areas with pores using the function of Thresholding, the program generates the separate image only with porosity and can calculate it in percent. The porosity measurements result of carburized in fluidized bed samples using Image J software are presented in Table 2 and Fig. 3.

Table 2. *The porosity of analysed alloys in carburized in fluidized bed state*

Powder type	Porosity from conventional method (%)	Porosity from image analysis (%)
P_1	9.85	11.73
P_2	8.91	10.44

THE ANNALS OF "DUNAREA DE JOS" UNIVERSITY OF GALATI
FASCICLE IX. METALLURGY AND MATERIALS SCIENCE
Nº. 4 - 2021, ISSN 2668-4748; e-ISSN 2668-4756
Article DOI: https://doi.org/10.35219/mms.2021.4.07

The measurements of porosity resulted from density technique are ranging from 8.91% to 9.85%. The measurements of porosity resulted by using the Image J software are ranging from 10.44 % for 6.93 g/cm^3 to 11.73% for 6.98 g/cm^3. A correlation between higher density and a decreasing in porosity was established. The sample P2 had a lower porosity. Also, the Image J software can generate a 3D image of the surface for the carburized in fluidized bed samples presented in Fig. 4.

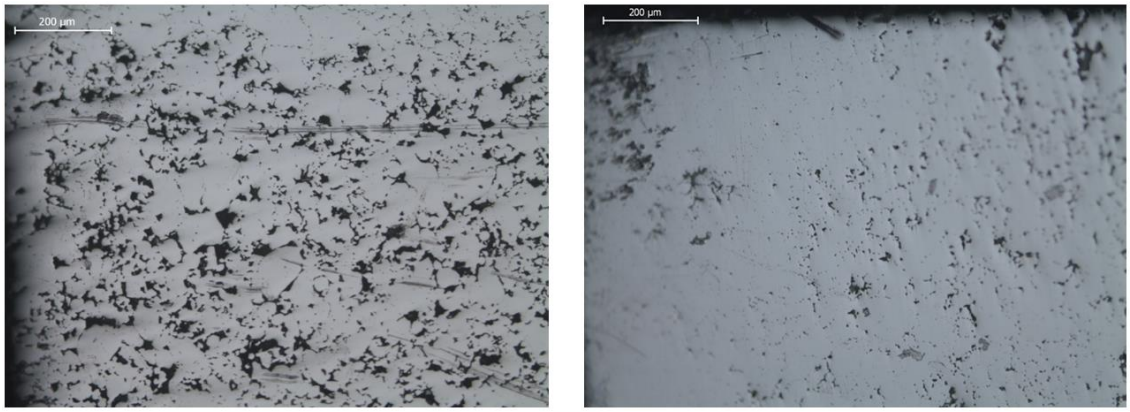

Fig. 2. *Micrographs of the non-etched carburized in fluidized bed samples a) P1; b) P2*

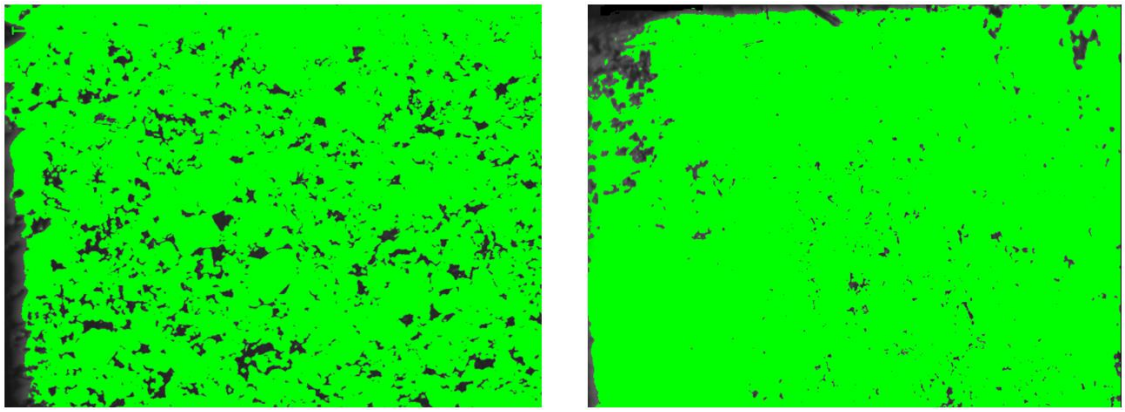

Fig. 3. *Processed images by using the image software for porosity measurements of carburized in fluidized bed samples: a) P1; b) P2*

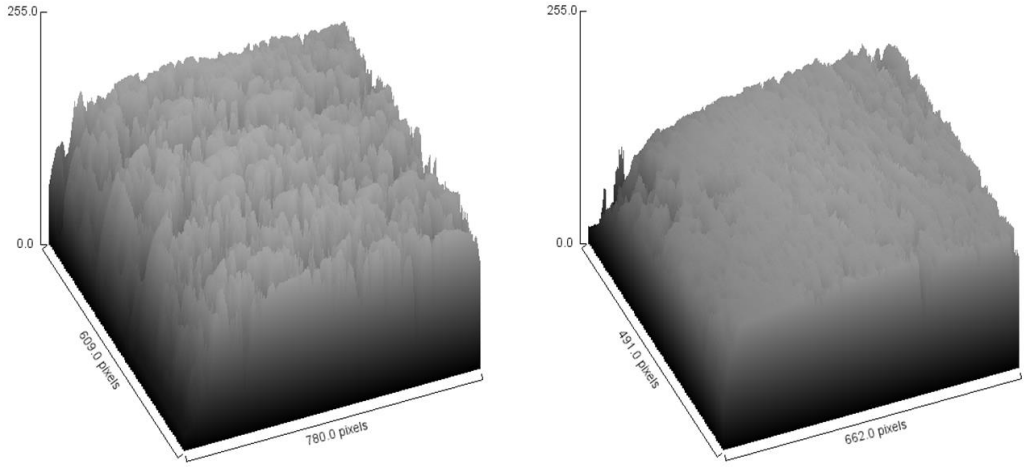

Fig. 4. *3D image of the surface for the carburized in fluidized bed samples, obtained using image software: a) P1; b) P2*

THE ANNALS OF "DUNAREA DE JOS" UNIVERSITY OF GALATI
FASCICLE IX. METALLURGY AND MATERIALS SCIENCE
Nº. 4 - 2021, ISSN 2668-4748; e-ISSN 2668-4756
Article DOI: https://doi.org/10.35219/mms.2021.4.07

4. Conclusions

The measurements of porosity in fluidized bed carburized state of analysed samples, using image analysis software - Image J was correlated to the density results obtained by geometrical method.

A correlation between higher density and a decreasing in porosity was established. The sample P2 had a lower porosity.

A correlation between the experimental and software data analysis was established, the porosity measured from image analysis was higher than from density technique due to the fact that only open porosity is considered in the image analysis technique, so the closed porosity is not accounted in the image analysis. An increase in the sintered and carburizing in fluidized bed density of the samples was correlated with a lower porosity and smaller pore size.

References

[1]. Narasimhan K. S., *Sintering of powder mixtures and the growth of ferrous powder metallurgy*, Materials Chemistry and Physics, vol. 67, p. 56-65, 2001.
[2]. Jang G. B., Hur M. D., Kang S. S., *A study on the development of a substitution process by powder metallurgy in automobile parts*, J Mater Process Technol, p. 110-115, 2000.
[3]. Hamiuddin M., *Correlation between mechanical properties and porosity of sintered iron and steels-a review*, Powder Metall. Int. 18, p. 73-76, 1986.
[4]. Wu M. W., Tsao L. C., Shu G. J., Lin B. H., *The effects of alloying elements and microstructure on the impact toughness of powder metal steels*, Materials Science and Engineering: A 538, p. 135-144, DOI: 10.1016/j.msea.2011.12.113, 2011.
[5]. Maheswari N., Ghosh Chowdhury S., Hari Kumar K. C., Sankaran S., *Influence of alloying elements on the microstructure evolution and mechanical properties in quenched and partitioned steels*, Materials Science and Engineering: A, 600, p. 12-20, 2014.
[6]. Wu M. W., Tsao L. C., Shu G. J., Lin B. H., *The effects of alloying elements and microstructure on the impact toughness of powder metal steels*, Materials Science and Engineering: vol. A 538, p. 135-144, 2012.
[7]. Trivedi S., Mehta Y., Chandra K., Mishra P. S., *Effect of carbon on the mechanical properties of powder-processed Fe–0·45 wt% P alloys*, Indian Academy of Sciences, vol. 35, part 4, p. 481-492, 2010.
[8]. Angel W. D., Tellez L., Alcala J. F., Martinez E., Cedeno V. F., *Effect of copper on the mechanical properties of alloys formed by powder metallurgy*, Materials and Design, vol. 58, p. 12-18, 2014.
[9]. Marucci M. L., Hanejko F. G., *Effect of copper alloy addition method on the dimensional response of sintered Fe-Cu-C steels*, Advances in Powder Metallurgy and Particulate Materials, MPIF, p. 1-11, 2010.
[10]. Dong Y., Jun L., Wen J., Jie S., Kunyu Z., *Effect of Cu addition on microstructure and mechanical properties of 15%Cr super martensitic stainless steel*, Mater Des, vol. 41, p. 16-22, 2012.
[11]. Takaki S., Fujioka M., Aihara S., Nagataki Y., Yamashita Y., Sano N., Adachi Y., Nomura M., Yaguchi K., *Effect of Copper on Tensile Properties and Grain-Refinement of Steel and its Relation to Precipitation Behavior*, Mater Trans, vol. 45, p. 2239-2244, 2005.
[12]. Bernier F., Plamondon P., Bailon J. P., Esperance G. L., *Microstructural characterisation of nickel rich areas and their influence on endurance limit of sintered steel*, Powder Metallurgy, vol. 54, issue 5, p. 559-565, 2011.
[13]. Sulowski M., *Structure and mechanical properties of sintered Ni free structural parts*, Powder Metallurgy, vol. 53, no. 2, p. 125-140, 2010.
[14]. Sanjay S. R., Milind M. S., Vikram V. D., *Effect of molybdenum addition on the mechanical properties of sinter-forged Fe Cu C alloys*, Journal of Alloys and Compounds 649, p. 988-995, 2015.
[15]. Mansoorzadeh S., Ashrafizadeh F., *The effect of thermochemical treatments on case properties and impact behaviour of Astaloy CrM*, Surface and Coatings Technology, vol. 192, issue 2-3, p. 231-238, 2005.
[16]. Kazior J., Janczur C., Pieczonka T., Ploszczak J., *Thermochemical treatment of Fe–Cr–Mo alloys*, *Surface and Coatings Technology*, vol. 151-152, p. 333-337, 2002.
[17]. Krauss G., *Principles of Heat Treatment of Steels*, *American Society for Metals*, ASM International, 2003.
[18]. Radomyselsk I. D., Zhornyak A. F., Andreeva N. V., Negoda G. P., *The pack carburizing of dense parts from iron powder*, Powder metallurgy and metal ceramics, vol. 3, p. 204-211, 1964.
[19]. Askaria M., Khorsand H., Mohamad Aghamiri, *Influence of case hardening on wear resistance of a sintered low alloy steel*, Journal of Alloys and Compounds, vol. 509, issue 24, p. 6800-6805, 2011.
[20]. Krauss G., *Microstructure residual stress and fatigue of carburized steels*, Proceedings of the Quenching and Carburizing, The Institute of Materials, p. 205-225, 1991.
[21]. Georgiev J., Pieczonka T., Stoytchev M., Teodosiev D., *Wear resistance improvement of sintered structural parts by C7H7 surface carburizing*, Surface and Coatings Technology, vol. 180-181, p. 90-96. 2004.
[22]. Sulowski M., *How processing variables influence mechanical properties of PM Mn steels?*, Powder Metallurgy Progress, vol. 7, no. 2, 2007.
[23]. ***, Image J software- https://imagej.nih.gov/ij/.
[24]. Marin M., Potecaşu F., Potecaşu O., Marin F. B., *Image Analysis Software for Porosity Measurements in Some Powder Metallurgy Alloys*, Advanced Materials Research, vol. 1143, p. 103-107, Trans Tech Publications, Ltd., 2017.
[25]. Dobrzanski L., Musztyfaga M., Actis Grande M., Rosso M., *Computer aided determination of porosity in sintered steels*, Archives of Materials Science and Engineering, vol. 38, no. 2., p. 103-11, 2009.
[26]. Dobrzanski L. A., Musztyfaga-Staszuk M., Luckos A., *The comparison of computer methods for porosity evaluation in sintered constructional steels*, Journal of Achievements in Materials and Manufacturing Engineering, vol. 61, no. 2, p. 395-402, 2013.

THE ANNALS OF "DUNAREA DE JOS" UNIVERSITY OF GALATI
FASCICLE IX. METALLURGY AND MATERIALS SCIENCE
Nº. 4 - 2021, ISSN 2668-4748; e-ISSN 2668-4756
Article DOI: https://doi.org/10.35219/mms.2021.4.08

CFD MODELING OF AERODYNAMIC CAR BRAKE COOLING SYSTEM

Florin-Bogdan MARIN, Mihaela MARIN
"Dunarea de Jos" University of Galati, Romania
e-mail: flmarin@ugal.ro

ABSTRACT

The objective of this experimental research is to identify solutions for an optimal cooling of the disks. The aerothermal brake cooling calculation is used to determine how the brake cooling process evolves. The techniques for simulating the dynamics of the CFD fluid allow us to simulate the cooling of the brakes in air current and then to compare the results obtained in the wind tunnel.

KEYWORDS: CFD, modeling, simulation, car brake, cooling

1. Introduction

The braking system is an important control system of an automotive. Computational Fluid Dynamics (CFD) is the part of CAE that analysis the fluid motion and heat transfer using numerical solution methods. This technology is used in many industries like aeronautical engineering, electronics engineering, HVAC engineering, automotive, medical research, power generation, chemical engineering and way more [1-13].

CFD can be used to simulate disc brake cooling system. There are some differences between aerothermal calculation and classical CFD calculation. These differences are located on the elements that will be coupled. As for the rest of the vehicle, the geometry preparation is similar to a simulation of external air flow. Aerothermal calculations on the brake proved to be complex and time-consuming for implementation, due to the large number of steps prior to the calculation of the cooling constant. The aerothermal brake cooling calculation is used to determine how the brake cooling process evolves. The techniques for simulating the dynamics of the CFD fluid allow to simulate the brakes cooling in air current and then to compare the results contained in the wind tunnel. In addition, given the expectation of this type of calculation, to prepare the parts of the front wheel assembly, which will be used later in the thermal coupling, a special care is required. The different meshing stage depending on the surfaces of the brake system components is a particular interest [14-20]. In the brake system, a major problem is the overheating between disc brake and brake pad. To avoid this process, the heat generated should be evacuated into the atmosphere.

Brake cooling aerothermal calculation is used in order to determine a constant related to brake cooling. Brake cooling simulation requires coupled simulations as well as coupled calculations. Front wheel air deflector poses an important place in better cooling the brakes as it orientates the flow of air in order to assure a better cooling. In this paper we aim to determine dimension of the front wheel air deflector for specific scenario.

2. Experimental procedure

In the first stage we prepare the models for aero, thermal and coupled calculations. These calculations require several preparation steps before a simulation is launched. For aerodynamic calculation, to clean the geometry of intersections of surfaces, lines and points is a necessary step. After the geometry is cleaned, the geometry is meshed, the conditions are set and the calculation is launched. In the case of thermal calculation, the geometry of the brake assembly is cleaned, the contacts between the PIDs are created, the conditions are set and then the calculations are launched. Finally, the two calculations are coupled and then released to determine the cooling of the brake. The brake cooling is calculated thermally, transiently and consequently an independent calculation is made.

The results of the brake cooling calculation are processed compared with the results obtained in the wind tunnel, where the physical product is tested at different wind speeds.

THE ANNALS OF "DUNAREA DE JOS" UNIVERSITY OF GALATI
FASCICLE IX. METALLURGY AND MATERIALS SCIENCE
Nº. 4 - 2021, ISSN 2668-4748; e-ISSN 2668-4756
Article DOI: https://doi.org/10.35219/mms.2021.4.08

The physical tests are performed by heating the disc, by repeated braking and acceleration in as short a time as possible to a temperature of 600 °C, maintaining this temperature for 4 minutes and then allowing it to cool in the air for 10 minutes until reaches ambient temperature (20 °C). We have simulated the cooling of car breaks in several situations. The brake cooling is calculated thermally, transiently and an independent calculation is made. The purpose of the simulations is to determine how the brakes are cooled for the general purpose of identifying methods to improve their cooling. The scenarios considered take into account extreme conditions of ambient temperature as well as disk temperature. The simulation setup takes into account, also, the rotation of the wheels. The surface on which the car (road) rests does not move - a matter that is not respected for the total replication of situations in reality. However, the influence of road traffic does not influence the cooling of the brakes as there is an important distance between the disc and the road. In this research, the following conditions are considered: car speed: 100 km/h, disc temperature of the brake: 400 °C, outdoor temperature: 20 °C and wind speed of 0 km/h.

3. Results and discussions

Fig. 1. Shows the 3D model considered at a real scale. In Figure 2 is presented the three variations of the dimension (depth) of air deflector.

Fig. 3 shows the temperature variation in a vertical plane at a distance of 5 mm from the brake disc. The fluid temperature distribution is also observed. The higher temperature is towards the back of the car and it is observed that in the space between the wheels, under the body, there is a temperature around 44 °C. If the car had an acute lower ground clearance, the temperature would have been higher. If there were plastic components (pipe guards, decorative elements) the relatively high temperature would influence both its strength and aging.

In Fig. 4 we observe the temperature distribution in a plane at 300 mm from the wheel plane in which the results show that the components of the front wheel braking elements will be better cooled than the rear ones. It follows that the geometry of the car must be intervened in order to improve the cooling of the rear wheel.

In Figures. 4 and 5 are observed that the fluid trajectories are different, as we previously concluded. This results in a different cooling.

In Fig. 6 is observed that the design of the rim allows a good cooling, acting as a fan, which allows the rapid air evacuation to cool the braking components.

In Fig. 7, which shows the temperature distribution in the front wheel area, it is observed that the air currents that are deviated from the side of the rim and the tire from the front, do not allow uniform cooling of the disc. It is observed that if the disk were arranged further inwards, the situation would change and the cooling would be better. However, there are other conditions related to the braking mechanism, wheel resistance, protection of the disc from rain and objects that can hit the disc (such as stones).

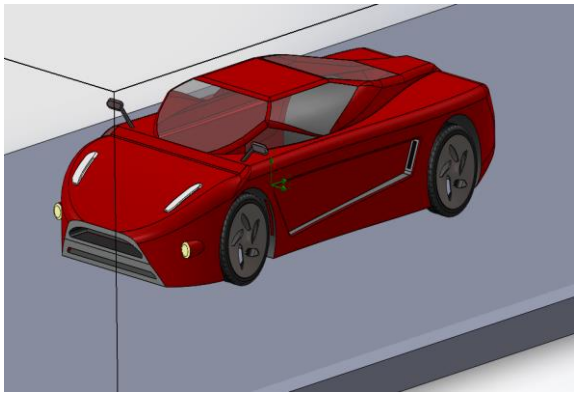

Fig. 1. *3D CAD model considered*

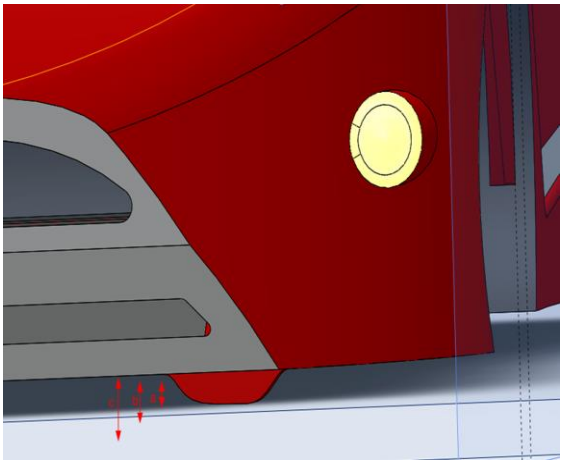

Fig. 2. *The three scenarios considered as dimensions for the front wheel deflector case a - 60 mm case b 80 mm and c 120 mm*

We considered three cases where the depth of the air deflector is 60 mm, 80 and 120 mm respectively (as seen in Figure 2). The results showed that the second case b, with the dimension of 80 mm mean better cooling of the brake disc with an average of 10 ºC degree for the scenario considered. The third case where de depth of deflector is 120 mm indicated worse cooling than a case and b case. It seems that the air is deflector to a region of the brake disc and the air is not director to the rim to the exterior of the car as it should.

THE ANNALS OF "DUNAREA DE JOS" UNIVERSITY OF GALATI
FASCICLE IX. METALLURGY AND MATERIALS SCIENCE
No. 4 - 2021, ISSN 2668-4748; e-ISSN 2668-4756
Article DOI: https://doi.org/10.35219/mms.2021.4.08

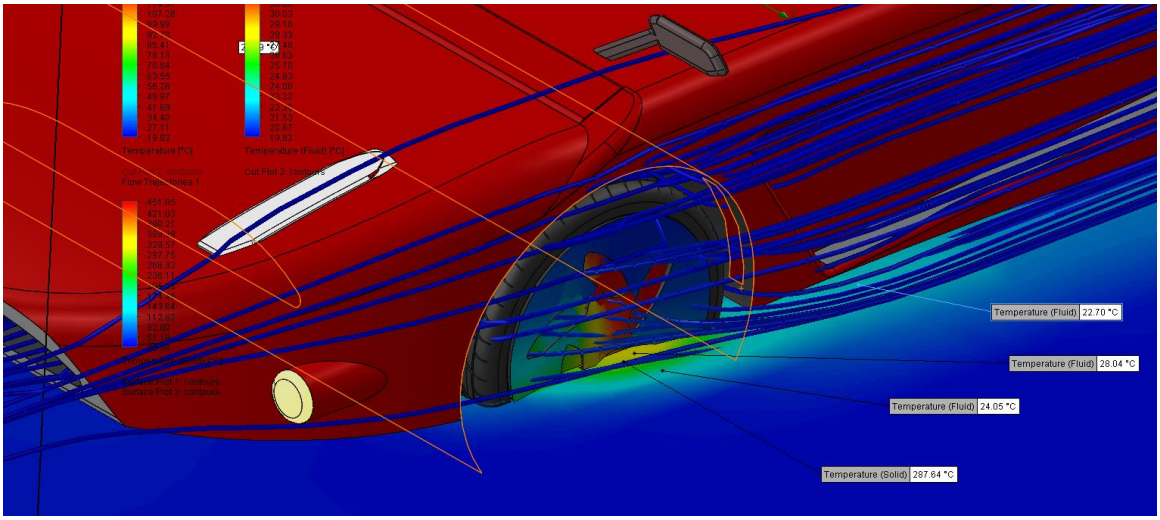

Fig. 3. *Fluid trajectories and temperature distribution*

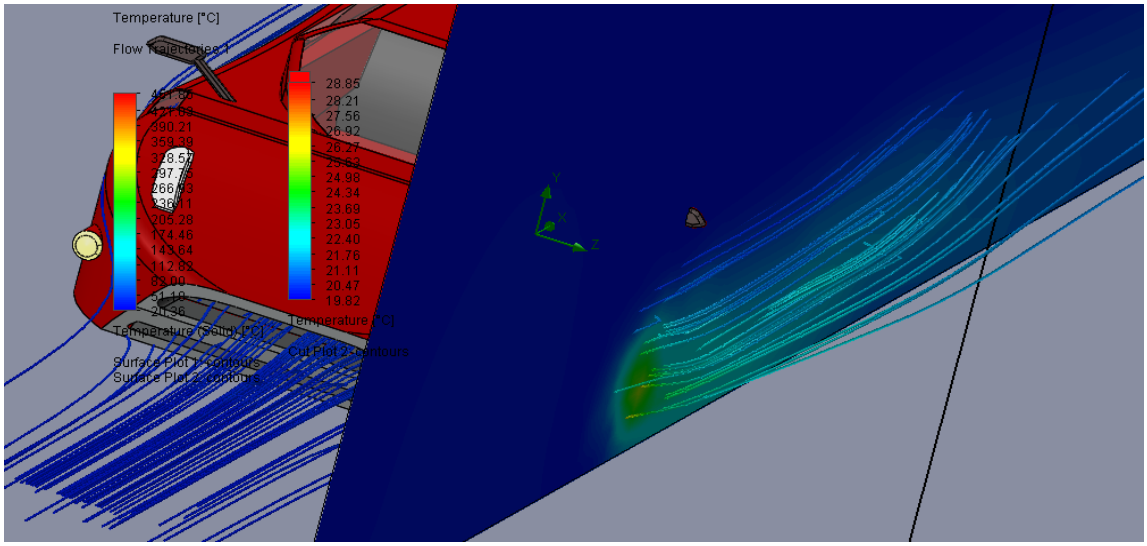

Fig. 4. *Temperature distribution in a horizontal plane at a distance of 200 mm from the ground*

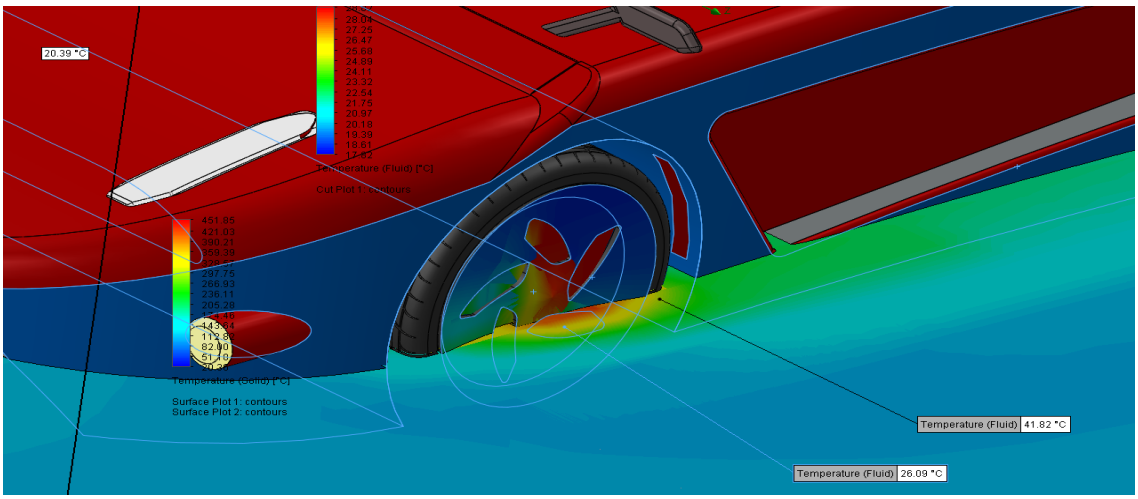

Fig. 5. *Temperature distribution in the front wheel area*

THE ANNALS OF "DUNAREA DE JOS" UNIVERSITY OF GALATI
FASCICLE IX. METALLURGY AND MATERIALS SCIENCE
Nº. 4 - 2021, ISSN 2668-4748; e-ISSN 2668-4756
Article DOI: https://doi.org/10.35219/mms.2021.4.08

4. Conclusions

The main conclusions are the following:

- Braking system cooling is an important objective both for the safe operation of the braking system and especially for not affecting other components.

- The brake disc heating determines the heat transfer to other components and is a particularly important part for the design of the braking system.

- From simulated scenario, it was observed that the rim design allowed a good cooling, acting as a fan, which allowed the rapid air evacuation to cool the braking components.

- The design of front wheel deflector is important taking into account the car body and rim dimensions.

- Further development should refer to compare different design of the deflector for different car speeds.

References

[1]. Silvestri L., *CFD modeling in Industry 4.0: New perspectives for smart factories*, Procedia Computer Science, vol. 180, p. 381-387, ISSN 1877-0509, 2021.

[2]. Wutz J., Waterkotte B., Heitmann K., Wucherpfennig T., *Computational fluid dynamics (CFD) as a tool for industrial UF/DF tank optimization*, Biochemical Engineering Journal, vol. 160, 107617, ISSN 1369-703X, 2020.

[3]. Moon H.-G., Park S., Ha K., Jeong J.-H., *CFD-Based In-Depth Investigation of the Effects of the Shape and Layout of a Vortex Generator on the Aerodynamic Performance of a Multi-MW Wind Turbine*, Appl. Sci. 2021, 11, 10764. https://doi.org/10.3390/app112210764, 2021.

[4]. Pavlin-Premrl D., Sethu R., Nemes A., Mohammadzadeh M., Monajemi S., Brian S., Campbell C. V., *Computational Fluid Dynamics in Intracranial Atherosclerosis - Lessons from Cardiology: A Review of CFD in Intracranial Atherosclerosis*, Journal of Stroke and Cerebrovascular Diseases, vol. 30, issue 10, 106009, ISSN 1052-3057, 2021.

[5]. Zobaer T., Sutradhar A., *Modeling the effect of tumor compression on airflow dynamics in trachea using contact simulation and CFD analysis*, Computers in Biology and Medicine, vol. 135, 104574, ISSN 0010-4825, 2021.

[6]. Perinajov R., Juffermans J., Westenberg J. M., Roel L. F., Palen Pieter J., Boogaard Hildo J., Lamb Sas a Kenjeres, *Geometrically induced wall shear stress variability in CFD-MRI coupled simulations of blood flow in the thoracic aortas*, Computers in Biology and Medicine, vol. 133, 104385, ISSN 0010-4825, 2021.

[7]. Shoeibi S., Kargarsharifabad H., Rahbar N., Ahmadi G., Reza M. S., *Performance evaluation of a solar still using hybrid nanofluid glass cooling-CFD simulation and environmental analysis*, Sustainable Energy Technologies and Assessments, vol. 49, 101728, ISSN 2213-1388, 2022.

[8]. Zhu X., Dai Y., Ma F., *CFD modelling and numerical simulation on windage power loss of aeronautic high-speed spiral bevel gears*, Simulation Modelling Practice and Theory, vol. 103, 102080, ISSN 1569-190X, 2020.

[9]. Fujii K., *Progress and future prospects of CFD in aerospace-Wind tunnel and beyond*, Progress in Aerospace Sciences, vol. 41, issue 6, p. 455-470, ISSN 0376-0421, 2005.

[10]. Xia H., Tucker P. G., Dawes W. N., *Level sets for CFD in aerospace engineering*, Progress in Aerospace Sciences, vol. 46, issue 7, p. 274-283, ISSN 0376-0421, 2010.

[11]. Wang C., Li F., Ding Z., Zhang L., *Numerical Simulation of Hypersonic Flow Around an Aerospace Plane by Parallel RANS based CFD*, Procedia Engineering, vol. 61, p. 23-27, ISSN 1877-7058, 2013.

[12]. Rizzi A., Jluckring J. M., *Historical development and use of CFD for separated flow simulations relevant to military aircraft*, Aerospace Science and Technology, vol. 117, 106940, ISSN 1270-9638, 2021.

[13]. Wang M., Wang Y., Tian W., Qiu S., Su G. H., *Recent progress of CFD applications in PWR thermal hydraulics study and future directions*, Annals of Nuclear Energy, vol. 150, 107836, ISSN 0306-4549, 2021.

[14]. Seshaiah T., Vasu B., Vijaya K., Reddy K., Bridjesh P., *Analysis on air craft winglet at different angles by using CFD simulation*, Materials Today: Proceedings, ISSN 2214-7853, 2021.

[15]. Garcia-Ribeiro D., Flores-Mezarina J. A., Bravo-Mosquera P. D., Cerón-Muñoz H. D., *Parametric CFD analysis of the taper ratio effects of a winglet on the performance of a Horizontal Axis Wind Turbine*, Sustainable Energy Technologies and Assessments, vol. 47, 101489, ISSN 2213-1388, 2021.

[16]. Zurin W. M., Talib R. J., Ismail N. I., *Thermal Analysis on Motorcycle Disc Brake Geometry*, International Conference on Applied Physics and Engineering (ICAPE2016) AIP Conf. Proc. 1875, 030022-1-030022-8, doi: 10.1063/1.4998393, 2017.

THE ANNALS OF "DUNAREA DE JOS" UNIVERSITY OF GALATI
FASCICLE IX. METALLURGY AND MATERIALS SCIENCE
Nº. 4 - 2021, ISSN 2668-4748; e-ISSN 2668-4756
Article DOI: https://doi.org/10.35219/mms.2021.4.09

THE IMPACT OF VARIOUS FUELS ON PARTICULATE EMISSIONS FOR A COMPRESSION IGNITION ENGINE EQUIPPED WITH A DIESEL PARTICULATE FILTER

Bogdan Manolin JURCHIȘ
Technical University of Cluj-Napoca, Romania
e-mail: bogdan.jurchis@auto.utcluj.ro

ABSTRACT

The aim of this research was to highlight the impact of using different types of fuels on particulate emissions and also on the operation on particulate filters on diesel engines. For all the results obtained from the experimental tests, comparative studies were performed to find the optimal fuel mixture that can be used in order to obtain the optimal performance of the particle filter, without affecting the engine performance. Following the initial tests performed without DPF, the case with the highest smoke emission value (2000 1/min) was identified. For this case, continuous measurement tests were then performed. For this reason, a more detailed analysis was made only for this case.

KEYWORDS: particulate emissions, particulate filters, smoke emission

1. Introduction

One of the main issues of diesel engines is related to particulate emission which results from the combustion process. They are divided into several categories depending on their size. Thus, there are the so-called "TSPs" which represent all suspended particles in the air, PM10 are inhalable suspended particles so-called "coarse fractions" with a diameter between 10 µm and 2.5 µm, PM2.5 also called fine inhalable particles with dimensions less than 2.5 µm. Another category is ultrafine particles, which are denoted by PM0.1 and represent particles smaller than 0.1 µm. The last category are nanoparticles, their size is less than 0.05 µm [1, 2].

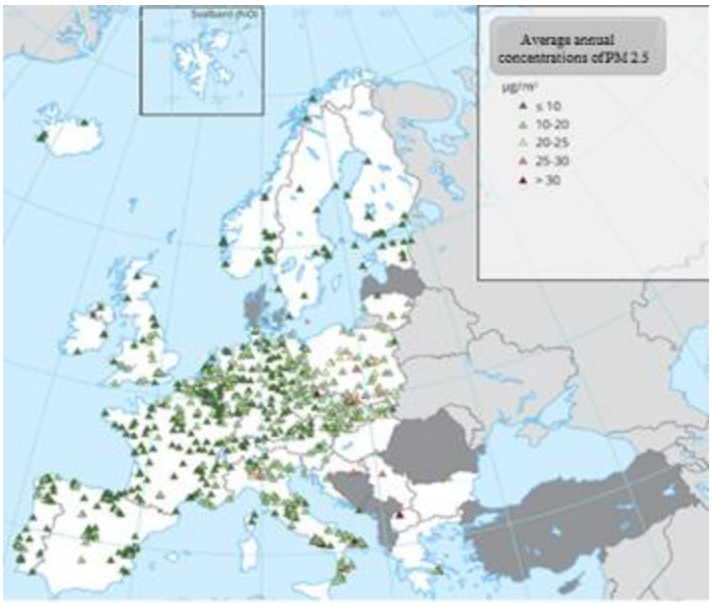

Fig. 1. *Average annual PM2.5 concentrations in Europe (2019)* [12]

THE ANNALS OF "DUNAREA DE JOS" UNIVERSITY OF GALATI
FASCICLE IX. METALLURGY AND MATERIALS SCIENCE
Nº. 4 - 2021, ISSN 2668-4748; e-ISSN 2668-4756
Article DOI: https://doi.org/10.35219/mms.2021.4.09

These PM emissions are continuously monitored by the emission monitoring stations. The highest concentration of PM is found in large urban areas or in industrial areas. The average annual concentrations of PM2.5 recorded by the European Environment Agency for 2019 in [µg/m^3] can be found in Figure 1.

The emission analysis was reduced for the cases in which biodiesel was used in the mixture at a speed of 2000 1/min. Experimental research has shown that the presence of oxygen in the fuel structure increases the supply of oxygen in the combustion process and has beneficial effects on smoke emissions.

2. Materials and methods

The experimental tests were performed on the single-cylinder engine AVL 5402 of the Testecocel laboratory, from The Department of Automotive Engineering and Transports of Cluj Napoca. The technical data of the engine can be found in Fig. 2. DPF loading with solid particles was monitored with a pressure sensor adapted before the diesel particulate filter. As the number of particles (PM1, PM2.5, PM10 or higher) in the filter increased, there was an increase of pressure before it. Because the sensor provided a relative pressure value, the impact of variations in atmospheric pressure was eliminated. To achieve this goal, a particle filter and a noise attenuator (Fig. 3). have been adapted to the exhaust system. Two particulate filters with asymmetrical square channels were used for experimental tests. The tests performed in this paper focused on determining the amount of soot loading of the particulate filter walls for several mixtures.

Parameter	Value	M.U.
Number of cylinders	1	[-]
Bore x Stroke	85 x 90	[mm]
Compression ratio	17.1	[-]
Maximum power	6	[kW]
Rated speed	4200	[min^{-1}]
Combustion system	4 valve	[-]
Displacement	510.7	[cm^3]

Fig. 2. *AVL 5402 Engine Technical Data*

In the first stage, measurements were made only with diesel (D100) at 3 different speeds and constant load to identify the least favorable point in terms of PM emissions. The second stage comprised performing tests with 20% biodiesel (B20) in the mixture and in the third stage experimental tests with 30% biodiesel (B30) in the mixture were performed. The formation of the mixture was performed by applying a formula for the exact calculation of the amount of fuel to be used in the mixture to reach the percentage of biodiesel of 20% and 30%, respectively. In order to determine the additional volume, it was taken into account that in D100 is already a percentage of 6.5% biodiesel. The soot load analysis was performed by continuous testing (engine operation without interruption) for 5 hours at 2000 rpm. The injection parameter values were taken from the injection map provided by the manufacturer of the engine (Table 1).

Fig. 3. *Diesel particulate filters mounted on the experimental engine AVL 5402*

Table 1. *Parameters used for experimental tests*

Fuels	Speed [1/min]	Ramp Pressure [bar]	Q_Pilot [mm^3]	Preinjection advance [°RAC]	Q_Main [mm3]	Main injection advance [°RAC]
D100, B20, B30	2000	700	2	22.125	21.6	8.625

THE ANNALS OF "DUNAREA DE JOS" UNIVERSITY OF GALATI
FASCICLE IX. METALLURGY AND MATERIALS SCIENCE
Nº. 4 - 2021, ISSN 2668-4748; e-ISSN 2668-4756
Article DOI: https://doi.org/10.35219/mms.2021.4.09

3. Results and discussion

There are multiple causes of the decrease in soot emissions as the oxygen content of the fuel increases. A first cause is that the presence of oxygen inhibits the formation of soot precursors in fuel-rich areas (by preventing carbon from entering the reactions that lead to their formation) and directly forms CO and CO_2, respectively, which makes a number of atoms available. for soot formation to decrease [3, 5]. Another cause is that oxygen leads to an increase in the temperature of the flame [6], which amplifies the oxidation of soot during the combustion process. If in the case of diesel, in the phase of diffusive combustion, an intense movement of the air is necessary to ensure the oxygen necessary for the oxidation of the soot, in the case of biodiesel this is compensated by the presence of oxygen in its structure. As a result, due to the fact that the testing was performed under the same conditions, soot emissions decreased as the percentage of biodiesel increased.

At the same time, it is highlighted that the stoichiometric ratio of biodiesel is lower, which under the conditions of the same air mass has the effect of reducing the rich regions during the combustion process [7]. In addition, it was found that, compared to the combustion of diesel, the combustion of biodiesel and diesel mixtures starts faster due to the reduction of the self-ignition delay caused by a higher cetane number, but also by an advance of the injection. Even if the higher viscosity disadvantages the mixture formation process (in this case, an advantage for biodiesel and diesel mixtures is that the load is reduced which negatively affects the self-ignition delay of diesel). This leads to more complete and uniform combustion of the fuel and thus to a decrease in soot emissions.

The decrease in PM is also due to the fact that biodiesel contains fewer aromatic hydrocarbons and does not contain Sulphur, the aromatic hydrocarbons being considered the precursors of solid particles [8]. The favourable factor for the formation of solid particles is a rich mixture followed by incomplete combustion resulting higher smoke emissions. The presence of oxygen in biodiesel also improves the combustion process through the chemical reaction that is achieved through the presence of oxygen, so oxygen molecules combine with soot molecules that are formed mostly of carbon resulting in CO_2.

For the analysed cases (Fig. 4) following tests performed, a relative decrease of the smoke emissions resulted after 5 hours of continuous operation with biodiesel mixture, at the speed of 2000 1/min as follows:

- the value of the differential pressure related to the charge of the particulate filter was 22.56% lower for B20 and 31.28% lower for B30 compared to D100;
- the value of the differential pressure was lower by 11.25% for B30 compared to B20.

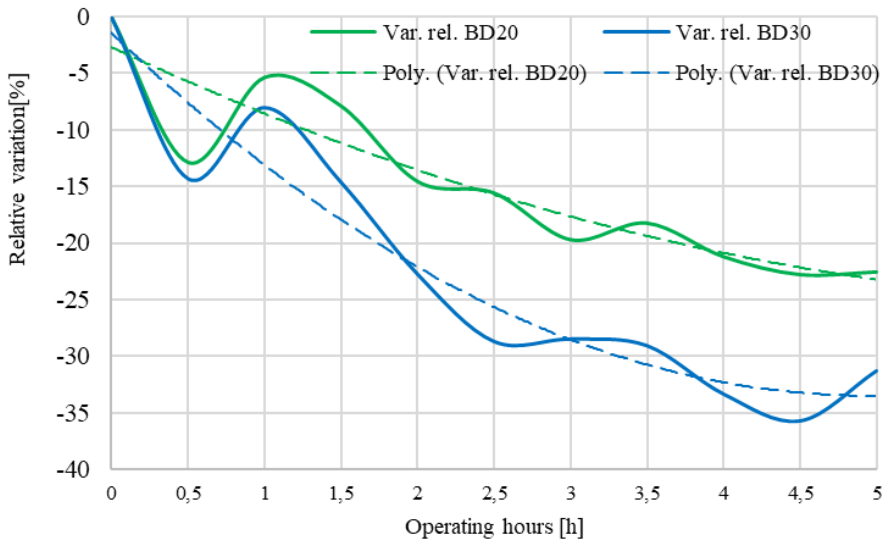

Fig. 4. *Relative polynomial variations of pressure drops for B20 and B30 related to D100 [%]*

The measured value of the pressure difference on the filter, after 5 hours of testing, was 19.5 mbar for D100, 15.1 mbar for B20 and 13.4 mbar (Fig. 5). Specialty literature confirms the results of experimental tests on the reduction of solid particulate emissions in direct proportion to the increase in the percentage of biodiesel in the mixture [9-11].

THE ANNALS OF "DUNAREA DE JOS" UNIVERSITY OF GALATI
FASCICLE IX. METALLURGY AND MATERIALS SCIENCE
Nº. 4 - 2021, ISSN 2668-4748; e-ISSN 2668-4756
Article DOI: https://doi.org/10.35219/mms.2021.4.09

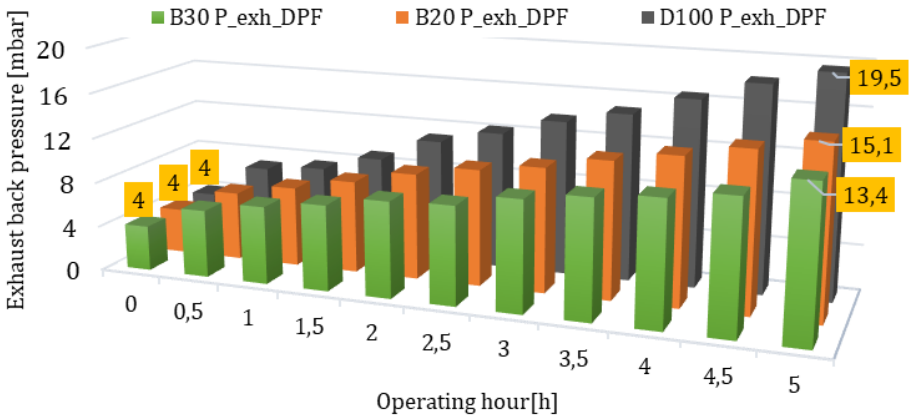

Fig. 5. *Variation of exhaust backpressure during 5 hours of continuous testing*

In order to be able to analyse in even more detail the load of the diesel particulate filters apart from the experimental test, a microscopic study of the particulate filter channels used in the experimental tests was performed. It was possible to analyse the channels of the diesel particulate filter in detail due to the high resolution that the device has and due to the fact that the optical zoom can be set up to 100 X. The images captured with the microscope were exported on an LED screen for a detailed analysis. In the first phase, the channel of the new particle filter was analysed and dimensioned (Fig. 6). As an element of analysis, the microscopically studied channel was chosen so as to be exactly in the same area of the DPF for all 3 cases studied as seen in Figure 6. The size of a cell following the measurements was 1.5 mm and the wall thickness was 0.225 mm.

Fig. 6. *Filter channels before the experimental tests and the area chosen for the microscopic study*

The objective of this microscopic research was to highlight the impact of various fuels on the loading of soot channels, but also to compare the results obtained experimentally with the results obtained by microscopic research. This impact was assessed by the effective measurement of the soot layer deposited on the channels with the help of Motic software.

The data obtained from microscopic measurements confirmed the results and the trend obtained in experimental tests. The first microscopic analysis was performed for D100 (Figure 7). From the detailed analysis that was transposed on a high-resolution LED screen it was observed that the maximum thickness for the soot layer deposited on the edge of the filter walls (referring to all 3 analysed cases D100, B20 and B30), was achieved for D100. Detailed microscopic analysis of the filter channel resulted in a thickness of 581 μm for the soot layer deposited in the filter. It is necessary to specify that these deposits were made without any regeneration during the entire experimental testing process. Microscopic analysis of the DPF channels for B20 led to lower thicknesses than the D100 for the soot layer, as can be seen in Figure 8. It is clear that with the increase of the percentage of biodiesel, the average thickness for the soot layer also decreased, having a maximum size for the soot layer of 441 μm. For the B30 case, the trend of decreasing soot mass-produced in the particulate filter is very pronounced. It can be seen from Figure 9 that the maximum layer size was up to 300 μm, which represent almost half of the soot deposited for B30 compared to D100.

THE ANNALS OF "DUNAREA DE JOS" UNIVERSITY OF GALATI
FASCICLE IX. METALLURGY AND MATERIALS SCIENCE
Nº. 4 - 2021, ISSN 2668-4748; e-ISSN 2668-4756
Article DOI: https://doi.org/10.35219/mms.2021.4.09

Fig. 7. *Microscopic analysis of DPF channels after experimental tests for D100*

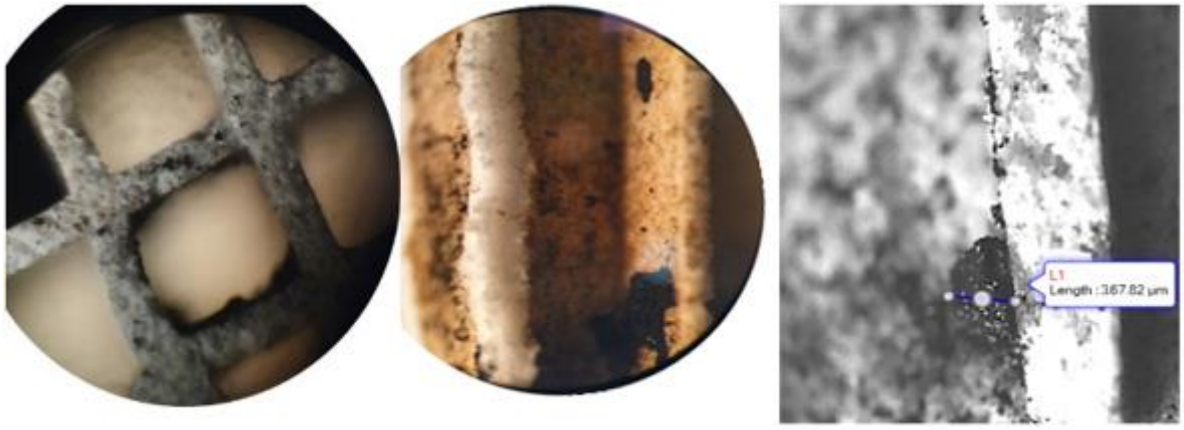

Fig. 8. *Microscopic analysis of DPF channels after experimental tests for B20*

Fig. 9. *Microscopic analysis of DPF channels after experimental tests for B30*

4. Conclusions

The main points and conclusions that emerge from this research, after the interpretation and analysis of data obtained from theoretical and experimental research are the following:

- for the cases analysed with DPF mounted on the exhaust, at a speed of 2000 1/min, for B20 the smoke emissions were 22.56% lower, respectively 31.28% for B30 compared to D100;

- soot emissions for B30 compared to B20 were lower by 11.25%;

- the measured value of the differential pressure on the particulate filter, after testing, was 19.5 mbar for D100, 15.1 mbar for B20 and 13.4 mbar for B30. Thus, it could be concluded that a higher percentage

of biodiesel in the mixture leads to a slower soot loading of the particulate filter;

- the trend of soot emissions is directly proportional to the total pressure drop. Thus, for D100 there was an increase of 25.12% in soot emissions compared to B20, respectively by 47.5% compared to B30;

- the data obtained from microscopic measurements confirmed the results and the trend obtained in experimental and numerical research. Microscopic analysis of the DPF channels for B20 led to lower thicknesses than the D100 for the soot layer. It is obvious that with the increase of the percentage of biodiesel, the average thickness for the soot layer also decreased, having a maximum size for the soot layer of 441 μm. For the B30 case, the decreasing trend of the soot mass produced in the particle filter is very accentuated, the maximum size of the deposited layer being up to 300 μm.

Acknowledgements

The data presented in this paper were obtained from my PhD thesis "Studies and research on improving the operation of particulate filters in the use of various fuels" F-CA-39032/23.06.2021. I would like to thank AVL company for the support provided in this research.

References

[1]. ***, www.epa.gov, Particulate Matter (PM) Basics 2015.
[2]. ***, *Environmental Protection Agency.: Particulate Matter (PM10) Trends | National Air Quality: Status and Trends of Key Air Pollutants | US EPA n.d*.
[3]. Mueller C. J., Martin G. C., *Effects of oxygenated compounds on combustion and soot evolution in a DI diesel engine: broadband natural luminosity imaging*, SAE Transactions, 2002.
[4]. Rakopoulos C. D., Hountalas D. T., Zannis T. C., Levendis Y. A., *Operational and environmental evaluation of diesel engines burning oxygen-enriched intake air or oxygen-enriched fuels: a review*, SAE Transactions, 2004.
[5]. Seong H. J., Boehman A. L., *Impact of Intake Oxygen Enrichment on Oxidative Reactivity and Properties of Diesel Soot*, Energy & Fuels, vol. 25, 2011.
[6]. Jha S. K., Fernando S., To S. D. F., *Flame temperature analysis of biodiesel blends and components*, Fuel, vol. 87, 2008.
[7]. Cheng A. S., Upatnieks A., Mueller C. J., *Investigation of the impact of biodiesel fuelling on NOx emissions using an optical direct injection diesel engine*, International Journal of Engine Research, vol. 7, 2006.
[8]. Wang Y., Liu H., Lee C. F. F., *Particulate matter emission characteristics of diesel engines with biodiesel or biodiesel blending: A review*, Renewable and Sustainable Energy Reviews, vol. 64, 2016.
[9]. Song H., Tompkins B. T., Bittle J. A., Jacobs T. J., *Comparisons of NO emissions and soot concentrations from biodiesel-fuelled diesel engine*, Fuel, vol. 96, 2012.
[10]. McGill R., *et al.*, *Emission performance of selected biodiesel fuels*, SAE Transactions, 2003.
[11]. Sze C., *et al.*, *Impact of test cycle and biodiesel concentration on emissions*, SAE Transactions, 2007.
[12]. ***, *Annual mean PM2.5 concentrations in 2019*, European Environment Agency n.d.

THE ANNALS OF "DUNAREA DE JOS" UNIVERSITY OF GALATI
FASCICLE IX. METALLURGY AND MATERIALS SCIENCE
Nº. 4 - 2021, ISSN 2668-4748; e-ISSN 2668-4756
Article DOI: https://doi.org/10.35219/mms.2021.4.10

RESEARCHES ON SOOT FILTRATION PROCESS BY COMPARING SIMULATION AND EXPERIMENTAL TESTS

Bogdan Manolin JURCHIȘ
Technical University of Cluj-Napoca, Romania
e-mail: bogdan.jurchis@auto.utcluj.ro

ABSTRACT

In this paper, the main objective of using numerical simulation was to highlight and analyse details that are very difficult to highlight through experimental tests. The development of the simulation model was also done for predictive purposes. In other words, after validation of the model, it can be used to estimate the filter load in other conditions than the experimental ones, respectively to evaluate how the particulate filter affects the operation of the internal combustion engine. In order to achieve the desired result, the creation of the model was done in two stages, the first stage was the creation of a model containing all the components of the engine, except the particle filter in order to identify the parameters of the combustion process and pollutant emissions - model validated on the basis of the indicated pressure curves, and the second stage was to complete the initial model with a particle filter and validate it from the point of view of the pressure drop, respectively of the engine performance, the aim was to obtain a trend, respectively values similar to the experimental ones.

KEYWORDS: simulation model, combustion engine, pollutant emissions

1. Introduction

The soot particles resulting from the combustion process are microscopic carbon particles. Based on the analysis with an electron microscope, it is found that the soot particles are arranged randomly and that they have a certain degree of overlap. The size of the primary particles and their degree of overlap depends on quantity of fuel injected and also about the initial conditions regarding combustion process. Approximately 0.5% of the mass of fuel is emitted as very small solid particulates matter with a diameter of about 0.1 μm [1]. Soot is produced during pyrolysis at high temperatures [2, 3]. Figure 1 shows a micrograph of the Diesel soot in which particles can be observed, consisting of spherical agglomerates. Due to the extremely small size of the solid particles, it was necessary to create a simulation model for a better highlight the amount of soot deposited in the particle filter.

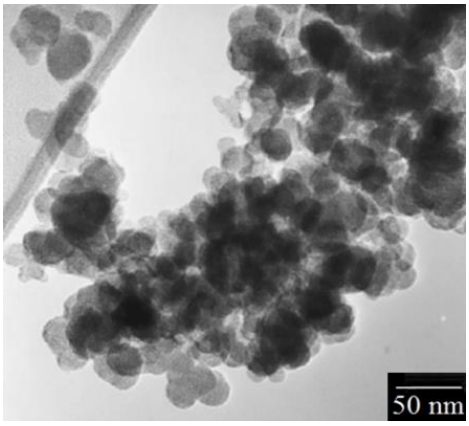

Fig. 1. *Soot micrograph consisting of groups of spherical particles* [4]

THE ANNALS OF "DUNAREA DE JOS" UNIVERSITY OF GALATI
FASCICLE IX. METALLURGY AND MATERIALS SCIENCE
N°. 4 - 2021, ISSN 2668-4748; e-ISSN 2668-4756
Article DOI: https://doi.org/10.35219/mms.2021.4.10

The DPF model implemented in BOOST combines in a single global solution detailed and pragmatic approaches for the flow of filtration and regeneration. It allows the user to take into account the ash or not, to choose the structure of his cups and also to use different materials for the particle filter on which the simulations are performed. For the simulation model created in this doctoral dissertation, a model of square cell particle filters was used in which a pair of inlet and outlet channels, channels loaded with soot and ash are presented. In the AVL BOOST program, different geometric shapes of the input channel were studied, namely: square, hexagonal, octagonal, rectangular. The soot is divided into two distinct layers: a deep layer and an outer layer, therefore the model made distinguishes between the soot located in the porous wall of the filter and the soot formed at the surface of the channel. An increased soot burning rate can be simulated in the deep layer by applying catalytically supported regeneration mechanisms. The presence of a layer of ash causes a pressure drop because it induces an additional flow resistance and a front flow surface [5]. In models where soot is described by a depth layer and a filtration layer, the ash layer can be understood as a barrier between the two layers of soot. Thus, soot cannot be stored in the deep layer as long as a layer of ash is present. The existence of an ash plug leads to a reduced filtration efficiency and therefore to an additional pressure drop. The actual filter length is also reduced by the size of the ash accumulations in the filter channels. A time finding for the whole filtration process based on the simulations, especially for the flow rates and for the increase of the soot layer, revealed that the gas phase processes can be assumed to be constant. The thickness of the soot layer, from the depth filtration layer of a channel with 4 filter walls, the height of the soot layer and the thickness of the ash layer δ_{ac} were calculated with the relation [6]:

$$\delta_{sd} = \frac{m_{sd} \cdot A_{front}}{n_1 \cdot \rho_{sd}} \cdot \frac{1}{n_{fw} d_1} \quad (1)$$

where: m_{sd} - represents the soot loading in the deep layer; A_{front} - the front surface of the filter; n_1 - number of input channels; ρ_{sd} - soot density in the deep layer; n_{fw} - number of active filtered walls; d_1 - diameter of the inlet channel.

2. Materials and methods

The simulation model created in AVL BOOST is based on the experimental engine AVL-5402 used in experimental research. The technical data provided by the manufacturer of the engine was used to create the simulation model. The model created in AVL BOOST fully complied with the parameters and related connections that were on the experimental model (Fig. 2). The simulation process consisted of the creation in the first phase of the single-cylinder engine model used in the experimental research in order to be able to extract the data regarding the gas flow resulting from the combustion process. The second phase consisted of creating and adapting a particle filter on the exhaust system defining each parameter separately. The "DPF" particle filter was modeled to highlight the correlation between the quantity of soot produced, the model of the channels, the channel structure, and the blend of fuel used in the research process.

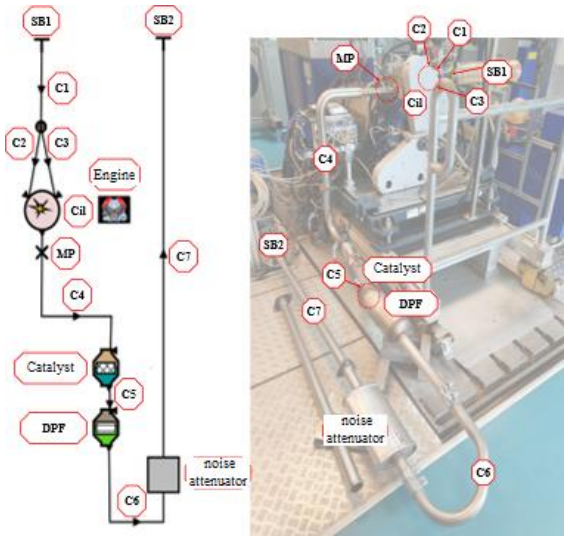

Fig. 2. *The simulation model created and the experimental engine equipped with DPF*

THE ANNALS OF "DUNAREA DE JOS" UNIVERSITY OF GALATI
FASCICLE IX. METALLURGY AND MATERIALS SCIENCE
Nº. 4 - 2021, ISSN 2668-4748; e-ISSN 2668-4756
Article DOI: https://doi.org/10.35219/mms.2021.4.10

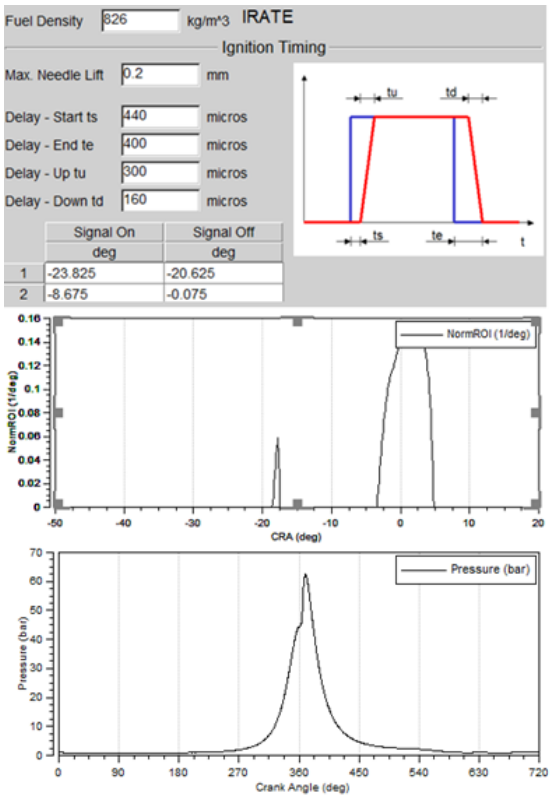

Fig. 3. *Input data for injection parameters*

The comparison of the simulation results was performed by overlapping the experimental data with those obtained in the simulation. The amount of fuel injected per cycle differs depending on the engine speed amount which is changed depending on the operating speed. The model used for combustion process was AVL MCC MODEL with this model it was possible to predict the amount of soot produced in relation to the amount of fuel injected [7]. In this model, in addition to the amount of fuel injected through the injector nozzles, it was necessary to perform synchronization with injection times and injector opening times. Injector opening times for pilot injection and main injection were controlled by an ON/OFF signal, which is in agreement with the delay of opening the injector. The main injector nozzle opening parameters are presented in Figure 3

The simulation model created was validated by comparing the pressure curves at 2000 1/min (Fig. 4) between the experimental case and the simulation case using diesel fuel, given the fact that at this speed both experimental tests were performed, as well as tests run by simulation. In order to validate the model, it was intended that the input values used for the simulation case be as similar as possible to the input data from the experimental case in order to create a valid model for the simulation. Although there is a small difference between the 2 pressure curves, the model was considered valid given that these differences are below 0.5% so we have an almost complete overlap of the pressure curves.

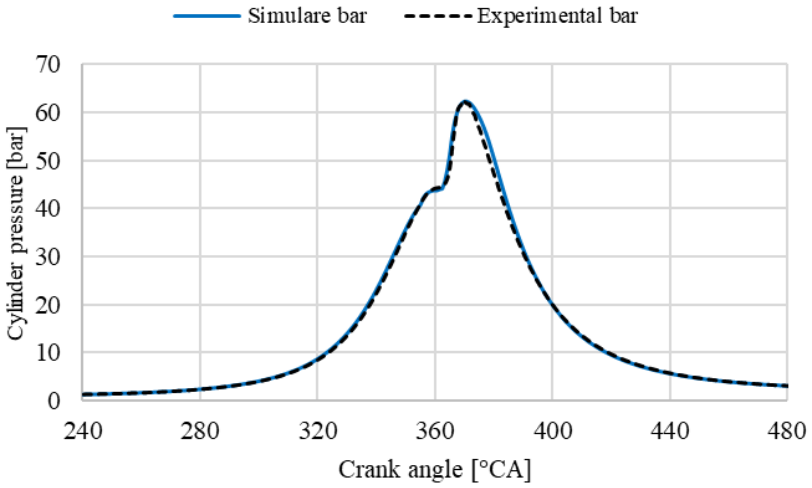

Fig. 4. *Comparison of pressure curves at 2000 [1/min]*

3. Results and discussion

In order to create a model capable of simulating the exhaust gas after-treatment process (Fig. 5) the boundary conditions for the inlet and outlet channels of the particulate filter system had to be defined. At the inlet, the mass gas flow obtained after simulating the combustion process was specified the pressure and boundary conditions for the exit of the filter were specified, the conditions of adiabatic gasodynamic resistance had to be defined in order not to change the thermal gradient or the species of the gas mass fractions. The following data were required for modeling the inlet to the exhaust after-treatment

THE ANNALS OF "DUNAREA DE JOS" UNIVERSITY OF GALATI
FASCICLE IX. METALLURGY AND MATERIALS SCIENCE
Nº. 4 - 2021, ISSN 2668-4748; e-ISSN 2668-4756
Article DOI: https://doi.org/10.35219/mms.2021.4.10

system: definition of the main dimensions of the DPF (monolith dimensions and monolith volume), mass gas flow, temperature, molar fraction of the exhaust gas and the solid mass fraction (Fig. 6). This simulation was followed by pressure drops depending on the degree of filter loading.

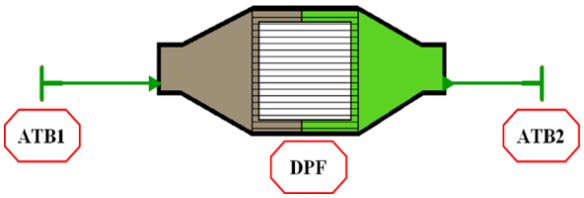

Fig. 5. *The DPF model created in AVL BOOST*

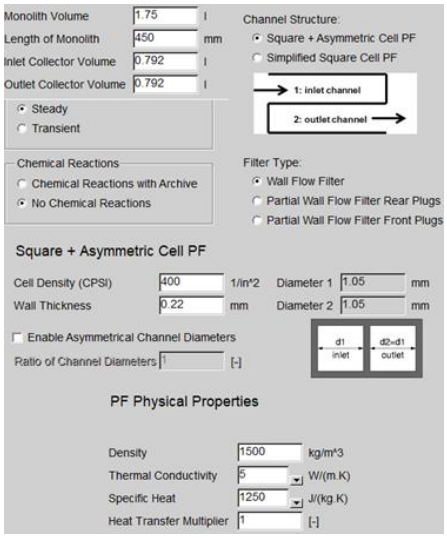

Fig. 6. *Parameter used to create the simulation model*

The discretization of the model was done by assigning the correction factor "Grid Shape Factor = 1" and by dividing the model axially into 100 measurement points, points that are equal as can be seen in Figure 7. These points determined the number of cells that entered the DPF simulation calculation. The physical properties of the particle filter that were introduced to create the model were necessary to be able to observe its thermal behavior, especially the heat transfer that takes place between the walls of the filter. All the physical properties of the filter, its specific density, and heat have been introduced, so that the heat transfer that takes place between the walls of the particle filter can be calculated.

The simulation aimed to highlight, based on the model created and validated in AVL Boost, the total mass of soot emitted in 5 hours of operation for the 3 fuels analysed (D100 - means pure diesel, B20 - means pure diesel with 20 % of biodiesel in blend and B30 means pure diesel with 30 % of biodiesel in blend). The pressure drops on the soot layer as shown in figure 8 was directly proportional to the total mass of soot obtained after 5 hours of operation. Thus, for D100, the largest pressure drop on the soot layer was found, namely 12.94 mbar, for B20 we had 8.71 mbar and 6.07 mbar for B30. The simulation data confirm the experimental results, namely that B30 produced the lowest solid particulate emissions. Due to the limitations, it is very hard to measure exactly the amount of soot emitted, but by simulation it was possible to calculate the exact soot emission in [mg]. As shown in figure 9 the trend of soot emissions is directly proportional to the total pressure drop. Thus, for D100, a 25.12% increase in soot emissions compared to B20 was obtained, respectively by 47.5% compared to B30.

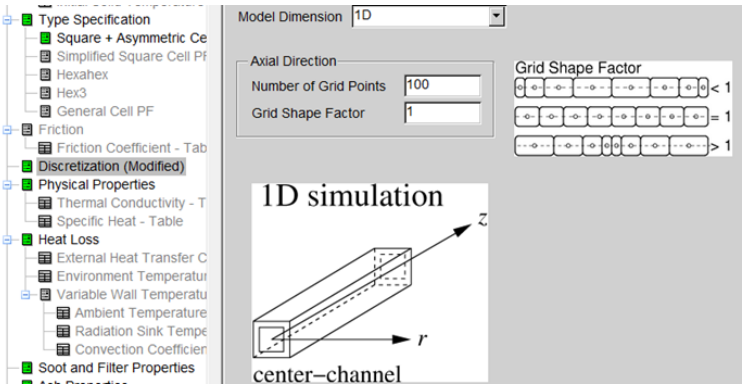

Fig. 7. *Discretization of the particulate filter model*

THE ANNALS OF "DUNAREA DE JOS" UNIVERSITY OF GALATI
FASCICLE IX. METALLURGY AND MATERIALS SCIENCE
Nº. 4 - 2021, ISSN 2668-4748; e-ISSN 2668-4756
Article DOI: https://doi.org/10.35219/mms.2021.4.10

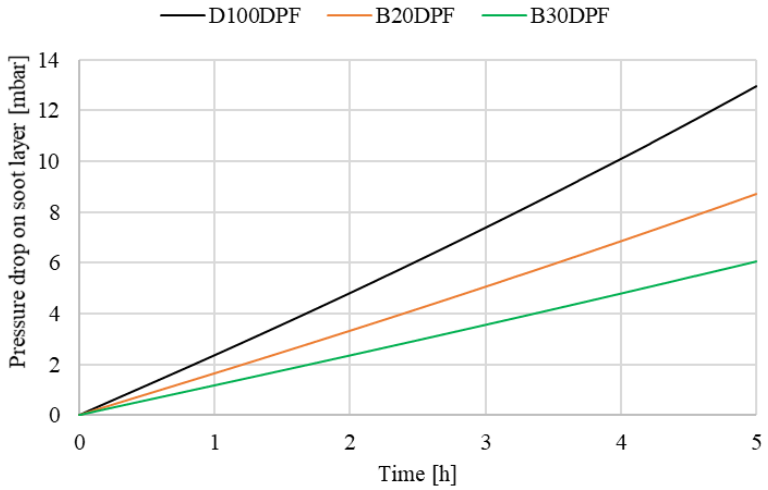

Fig. 8. *Pressure drop for the cases studied by simulation*

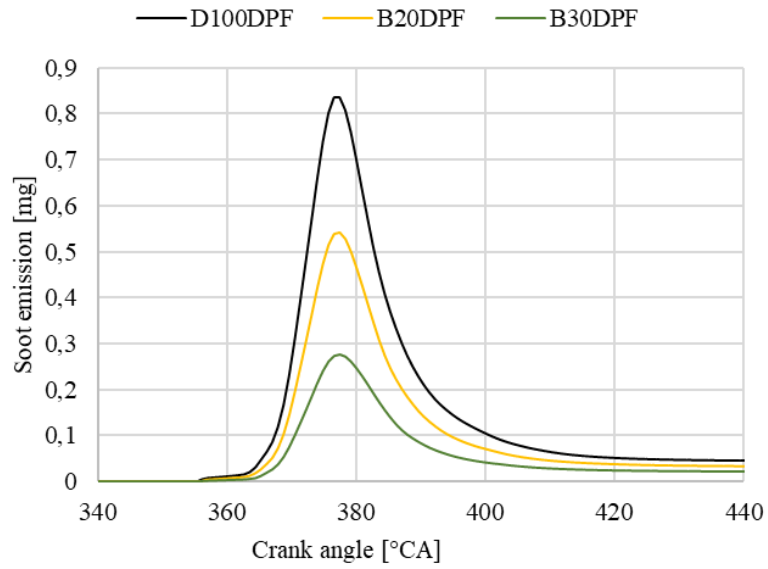

Fig. 9. *Soot emission obtained by simulation B20_DPF; B30_DPF; Diesel_DPF*

4. Conclusions

- The simulation model created in AVL Boost was validated by comparing the pressure curves. The overlap is almost perfect, and it can be concluded that the simulation model created is valid.

- The results obtained by simulation regarding the pressure drop were 12.94 mbar for D100DPF, 8.71 mbar for B20DPF and 6.07 mbar for B30DPF.

- The trend of soot emissions is directly proportional to the total pressure drop. Thus, for D100 there was an increase of 25.12% in soot emissions compared to B20, respectively by 47.5% compared to B30.

- The DPF model created by the simulation can be used for various future research using various fuels and using various injection strategies

Acknowledgements

The data presented in this paper were obtained from my PhD thesis "Studies and research on improving the operation of particulate filters in the use of various fuels" F-CA-39032/23.06.2021. I would like to thank AVL company for the support provided in this research.

References

[1]. Mathis U., Mohr M., Forss A.-M., *Comprehensive particle characterization of modern gasoline and diesel passenger cars at low ambient temperatures*, Atmospheric Environment, vol. 39, 2005.

[2]. Böhm H., Jander H., Tanke D., *PAH growth and soot formation in the pyrolysis of acetylene and benzene at high*

temperatures and pressures: Modeling and experiment, Symposium (International) on Combustion, vol. 27, 1998.

[3]. Ruiz M. P., de Villoria R. G., Millera A., Alzueta M. U., Bilbao R., *Influence of the temperature on the properties of the soot formed from C_2H_2 pyrolysis*, Chemical Engineering Journal, vol. 127, 2007.

[4]. Xi J., Zhong B.-J., *Soot in Diesel Combustion Systems*, Chemical Engineering & Technology, vol. 29, 2006.

[5]. Awais M., Bhuiyan A. A., *Recent advancements in impedance of fouling resistance and particulate depositions in heat exchangers*, International Journal of Heat and Mass Transfer, vol. 141, 2019.

[6]. Engeljehringer K., *AVL Emission Test Systems Light-Duty Application: Cars and LCV*, 2013.

[7]. Jurchiș B., Nicolae B., Iclodean C., Burnete N., *Study of emissions for a compression ignition engine fueled with a mix of DME and diesel*, vol. 252. 2017.

THE ANNALS OF "DUNAREA DE JOS" UNIVERSITY OF GALATI
FASCICLE IX. METALLURGY AND MATERIALS SCIENCE
Nº. 4 - 2021, ISSN 2668-4748; e-ISSN 2668-4756
Article DOI: https://doi.org/10.35219/mms.2021.4.11

ANALYSIS OF THE INFLUENCE OF PESTICIDES ON THE SOIL IN AN AGRICULTURAL AREA

Beatrice Daniela TUDOR, Bianca Teodora BUCEVSCHI
"Dunarea de Jos" University of Galati, Romania
e-mail: beatrice.tudor@ugal.ro

ABSTRACT

The paper presents an analysis of the soil in an agricultural area, to determine the influence of pesticides on the soil where agricultural production is carried out. For the research of the soil quality, were analysed areas, for harvesting soil samples. On the samples collected were determined, the amount of nitrates and nitrites from the soil, were determination of heavy elements from soil composition, soil pH and it was observed of the impact of pollutants on the soil.

KEYWORDS: pollutants, pesticides, nitrates, nitrites

1. Introduction

The soil represents the easy layer of the bark, having a thickness of a few cm, up to 2-3 m. It was formed as a result of simultaneous actions, such the atmosphere, hydrosphere and biosphere, on rocks and parenteral matter.

The chemical composition of the soil includes almost all known chemical, mineral and organic elements.

The mineral part of the soil is determined by its origin. The organic part of the soil is made up of animal and vegetable waste.

The amount of humus in the soil represents the natural fertility of the soil, which can be raised by applying organic fertilizers.

The soil has specific physical, chemical and morphological properties.

The physical properties of the soil include colour, texture, structure, porosity, density, consistency, temperature and air [1, 3].

The chemical properties are soil acidity, humification.

Soil pollution is defined by the presence of toxic substances (pollutants or contaminants) in the soil, in sufficient concentrations, to represent a risk, a health risk. Soil pollution, it is produced if the levels of soil contaminants, exceed the levels that should be present in a natural way.

The soil can be polluted by direct methods, i.e., by landfills, and by indirect methods, fertilizers and pesticides discarded on agricultural land; by the deposition of pollutants evacuated into the atmosphere; rainwater contaminated with pollutants; the transport of pollutants from the wind, from one place to another; infiltration through the soil of contaminated water.

The use of pesticides and chemical fertilizers has increased, for the cultivation of more crops, and these pollutants have made the soil poisonous and, in many places, the soil has become infertile [2, 5].

Pesticides, once in the soil, in addition to their action on diseases, pests, weeds, extend their action on microorganisms, so that there are quantitative changes and qualitative both in the structure of the edaphic population and in the physiological activities. The importance of knowing these changes is supported both by the requirements of a scientific agriculture and by the protection of soil ecosystems.

The chemicalization of agriculture through fertilizers, herbicides, pesticides, phytohormones is closely linked to both the increase in agricultural production and environmental problems [6, 8].

2. Experimental research

For the research of the soil quality, the following objectives were analysed:

- Establishment of affected areas, for harvesting soil samples;
- Determination of nitrates and nitrites from the soil;
- Determination of heavy elements from soil composition;
- Determination of soil pH;
- Observation of the impact of pollutants on the environment.

THE ANNALS OF "DUNAREA DE JOS" UNIVERSITY OF GALATI
FASCICLE IX. METALLURGY AND MATERIALS SCIENCE
N°. 4 - 2021, ISSN 2668-4748; e-ISSN 2668-4756
Article DOI: https://doi.org/10.35219/mms.2021.4.11

Soil sampling is one of the most important steps in a fertilization program. As soil sampling for laboratory analysis is done only from a not very large area of land, it is necessary to collect a representative soil sample for accurate results.

Soil samples were taken from the Bădălan agricultural production area, near the municipality of Galaţi. The sampling was done from two different areas and from each area it was selected as many samples from the different depths.

Most of the plant's roots have the highest biological activity and the highest nutrient, content on the surface, so, the first 30 cm of soil is tested and analysed. The soil samples were taken according to the depth as follows:

-10 cm depth for sample 1;
- 20 cm depth for sample 2;
- 30 cm depth for sample 3.

2.1. Analysis of the concentration of heavy soil metals in soil samples

The soil behaves as a depository of heavy metals emitted into the environment; behavior favoured by their ability to accumulate over time. Different factors can act on these deposits, being taken up in the form of particles in the air and water or being absorbed by plants.

Heavy metals have a potentially toxic effect on all living organisms, if they exceed a certain limit. The plants can accumulate heavy metals directly from the soil [4].

In order to be analysed, the soil samples were first dried in a thermoregulatory oven for 24 hours at 105 °C. This is necessary to remove the water molecules physically bound to the soil (Fig. 1).

Fig. 1. *Placement of the soil sample in the special place inside the analytical block of the X-ray fluorescence spectrometer*

Table 1. *Concentrations of metals corresponding to the 3 soil samples*

Sample	As [ppm]	Pb [ppm]	Rb [ppm]	Sr [ppm]	Zr [ppm]
Sample 1	9	13	90	222	151
Sample 2	11	18	99	222	159
Sample 3	10	15	104	216	154
Limit values	**20**	**50-300**	**100-120**	**240**	**165**

The values of the determinations resulting from the analyses for the soil samples taken from the analysed perimeter were compared with the reference values according to the national norms in force, respectively MAPPM Order no. 756/1997 [6].

Table 1 comparatively presents the results of the analyses regarding the elemental concentrations corresponding to the 3 soil samples taken from different depths.

Figure 2 shows graphically and comparatively the results of the analyses regarding the elemental concentrations corresponding to the 3 soil samples taken from different depths.

It was observed that for the elements As, Pb, Sr and Zr, the highest concentrations were revealed for sample 2, with the exception of Rb element. This can be explained by the fact that for soil sample 1 which was taken from the smallest depth (10 cm), the perimeter from which it was taken was subjected to rainfall and specific agricultural work, as it is known that the concentrations of pollutants are usually lower during precipitation.

Thus, the heavy metals analysed were "washed" and transported deeper into the soil, at a depth of 20 cm, corresponding to soil sample 2. The lower concentrations of heavy metals in the case of soil

THE ANNALS OF "DUNAREA DE JOS" UNIVERSITY OF GALATI
FASCICLE IX. METALLURGY AND MATERIALS SCIENCE
Nº. 4 - 2021, ISSN 2668-4748; e-ISSN 2668-4756
Article DOI: https://doi.org/10.35219/mms.2021.4.11

sample 3, taken from a depth of 30 cm can be explained by the fact that the mechanism of transport of pollutants in the soil was through the liquid phase, because most metals enter the soil in forms dissolved or suspended in water and, in fact, all interactions that take place between heavy metals and solid soil constituents take place at the solid-liquid interface. In this case, the pollutants did not penetrate too deep into the soil.

For no heavy metals analysed, the permissible limit values were not exceeded, so the soil samples taken do not indicate exceeding the level for heavy metal pollution.

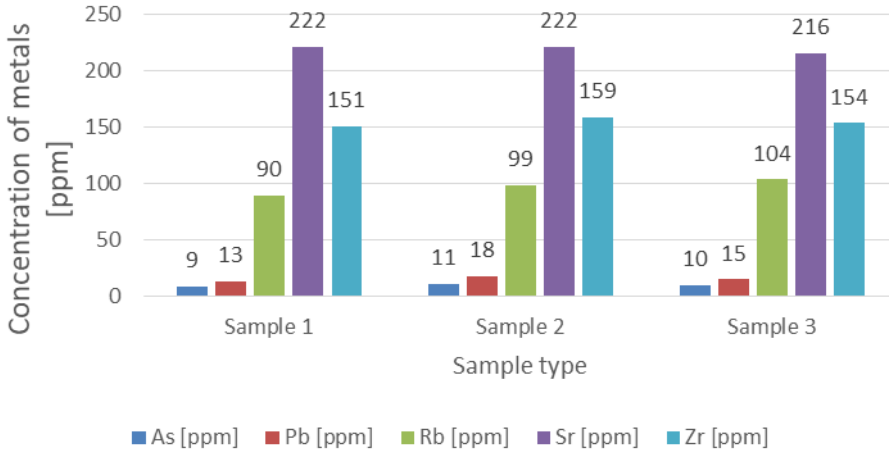

Fig. 2. *Concentrations of heavy elements related to the 3 soil samples analysed*

2.2. Determination of the pH of soil samples

Soil pH is one of the most common and indicative determinations of chemical properties, which specifies the acidic or basic character of the soil, indicating the type of crops suitable for each field, what type of fertilizer to apply or if necessary to correct the pH value of the soil. It also indicates the availability of essential nutrients, as well as the estimation of toxicity with certain elements [9, 10].

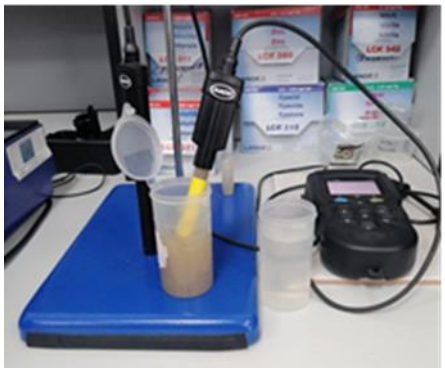

Fig. 3. *PH measurement with soil-water suspension sample*

Table 2 shows the pH values for the 3 types of samples studied and taken from different depths.

Table 2. *PH values corresponding to the 3 soil samples*

Sample	pH
Sample 1	7.60
Sample 2	7.99
Sample 3	7.97
Sample benchmark	7.29

Figure 4 shows graphically and comparatively the results of the analyses regarding the pH values corresponding to the 3 soil samples taken from different depths.

It was observed that, regardless of the depth from which the soil samples were taken, all measured pH values fell into the categories of "weakly alkaline" soils. As most plants support a pH in the low acid - neutral - low alkaline range, these results confirm that the soil samples taken do not indicate exceeding the level for pesticide pollution and/or chemical fertilizers.

THE ANNALS OF "DUNAREA DE JOS" UNIVERSITY OF GALATI
FASCICLE IX. METALLURGY AND MATERIALS SCIENCE
Nº. 4 - 2021, ISSN 2668-4748; e-ISSN 2668-4756
Article DOI: https://doi.org/10.35219/mms.2021.4.11

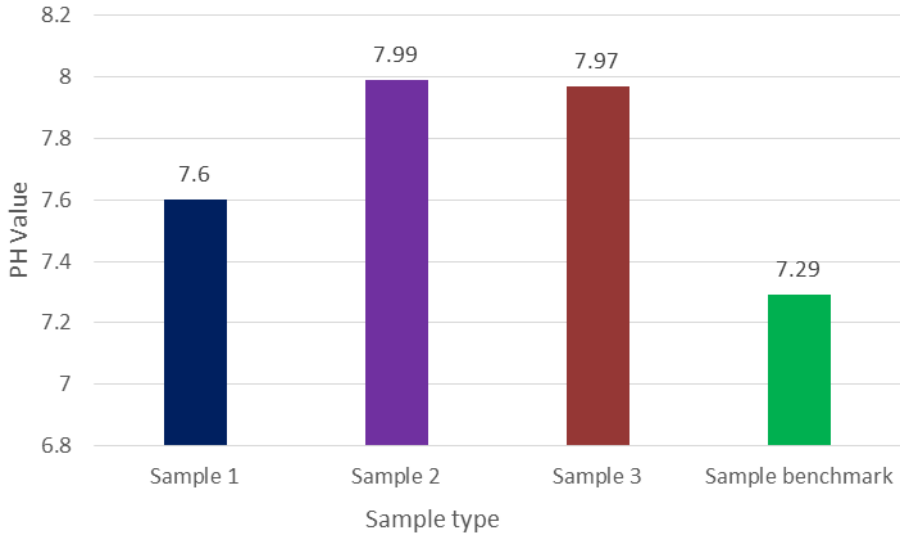

Fig. 4. *The pH values related to the 3 soil samples analysed*

2.3. Analysis of nitrate concentration in soil samples

Nitrates are nitrogen compounds that occur naturally in the soil, but which can also be spread by fertilization. Plants use nitrate nitrogen for their own metabolism and to produce protein. Nitrate is extracted from the soil through the roots and is distributed throughout the plant to be converted into high-energy protein compounds through photosynthesis. The remaining surplus contaminates the groundwater, being found in rivers, lakes or groundwater and, ultimately, in drinking water. Nitrate levels in soil and drinking water can become considerable, depending on the predominant form of land use. Nitrates in the soil come from the fixation of atmospheric nitrogen by many plant species (legumes), being present even in the absence of nitrogen fertilization, but the latter being a major source of them [7].

For this type of assay, for maximum safety, were used predetermined LCK 340 reagents.

Fig. 5. *Predetermined reagents LCK 340 for nitrate determinations*

Table 3 shows the values of nitrate concentrations related to the 3 types of samples studied and taken from different depths.

From Table 3 and Figure 6 it can be seen that regardless of the depth of soil sampling, the values of nitrate concentrations did not exceed the maximum level of contamination. These results confirm that the soil samples taken do not indicate exceeding the level for pollution with pesticides and/or chemical fertilizers. It can also be seen that the nitrate concentration shows an increasing trend with depth.

THE ANNALS OF "DUNAREA DE JOS" UNIVERSITY OF GALATI
FASCICLE IX. METALLURGY AND MATERIALS SCIENCE
Nº. 4 - 2021, ISSN 2668-4748; e-ISSN 2668-4756
Article DOI: https://doi.org/10.35219/mms.2021.4.11

Table 3. *Values of nitrate concentrations related to the 3 types of samples studied and taken from different depths*

Sample	NO_3^- [mg/L]
Sample 1	2.8
Sample 2	2.8
Sample 3	4.7
Sample benchmark	3.8
Maximum level of contamination	44

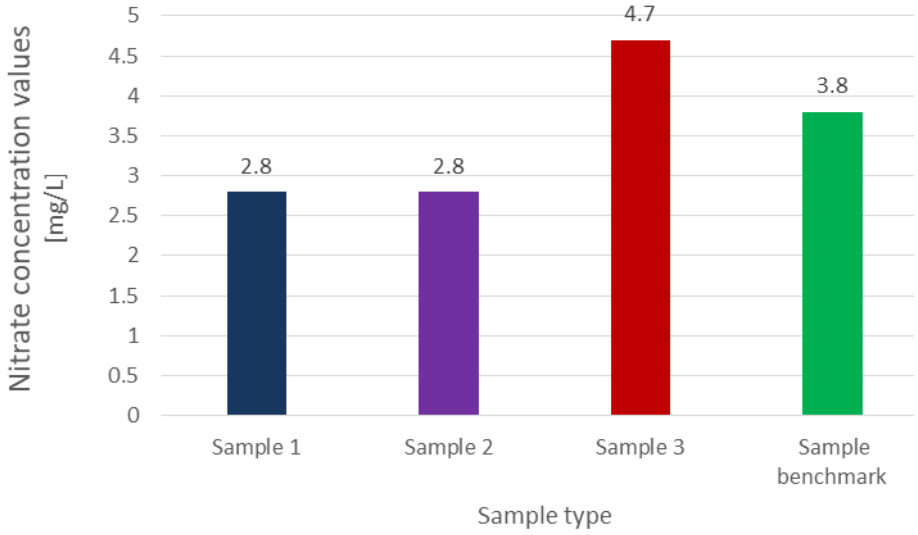

Fig. 6. *The values of nitrate concentrations related to the 3 soil samples analysed*

2.4. Analysis of the nitrite concentration in the soil samples

Nitrite is an intermediate product in the nitrogen supply process of the plant. Because plants cover their nitrogen requirements with nitrate, plant-based foods - especially various varieties of vegetables - can contain relatively large amounts of nitrogen. In vegetables that contain nitrates, microbiological or enzymatic processes can cause the conversion of nitrate to nitrite. This may be due to improper storage, improper transport or non-compliance with standard hygiene regulations.

For this type of assay, for maximum safety, were used predetermined LCK 342 reagents.

Table 4 indicates the values of nitrite concentrations related to the 3 types of samples studied and taken from different depths.

Figure 8 shows graphically and comparatively the results of the analyses regarding the values of nitrite concentrations corresponding to the 3 soil samples taken from different depths.

Table 4. *Nitrite concentrations corresponding to the 3 soil samples*

Sample	NO_2^- [mg/L]
Sample 1	0.009
Sample 2	0.010
Sample 3	0.028
Sample benchmark	0.009
Maximum level of contamination	3.3

THE ANNALS OF "DUNAREA DE JOS" UNIVERSITY OF GALATI
FASCICLE IX. METALLURGY AND MATERIALS SCIENCE
Nº. 4 - 2021, ISSN 2668-4748; e-ISSN 2668-4756
Article DOI: https://doi.org/10.35219/mms.2021.4.11

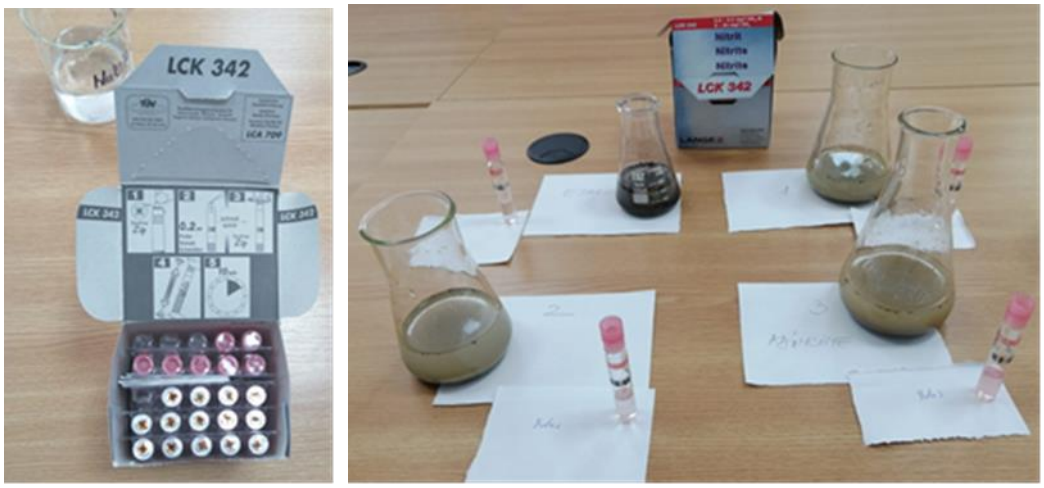

Fig. 7. *Predetermined reagents LCK 342 for nitrite determinations*

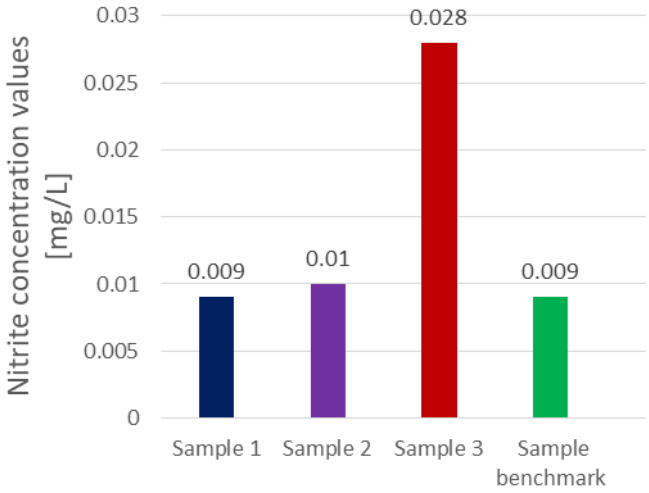

Fig. 8. *The values of nitrite concentrations related to the 3 soil samples analysed*

It was observed that regardless of the depth of soil sampling, the values of nitrite concentrations did not exceed the maximum level of contamination. These results confirm that the soil samples taken do not indicate exceeding the level for pollution with pesticides and/or chemical fertilizers.

It can also be seen that the nitrite concentration as in the case of nitrate concentrations shows an increasing trend with depth.

3. Conclusions

Following the analysis of the soil concentration, the determined elements fall within the limits imposed by the legislation in force on the limit values of heavy metals allowed in the soil, with the mention that in sample 2 (at a depth of 20 cm), were recorded the highest values of the determined elements which shows us that these pollutants migrate into the depths of the soil by diffusion and dissolution having as solvent water. The soil samples taken do not indicate exceedances of the permitted limit values.

The measured pH values fall into the category of weakly alkaline soils being beneficial for agricultural crops.

Nitrate concentration shows an increasing trend with depth. The highest value of nitrates was obtained in sample 3. However, the nitrate concentrations from all the samples studied did not exceed the maximum level of contamination.

The nitrite concentration shows an increasing trend with the sampling depth, but the determined values do not exceed the maximum level of contamination allowed.

References

[1]. Lăcătuşu R., *Agrochimie*, Ed. Helicon, Timişoara, 2000.

[2]. Lăcătuşu R., *Mineralogia şi chimia solului*, Ed. Universităţii „Al. I. Cuza" Iaşi, 2000.
[3]. Lăcătuşu R., Kovacsovics Beatrice, Plaxienco Doina, Rîşnoveanu I., Lungu Mihaela, Mihalache Daniela, *Încărcarea cu poluanţi proveniţi din îngrăşăminte şi pesticide a unor soluri, legume şi a apei freatice din partea sudică şi estică a municipiului Bucureşti*; Lucr. Simpoz. „Protecţia Mediului în Agricultură", vol. 1, p. 279-293, 2000.
[4]. Andreiaș S., *Optimizarea regimurilor nutritive ale solurilor și productivitatea plantelor de cultură*, Ed. Pontos, Chișinău, 2007.
[5]. Batjes N. H., *Total carbon and nitrogen in the soils of the world*, European J. Soil Sci., 47, p. 151-163, 1996.
[6]. Blair J., *Fertilizer recommendations as determined by chemical and physical parameters of soil and K requirement of crops*, Potassium in Ecosystems, p. 79-90, 1992.
[7]. Borlan Z., Hera Cr., *Aplicarea îngrăşămintelor pentru cultura intensivă a principalelor plante de câmp*, Agrochimie, Ed. Lixandru şi colab., Ed. Didactică şi Pedagogică, p. 296-305, 1990.
[8]. Borlan Z., Gavriluţă I., Ştefănescu Daniela, Alexandrescu Ariadna, Nebunelea Dobriţa, *Fertilizarea în cadrul unor sisteme de producţie vegetală durabilă. II. Potasiul*, Şt. Solului XXXIII, 2, 1999.
[9]. Calancea L., *Bazele agrochimice ale fertilizării în raport cu cerinţele plantelor*, Agrochimie, Ed. Didactică şi Pedagogică, Bucureşti, p. 18-36, 1990.
[10]. Clapp C. E., Hayes M. H. B., Simpson A. J., Kingery W. L., *Chemistry of soil organic matter in Chemical processes in soil*, (Tabatabai A., Spark D., eds.) SSSA Book Series, no. 8, Madison, p. 1-150, 2005.

THE ANNALS OF "DUNAREA DE JOS" UNIVERSITY OF GALATI
FASCICLE IX. METALLURGY AND MATERIALS SCIENCE
Nº. 4 - 2021, ISSN 2668-4748; e-ISSN 2668-4756
Article DOI: https://doi.org/10.35219/mms.2021.4.12

NO_X AND CO EMISSION ANALYSIS USING OXYGENATED FUELS FOR A DIESEL ENGINE EQUIPPED WITH DIESEL PARTICULATE FILTER

Andrei-Constantin SOFIAN, Mădălin-Florin POPA, Bogdan Manolin JURCHIȘ
Technical University of Cluj-Napoca, Romania
e-mail: bogdan.jurchis@auto.utcluj.ro

ABSTRACT

The automotive industry is responsible for a big part of the pollutant emissions, and the measures that are being taken to reduce these emissions are extremely important. Compared to 1990 emissions of nitrogen oxides from internal combustion engines decreased approximately by 39%, and for PM 2.5 by 37%. Even so, emissions concerns have increased in recent years, so the EU has taken a series of measures to continuously reduce emissions of nitrogen oxides and carbon monoxide related to transport sector. It is well known that the replacement, even partial, of fossil fuels with alternative fuels has a significant contribution to the decarbonisation of trans-European transport, which reduces the environmental impact of this sector. With a share of around 4.7% of all fuels used in EU transport, biofuels are the main type of alternative fuel. In addition, if produced sustainably, biofuels help reduce emissions of carbon monoxide and solid particles, but at certain operating intervals, the engine can produce more NO_x emissions, which is why diesel engines must be equipped with additional NO_x emission treatment systems.

KEYWORDS: NO_x emission, CO emission, Diesel particulate filter, biodiesel

1. Introduction

Compared to the combustion of gasoline engines, the combustion of diesel engines can be described by three successive processes: self-ignition delay, preformed mixture combustion and controlled mixing (diffusive) combustion. Depending on the operating point, the contributions of the three processes to the total duration of the combustion process change. Self-ignition delay defines the phase of combustion of the preformed mixture by the amount of fuel injected into the cylinder that has not yet burned. The longer the self-ignition delay, the greater the amount of preformed mixture. Combustion usually starts at the periphery of the fuel jet, where the fuel has mixed well with the air and therefore allowed the creation of optimal ignition conditions (temperature and λ). Exothermic reactions in these areas lead to temperatures above 2300 K [1], which allows the rapid oxidation of the preformed mixture by self-accelerating chain reactions. Compared to the petrol engine, the diesel engine runs on excess air ($\lambda > 1$), which is why the use of the catalyst is only beneficial for the oxidation of HC and CO with excess oxygen from the flue gases. For this reason, reducing internal emissions is important for diesel engines. In addition to the emissions of petrol engines (CO_2, H_2O, NO_x, HC and CO), soot and particulate emissions must also be taken into account for diesel engines.

A catalyst and a particulate filter are needed to treat the pollutant emissions from combustion. The basic part of the catalyst is a honeycomb-shaped ceramic monolith, which is composed of several small channels through which flue gases circulate. If the ignition temperature is reached, the oxidation in the DOC (Diesel Oxidation Catalyst) is almost complete. The ignition temperature varies between 170 and 200 °C, depending on the nature of the exhaust gases, the flow rate, and the catalyst composition. From this temperature, the conversion reaches 90%. For an optimal oxidation process in the catalyst, there must be a high residual oxygen content in the flue gases. Unburned hydrocarbons are the result of incomplete combustion. Nitrogen oxides are produced at very high temperatures in the combustion

THE ANNALS OF "DUNAREA DE JOS" UNIVERSITY OF GALATI
FASCICLE IX. METALLURGY AND MATERIALS SCIENCE
Nº. 4 - 2021, ISSN 2668-4748; e-ISSN 2668-4756
Article DOI: https://doi.org/10.35219/mms.2021.4.12

chamber in places where there is a surplus of oxygen. NO_x emissions cannot be reduced by the oxidation catalyst, but only in the three-way catalyst (Fig. 1).

Diesel Oxidation Catalyst has a carrier ceramic or metal structure and a substrate coating covered with noble metals. The major purpose of the substrate coating is to ensure that the noble metal is slowing down the sintering of the catalyst, which occurs at high temperatures and results in an irreversible reduction in the catalyst's activity.

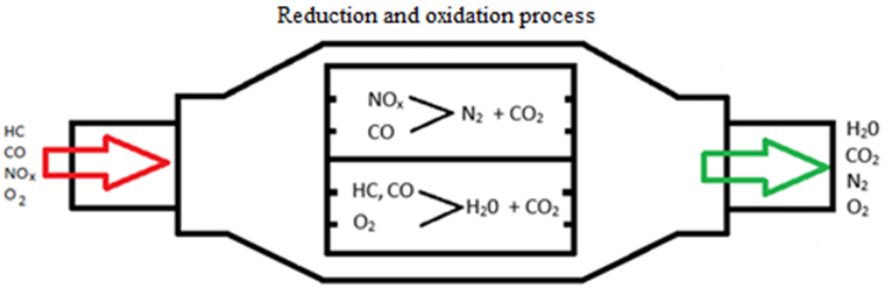

Fig. 1. *Three-way catalyst (DOC)*

2. Materials and methods

The experimental research for the analysis of the operation of particulate filters with biofuels was carried out in the "Laboratory for testing, research and certification of internal combustion engines" within the Faculty of Road Vehicles, Mechatronics and Mechanics Cluj Napoca. The laboratory offers the possibility of testing internal combustion engines with different fuels. Therefore, comparative studies can be performed between the operation of conventional fuels, respectively biofuels in terms of pollutant emissions, performance and combustion processes.

The specific objectives were:

- CO emission analysis for Diesel engine using different blends;
- NO_x emission analysis for Diesel engine using different blends.

In order to obtain and process the data generated by the experimental tests performed in the Testecocel laboratory, in order to fulfil the objectives of the present doctoral thesis, the following were taken into account:

- modification of the input parameters of the electronic engine control system
- measuring the mass air flow;
- measuring NOx and CO emissions;
- fitting a particle filter to the exhaust system.

The experimental single-cylinder engine AVL 5402 with a maximum power of [6 kW] was used for experimental tests. The entire process was controlled from the command-and-control room (Fig. 2), which consists of computing equipment and process monitoring systems.

Fig. 2. *Command chamber and AVL5402 engine used in experimental tests*

The TESTO 350 analyser (Fig. 3) was used to measure pollutant emissions (CO, NO_x), which is equipped with a modular probe that works at temperatures up to 1000 °C. After calibrating the device, the probe was introduced into the exhaust system to read NO_x and CO emissions (Fig. 4). The data acquisition was done in real time, by connecting the Testo unit to the PC using Bluetooth technology. The data was saved automatically every 5 seconds. The data used for the analysis were collected only after stabilization of temperature and NO_x and CO emissions. The change in values before collecting them had to be less than 1% within one minute.

THE ANNALS OF "DUNAREA DE JOS" UNIVERSITY OF GALATI
FASCICLE IX. METALLURGY AND MATERIALS SCIENCE
Nº. 4 - 2021, ISSN 2668-4748; e-ISSN 2668-4756
Article DOI: https://doi.org/10.35219/mms.2021.4.12

Fig. 3. *Testo Analyzer: 1 - Testo 350 analysis unit, 2 - modular exhaust gas probe*

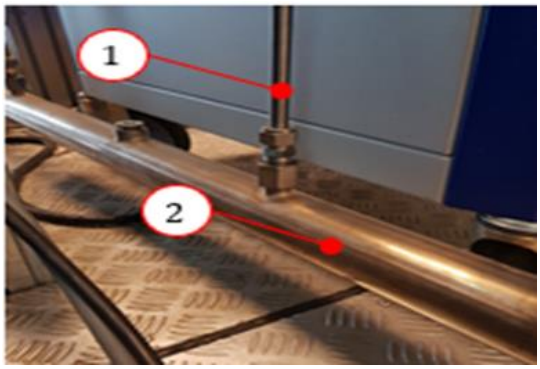

Fig. 4. *Adapting the modular probe to the exhaust system: 1 - modular probe, 2 - exhaust pipe*

3. Results and discussion

The working regime at which the experimental determinations were performed was 2000 1/min. The injection parameters were the same in all cases. For each fuel, 2 types of tests were performed:

1 - Tests without particulate filter;

2 - Tests with particulate filter.

The results obtained after the experimental tests performed with particulate filter and without particulate filter mounted on the exhaust are presented in Table 1. Three types of D100 fuel mixture were used - diesel, B20 - is a mixture of 20% biodiesel and 80% diesel and B30 - is a mixture of 30% biodiesel and 70% diesel. A first analysis of the results found that increasing the biofuel content from 6.5% v/v which D100 has to 20% and 30% v/v respectively has a beneficial effect on smoke and CO emissions, which can be justified by higher oxygen content. Instead, NO_x emissions increase, which is due to the local excess oxygen in the combustion chamber.

NO_x and CO emissions have been measured with the Testo device since the stabilization of the system, which was achieved when the engine oil and exhaust temperature fluctuated by less than 1% for a period of 1 minute. Another important aspect is that no gas recirculation system has been used to limit NO_x emissions. The NO_x and CO emission values were converted from PPM to g/kWh using the formula [2]:

$$EP_i = EV_{i,d} * \frac{M_i * \dot{m}_{E_{xh,d}}}{M_{Exh,d} * P_{eff}} = EV_{i,w} * \frac{M_i * \dot{m}_{E_{xh,w}}}{M_{exh,w} * P_{eff}} \quad (1)$$

Notes: EP_i - mass of pollutant "i" in relation to power in [g/kWh], EV_i - value of exhaust emissions "i" in [ppm], M_i - molar mass, M_{Exh} - molar mass of the exhaust gas, $\dot{m}_{Exh}$ - mass flow of the exhaust gas [kg/h], P_{eff} - effective power [kW], index *d* - dry exhaust gases without water vapor and index *w* - vapor exhaust gas.

Table 1. *Pollutant emissions at 2000 rpm - NO_X, CO*

Case nr.	Blend	NO_X [g/kWh]	CO [g/kWh]
1	Diesel_DPF	8.19	2.11
2	Diesel_noDPF	7.52	3.74
3	B20_DPF	10.41	1.91
4	B20_noDPF	8.43	3.60
5	B30_DPF	10.76	1.53
6	B30_noDPF	8.52	3.42

For the analysed cases (at a speed of 2000 1/min) (Fig. 5), the tests performed without a particulate filter showed an increase in NO_x emissions for B20 of 12.10% and 13.30% for B30 in the ratio with diesel. For DPF cases there is an increase in NO_x emissions for all mixtures. Thus, we have an increase

THE ANNALS OF "DUNAREA DE JOS" UNIVERSITY OF GALATI
FASCICLE IX. METALLURGY AND MATERIALS SCIENCE
Nº. 4 - 2021, ISSN 2668-4748; e-ISSN 2668-4756
Article DOI: https://doi.org/10.35219/mms.2021.4.12

of 8.91% for the Diesel_DPF case compared to the Diesel_No_DPF case, an increase of 23.49% for the B20_DPF case compared to B20_No_DPF and an increase of 26.30% for the B30_DPF case compared to B30_No_DPF. All these additional increases in NO_x emissions for a higher percentage of biodiesel in blend are confirmed by the specialty literature [3, 5].

The composition of biodiesel (oxygen content, length of molecules, unsaturated FAME, etc.) but also the effects of cetane number, viscosity and modulus of elasticity on the beginning of the combustion process, ensure conditions that favour the formation of nitrogen oxides. Higher flame temperatures [6], especially in regions where there is a high oxygen content coupled with the occurrence of dissociation reactions and sufficient residence time [7] lead to high NO_x emissions.

This is explained by the fact that the oxygen molecules in the mixture react with the existing nitrogen, increasing the maximum temperature during the combustion process, this being the main factor for increasing NO_x emissions. Although combustion is improved in the case of biodiesel blends, this has the consequence of increasing NO_x. Nitrogen oxides emissions can be reduced by applying temperature reduction measures: reducing the concentration of oxygen in the combustion zone or delaying the fuel injection, but also reducing the injection pressure.

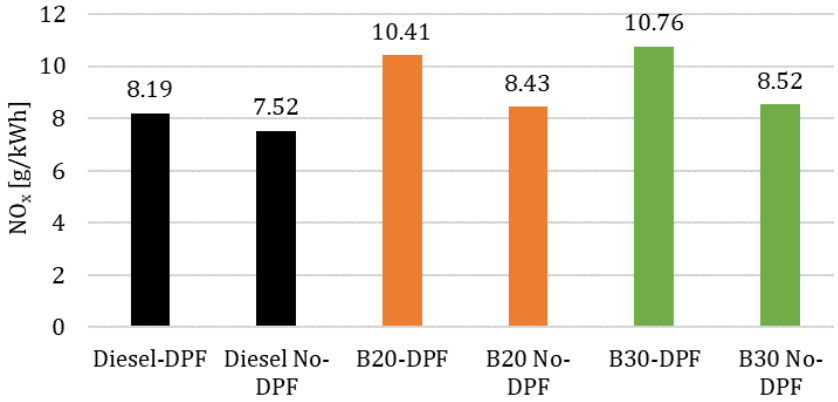

Fig. 5. *NO_x emissions at 2000 1/min*

CO emissions decreased in direct proportion to the addition of biodiesel to the mixture due to the presence of oxygen in the chemical composition of the biodiesel, resulting in a more complete combustion. Another reason why CO emissions fell was because biodiesel has a lower carbon content than diesel. For cases without exhaust particulate filter, the carbon emission decreased by 3.74% for B20 and by 8.56% for B30 compared to D100. Cases where particulate filter was used on discharge showed that the CO emission decreases by 43.58% for D100DPF compared to D100_No_DPF, by 46.94% for B20DPF compared to B20_No_DPF and by 55.26% for B30DPF compared to of B30_No_DPF (Fig. 6). The decrease in CO emissions for DPF cases is also confirmed by research conducted by Shao *et al.* [75].

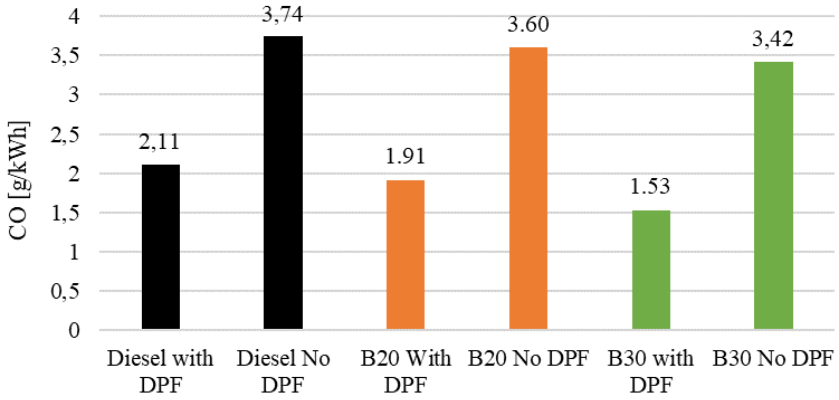

Fig. 6. *CO emissions at 2000 1/min*

4. Conclusions

The main conclusions that can be drawn from this research are:

- for the analysed cases (at a speed of 2000 1/min), the tests performed without a particulate filter showed an increase in NO_x emissions for B20 of 12.10% and 13.30% for B30 compared to D100;

- for cases with DPF there was an increase in NO_x emissions for all mixtures. Thus, we have an increase of 8.91% for the Diesel_DPF case compared to the Diesel_No_DPF case, an increase of 23.49% for the B20_DPF case compared to B20_No_DPF and an increase of 26.30% for the B30_DPF case compared to B30_No_DPF;

- CO emissions decreased in direct proportion to the addition of biodiesel to the mixture, due to the presence of oxygen in the chemical composition of biodiesel, helping to burn more completely; in the cases without the exhaust-mounted particulate filter, the carbon emission decreased by 3.74% for B20 and by 8.56% for B30 compared to D100;

- the cases in which exhaust particulate filter was used showed that the CO emission decreases by 43.58% for D100DPF compared to D100NoDPF, by 46.94% for B20DPF compared to B20NoDPF and by 55.26% for B30DPF compared to B30NoDPF.

Acknowledgements

The data presented in this paper were obtained from my PhD thesis "Studies and research on improving the operation of particulate filters in the use of various fuels" F-CA-39032/23.06.2021. I would like to thank AVL company for the support provided in this research.

References

[1]. Bazyn T., Krier H., Glumac N., *Combustion of nanoaluminum at elevated pressure and temperature behind reflected shock waves*, Combustion and Flame, vol. 145, 2006.
[2]. VDMA, *Exhaust emission legislation Diesel and gas engines*, 2017.
[3]. McGill R., Storey J., Wagner R., Irick D., Aakko P., Westerholm M., *et al.*, *Emission performance of selected biodiesel fuels*, SAE Transactions, 2003.
[4]. Sze C., Whinihan J. K., Olson B. A., Schenk C. R., Sobotowski R. A., *Impact of test cycle and biodiesel concentration on emissions*, SAE Transactions, 2007.
[5]. Abed K. A., Gad M. S., El Morsi A. K., Sayed M. M., Elyazeed S. A., *Effect of biodiesel fuels on diesel engine emissions*, Egyptian Journal of Petroleum, vol. 28, 2019.
[6]. Cheng A. S., Upatnieks A., Mueller C. J., *Investigation of the impact of biodiesel fuelling on NO_x emissions using an optical direct injection diesel engine*, International Journal of Engine Research, vol. 7, 2006.
[7]. Hoekman S. K., Robbins C., *Review of the effects of biodiesel on NO_x emissions*, Fuel Processing Technology, vol. 96, 2012.

THE ANNALS OF "DUNAREA DE JOS" UNIVERSITY OF GALATI
FASCICLE IX. METALLURGY AND MATERIALS SCIENCE
No. 4 - 2021, ISSN 2668-4748; e-ISSN 2668-4756
Article DOI: https://doi.org/10.35219/mms.2021.4.13

ANALYSIS OF THE WEAR PROCESS OF THE ELEMENTS IN THE BRAKING SYSTEM OF HEAVY TRUCKS

Mădălin-Florin POPA, Bogdan Manolin JURCHIȘ
Technical University of Cluj-Napoca, Romania
e-mail: madalin.popa@live.com

ABSTRACT

Today's commercial vehicles work in a very competitive environment, in an extremely active economic market and the requirements for the delivered performance make it imperative to study in detail each component element. In practice, all these aspects are found in the process of wearing the elements of different systems. Moreover, major changes are expected for the near future of motor vehicles in order to improve the ecological balance both by reducing the pollutant emissions of the propellants and by improving the percentage of recyclability and reduction of waste from maintenance (liquids and solutions such as oils, antifreeze or solutions with different detergents). In order to identify solutions to improve the mentioned problems, the current study analyses the types of wear identified in the elements of the braking system of commercial vehicles and their main factors of influence. The study is based on data obtained during analysis during operation for a number of trucks with different configurations.

KEYWORDS: brake, wear, brake pads wear, brake disk wear

1. Introduction

In order to be competitive, commercial vehicles must be able to carry heavy loads in the shortest possible time and very importantly, with minimal costs. The current braking systems that equip this type of vehicle are widely used and offer extremely good performance and low costs compared to previous generations. Until they are replaced with new variants of braking systems that allow in addition to high braking performance and total or partial energy recovery, improving performance and reducing maintenance costs remain two topics of major importance.

The identification of the impact that a number of external and operating factors have on the braking system as well as the analysis of the wear of the elements in the friction torque are also study elements that outline the main purpose of this study. It should be noted that this study provides an analysis based on the direct study of trucks operating in real working conditions. Moreover, extreme wear and tear situations resulting from over-stresses were also analysed.

Identification and analysis of problems during operation, because they are the starting point of experimental research. Occasionally, the problems of each system must be analysed and we can mention here systems such as: electrical, mechanical, hydrodynamic, main and auxiliary systems, etc. The analysis of each system with its particularities requires a large volume of data to be analysed, but based on them, conclusive and efficient solutions can be provided for the current major problems of motor vehicles. It should be noted that the paper seeks to address the analysis of situations encountered in operation from several perspectives. The proposal of solutions for the identified problems also touches on topics related to: materials used in the friction torque, constructive variants for the braking systems, the mode of operation and even aspects related to the problem of obsolete parts.

The analysis of the interventions in the service of heavy trucks led to the conclusion that they generate a large volume of used parts, which do not find their place in a well-developed recycling system. Another issue that needs to be clarified and requires increased attention is the decisive factor that determines the need to replace a part. In the absence of advanced systems for accurately measuring wear, many parts are replaced prematurely and others are replaced too late, leading to damage to other parts of the system, thus entering a vicious circle.

THE ANNALS OF "DUNAREA DE JOS" UNIVERSITY OF GALATI
FASCICLE IX. METALLURGY AND MATERIALS SCIENCE
Nº. 4 - 2021, ISSN 2668-4748; e-ISSN 2668-4756
Article DOI: https://doi.org/10.35219/mms.2021.4.13

2. Elements of analysis

One of the essential conditions for a braking system to deliver the specified performance is that its elements meet certain technical conditions. In addition to the assemblies, an essential factor is the quality of the parts. A good quality part will satisfy a range of use as accurately as possible, without causing unwanted wear to other parts. Wear elements are the brake pads, which are most often replaced due to wear and tear after friction with the brake disc. The latter is a more expensive part and more difficult to access, so it will have to withstand a longer period of operation. In addition to wear on discs and pads, defects are very common in the sealing gaskets either in the pistons in the brake calliper or in the sliding bolts in the brake callipers. Frequent damage caused by corrosion has also been found in vehicles older than 10 years.

All these defects must be prevented in such a way that it is not possible to carry out the braking process while driving, so that there must be regular intervals of preventive inspection. More recently, electronic assistance systems have been used to monitor system parts. However, at present, the only maintenance system for the brake system is based on the information transmitted to the brake pad wear sensor display (Figure 1). Based on this, service interventions will be required to replace the brake pads when the electronic system alerts the driver.

The wear and tear of discs and pads will be assessed by authorized workshop personnel on the basis of standards. However, this process can be subjective and inefficient and it would be preferable to have an automatic wear monitoring system or to identify new solutions, which would allow greater control over the wear phenomena in the friction torque.

Fig. 1. *Information provided to the user regarding the stage of wear of the brake pads*

Fig. 2. *Large volume of obsolete parts that do not have a recycling plan*

Fig. 3. *Worn brake discs for which there is no recycling plan*

3. Analysis of identified types of wear

3.1. Normal wear of the elements of the friction torque of the main braking system

All interventions for replacements to the braking system, apart from the maintenance program initially established, represent abnormal wear. These have different causes and, in the literature, there are a number of papers that address these issues [1-5]. Friction between the plate and the disc will result in a change in the size of the two parts. Normally, the wear elements are the friction linings of the brake pads. The reduction of their dimensions is done up to a certain maximum accepted value. Slowing down the wear process and identifying solutions by using new materials are elements frequently analysed in the literature [6-8].

THE ANNALS OF "DUNAREA DE JOS" UNIVERSITY OF GALATI
FASCICLE IX. METALLURGY AND MATERIALS SCIENCE
Nº. 4 - 2021, ISSN 2668-4748; e-ISSN 2668-4756
Article DOI: https://doi.org/10.35219/mms.2021.4.13

Figures 2 and 3 show parts replaced during a calendar month in the repair shop where the analysis was performed. There is a very large volume of replaced brake pads and a few worn brake discs. Among the parts in both figures can be seen some that have not yet reached the degree of wear but are still replaced. These issues related to the premature replacement of some elements require a careful analysis both for the efficiency of the economic balance and for the identification of solutions for electronic monitoring and evaluation of wear elements in order to determine the exact degree of wear and use of resources as efficiently as possible.

3.2. Excessive wear of the elements in the braking system

Braking efficiency is greatly influenced by the condition of the final brake effectors (brake calliper, brake pads, discs or brake shoes). Continuous monitoring of the condition of these elements increases traffic safety by continuously knowing the degree of wear of the parts in the system. However, the study [9] identifies and analyses a number of external factors, encountered in operation, which cause serious damage to the braking systems by the effect on the parts intended for maintenance control or by the direct damage of the brake pads or discs under conditions. extreme. In practice, the main problems that lead to excessive wear are caused by [9]: blockage of the brake callipers due to dust and mud on the road; suppression of the movement of the brake pads; non-compliant parts; overloads; uneven and unforeseen wear and tear; aggressive driving style.

Aspects related to the wear profile of certain sets of brake pads should also be considered. This can lead to the identification of areas of wear, on the basis of which an overview of wear can be outlined. These studies, unlike those performed on brake pads, reveal unforeseen issues encountered only in real operating conditions and the results can bring significant improvements, both in terms of performance and system reliability.

After analysing the wear intervals (by reading the values from the brake pad wear sensors), from the total number of trucks analysed, at 8.24% of them, at least a wear value greater than 99% was identified for one of the brake pads. The distribution of these cases (Figure 4) was analysed as in the other cases based on the current maintenance interval. As already mentioned, in the interval 4 the data cannot be completely analysed due to the large number of kilometres required to be covered until the beginning of the interval and then for the passage of the interval until the total wear. The "interval" represented the distance travelled between two brake pad replacements.

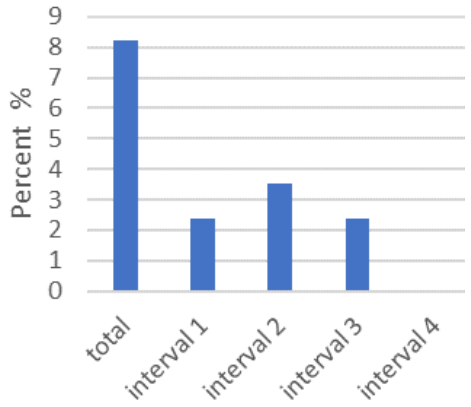

Fig. 4. *Cases with wear greater than 99 %*

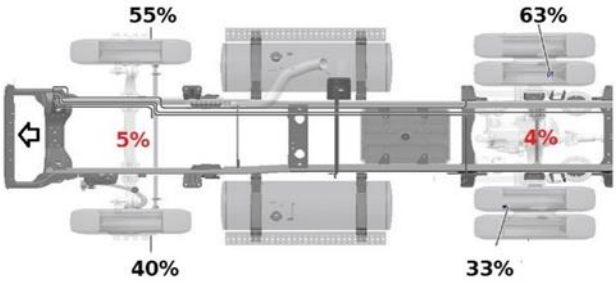

Fig. 5. *Cases in which there is a greater wear of the brake elements on the right wheel*

3.3. Different wear of the brake pads of the same axle

The study also carefully analysed the frequency of cases in which differentiated wear of the elements in the friction torque occurs. In general, there have been significantly more cases with more wear on the right-hand brake elements. Figure 5 shows the percentages in which the wear was higher on the respective wheel and in the middle are the percentages in which the wear was equal to the wheels of the same axle (with an error of 1%). In 55%

THE ANNALS OF "DUNAREA DE JOS" UNIVERSITY OF GALATI
FASCICLE IX. METALLURGY AND MATERIALS SCIENCE
N°. 4 - 2021, ISSN 2668-4748; e-ISSN 2668-4756
Article DOI: https://doi.org/10.35219/mms.2021.4.13

of cases on the front axle and in 63% of cases on the rear axle there was more wear on the right side, while only in 5% of cases on the front axle and 4% of cases on the rear axle respectively, no there were differences in wear.

3.4. Different wear of the brake pad on the inside than on the outside

Analysing the shape of the wear, it was found that a determining factor for the premature replacement of the brake pads or discs is due to the uneven wear of the elements in the system. This can be either a different wear of the brake pad from the inside than the outside or another case can be due to the different wear of the pads on the wheels of the same axle. Figure 6 shows an example of different wear of the outer pad from the inside and Figure 7 shows the effect of different wear on the brake pads.

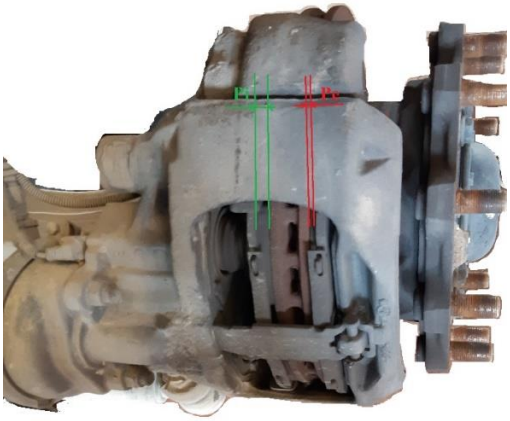

Fig. 6. *Wear difference on the inner brake pad (Pi) compared to the outer brake pad (Pe)*

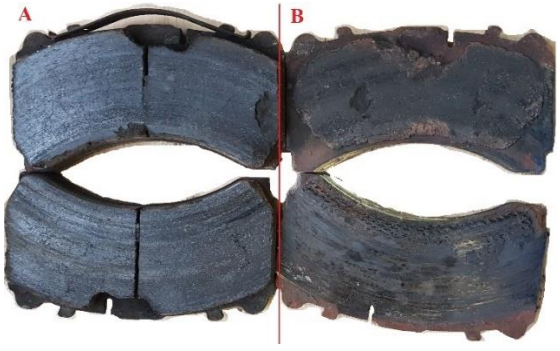

Fig. 7. *Brake pads of the same axle, worn differently (A-left; B-right)*

In both cases of wear and tear, the cause of the wear and tear was the suppression of the calliper or the plate. Specifically, Figure 6 shows the locking movement of the brake pad from the outside relative to its support, and Figure 7 shows the difference in wear between the left and right is caused by the locking movement of the left calliper on the bolts its. Without the calliper sliding, the braking on the axle was performed differently, which only led to the wear of the elements in the functional brake coupling. The operation of the calliper sliding system was discussed in the first part of the thesis. The translational movement of the calliper is absolutely necessary so that the pressing force of the pistons is applied uniformly on the surface of both brake pads.

3.5. The influence of external factors on brake wear

Suppression of the friction torque elements is a common cause of premature replacement of parts in the system. During the study it was found that although there is a complex maintenance system, this type of defect is not monitored electronically. Such a brake calliper position and movement monitoring system would be useful in this regard but would bring additional costs to the system. In this case, the question is whether these additional costs are lower than the damage caused by defects and whether a cheap system could be implemented to streamline the process.

The analysis of the factors that favour these defects is an essential element for the improvement of the performances, at the same time as the reduction of the maintenance costs. Figure 8 shows one of the external factors that most frequently contributes to blocking the translational motion, namely deposits of dust, mud and other materials from the outside environment.

During the analysis, a series of defects were identified caused by impurities from the external environment, the presence of which favors abrasion wear. In addition to the influence of abrasive materials from the outside environment, corrosion is also a major problem because there are a number of common factors that influence wear and tear and significantly reduce the life of the elements in the braking system. The combination of several types of wear based on common influencing factors generates defects such as those in Figure 9.

The main effects of the situations shown in Figure 9 lead to increased degradation and premature decommissioning of the pads and (in most cases) brake discs, leading to a significant increase in maintenance costs. As a side effect of these types of wear, there are a number of specific noises (rumble or sharp noises). The intensity and type of these noises significantly affect the quality of life in areas close to roads. At the same time, these noises are the main warning about the occurrence or existence of a fault.

THE ANNALS OF "DUNAREA DE JOS" UNIVERSITY OF GALATI
FASCICLE IX. METALLURGY AND MATERIALS SCIENCE
Nº. 4 - 2021, ISSN 2668-4748; e-ISSN 2668-4756
Article DOI: https://doi.org/10.35219/mms.2021.4.13

Fig. 8. *Deposits and corrosion under normal working conditions A-deposits on the stirrup; B-deposits on the guide bolts of the brake calliper*

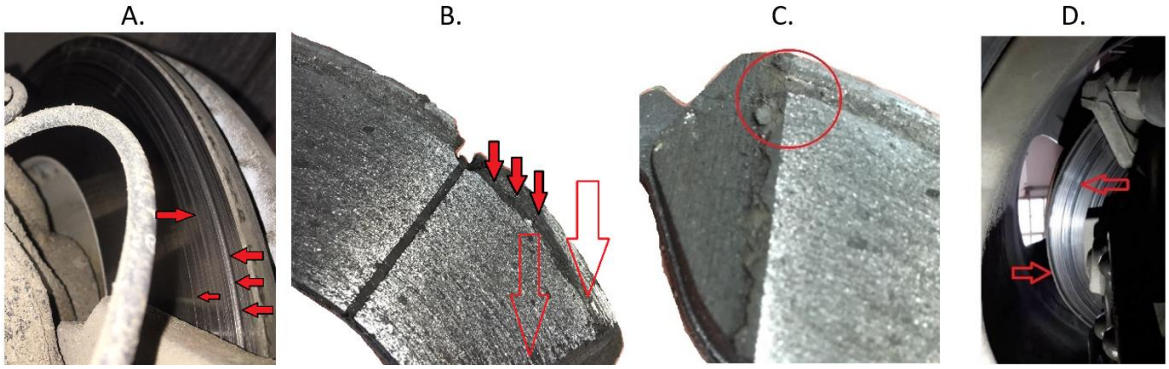

Fig. 9. *Combined effects of the influence of impurities and particles from the external environment on the wear of the brake discs and pads: A, D- the effects of abrasive wear on the brake disc; B, C- degradation of the brake pads under the action of external factors and corrosion*

4. Analysis of distances travelled until the replacement of the brake pads

Figure 10 shows the situation of another truck without an auxiliary braking system, which is running in internal traffic but which already has up to 477 000 km and has 4 brake pad replacements. This is a significant justification for the need to use auxiliary braking systems. During the work, several cases of accentuated wear of the elements in the braking system were found and frequent thermal overloads of the brakes were frequently identified with serious effects on the braking performance. It has also been found that when heavy wear occurs or in cases of thermal overload, repair costs increase significantly and, in most cases, it becomes necessary to replace the brake discs. The current study also contains an economic analysis of these maintenance costs for certain cases but also a part of the analysis of the effects of thermal overloads on the elements of the braking system.

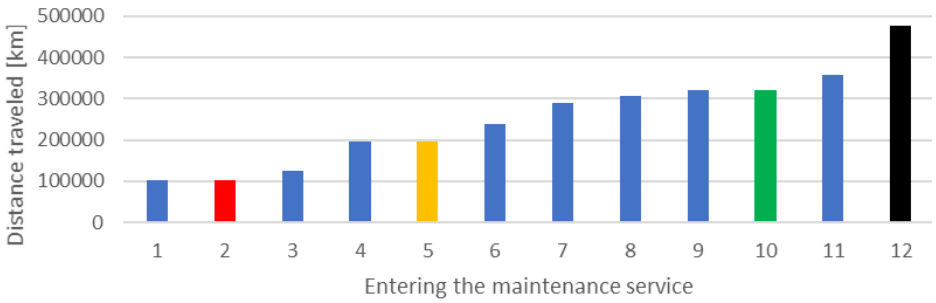

Fig. 10. *Distribution of service entries and replacement of brake pads on the front axle to a truck without an auxiliary braking system*

THE ANNALS OF "DUNAREA DE JOS" UNIVERSITY OF GALATI
FASCICLE IX. METALLURGY AND MATERIALS SCIENCE
N°. 4 - 2021, ISSN 2668-4748; e-ISSN 2668-4756
Article DOI: https://doi.org/10.35219/mms.2021.4.13

In the case of extreme wear and tear, it has been found that exceeding the maintenance intervals or exceeding the maximum wear limits comes with additional costs caused in many cases and the need to replace the brake discs. In order to avoid these situations, the evolution of wear and tear and the distribution of cases in which wear is close to the maximum values were studied.

The graphs in Figures 11 and 12 show the distribution of cases with wear greater than 95%. The degree of wear is read from the data taken from the brake pad wear sensors.

It is observed that both the front and the rear axle have a high weight in cases where the wear is higher than 95%. The technical documentation provided by the manufacturer recommends replacement from 90% (even 85% in some cases) so further use from values above 95% is not recommended. Above these values, the rate of serious defects increases exponentially, so the continued use is not only no longer justified but also with much higher risks.

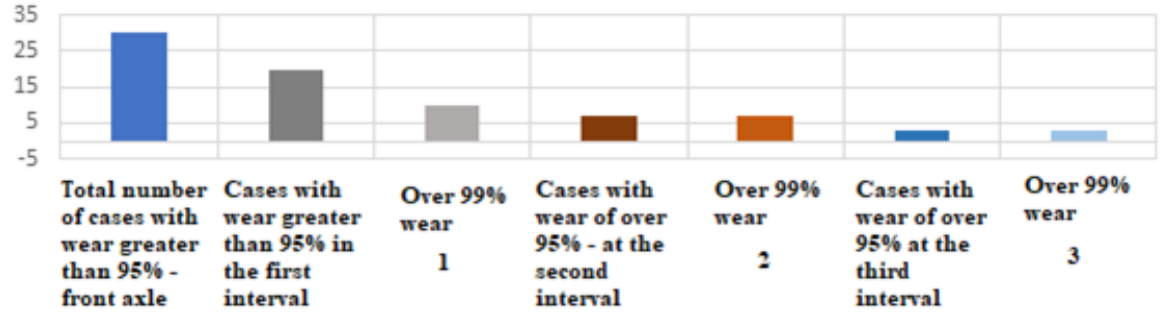

Fig. 11. *Distribution of wear cases close to the maximum limit for the front axle*

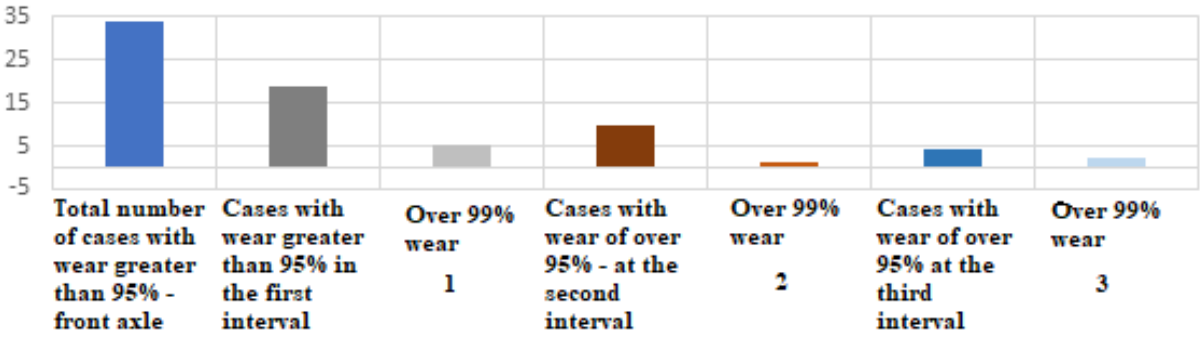

Fig. 12. *Distribution of wear cases close to the maximum limit for the rear axle*

5. Aspects and problems related to waste management resulting from the wear of the elements during braking

Figure 13 shows the parts replaced during a calendar month in the repair shop where the analysis was performed. There is a very large volume of replaced brake pads and a few worn brake discs. Among the parts, you can see some that have not yet reached the degree of wear but are still replaced. These issues related to the premature replacement of some elements require a careful analysis both for the efficiency of the economic balance and for the identification of solutions for electronic monitoring and evaluation of the elements of wear in order to determine the exact degree of wear and the most efficient use of resources.

Following the analysis of the problems encountered in operation on commercial vehicles, it was found that in addition to the problems of wear and defects, these vehicles also generate a large volume of waste resulting from the parts used. This aspect needs special attention, especially in the ecological context of environmental protection. In this sense, a major regulation of these situations would be useful, especially since these used parts are generated, as it was found, in quite large quantities (Fig. 13).

The production of a small volume of waste can be controlled from the period of use, when the main causes that cause premature or accentuated defects can be established and solutions can be identified to

THE ANNALS OF "DUNAREA DE JOS" UNIVERSITY OF GALATI
FASCICLE IX. METALLURGY AND MATERIALS SCIENCE
Nº. 4 - 2021, ISSN 2668-4748; e-ISSN 2668-4756
Article DOI: https://doi.org/10.35219/mms.2021.4.13

improve the processes. Thus, the analysis of braking systems becomes a component part of the environmental and quality of life problems, not only by the volume of waste generated but also by the direct effects of the noise produced by braking on people in the immediate vicinity of the roads.

Fig. 13. *The problem of used parts that generate a large volume of waste and for which there is no recycling plan*

6. Conclusions

Starting from the analysis of operational defects, it can be concluded that, in addition to the normal wear problems, there are a number of different wear situations, the effects of which can cause a drastic decrease in traffic safety and additional operating costs. In this context, the analysis of factors favouring wear and tear is a key element in increasing traffic safety and reducing additional operating costs.

The main problems identified in the operation refer to: the generation of a large volume of residual parts; premature replacement of parts; subjectivity to the decision to replace parts, without being monitored by a precise maintenance system; uneven wear of brake discs (shoulder wear); uneven wear of brake pads; deposits that suppress the freedom of movement of some elements of the friction torque; advanced corrosion in different areas; parts failures and serious defects identified as a result of overloading in heavy site conditions.

References

[1]. Vdovin A., *et al.*, *A coupled approach for vehicle brake cooling performance simulations*, International Journal of Thermal Sciences, 132, p. 257-266, 2018.
[2]. Hatam A., Khalkhali A., *Simulation and sensitivity analysis of wear on the automotive brake pad*, Simulation Modelling Practice and Theory, 84, p. 106-123, 2018.
[3]. Elgharbawy M., *et al.*, *Adaptive functional testing for autonomous trucks*, International Journal of Transportation Science and Technology, December 2018.
[4]. Blau P. J., Jolly B. C., *Wear of truck brake lining materials using three different test methods*, Wear, 259, p. 1022-1030, 2005.
[5]. Adamowicz A., Grzes P., *Influence of convective cooling on a disc brake temperature distribution during repetitive braking*, Therm. Eng., 31, p. 2177-2185, 2011.
[6]. Wahlström J., Olander A. S. L., Jansson A., Olofsson U., *A pin-on-disc simulation of airborne wear particles from disc brakes*, Wear, 268, p. 763-769, 2010.
[7]. Shiva Shanker P., *A review on properties of conventional and metal matrix composite materials in manufacturing of disc brake*, Mater. Today Proc., 5, p. 5864-5869, 2018.
[8]. Poletto J. C., *et al.*, *Analysis of the error in the estimation of the morphology of contact plateaus existing on the surface of brake pads*, Tribology International, 126, p. 297-306, 2018.
[9]. Popa M. F., Capătă D. M. S., Burnete N., *Aspects of wear braking process on brake discs and brake pads in the construction of commercial vehicles*, Fascicle of Management and Technological Engineering, May 2019.

THE ANNALS OF "DUNAREA DE JOS" UNIVERSITY OF GALATI
FASCICLE IX. METALLURGY AND MATERIALS SCIENCE
No. 4 - 2021, ISSN 2668-4748; e-ISSN 2668-4756
Article DOI: https://doi.org/10.35219/mms.2021.4.14

RACK AND PINION STEERING SYSTEM DESIGN FOR A PASSENGER CAR

Andrei-Constantin SOFIAN, Bogdan Manolin JURCHIȘ, Mădălin Florin POPA
Technical University of Cluj-Napoca, Romania
e-mail: madalin.popa@live.com

ABSTRACT

The steering system plays a crucial role in the stability of the automobile, especially in the safety of the passengers and pedestrians. The aim of this work is to design a rack and pinion steering system that could equip a passenger car. In this process, many parameters are considered for the correct and effective directional response behavior of the vehicle. 2D models were sketched to validate the kinematic algorithm calculus used to optimize and refine the dimensions of the components of the steering system. After a satisfactory Ackermann percentage was achieved, steering system is designed and analysed in one of the most used CAD and CAE software in automotive, CATIA.

KEYWORDS: rack and pinion, steering kinematics, Ackerman geometry, optimization, CAD, CAE, turning angle, turn centre

1. Introduction

Devised by the English physician Erasmus Darwin in 1758, designed by the German carriage builder George Lankensperger in 1817, and patented by the Anglo-German bookseller Rudolph Ackermann in 1818, Ackermann geometry proposed a new method of steering of horse-drawn carriages, whose stability in turning was very low at that time. This new method aims that the two front wheels should turn about a centre that lies on the extended line of the back axle of the carriage. Respecting this principle means that all four wheels will have concentric paths. These concentric paths of the wheels come with some important advantages: the front wheels both run tangential to the track, so there is no scuffing anymore of the wheels on the road, but more important, the carriage turns more smoothly and the probability of overturning decreases insignificantly. It is essential to know these facts because the automotive steering system is also designed considering this principle discovered by Darwin and Lankensperger [1].

Throughout this paper many parameters will be encountered, so it is absolute necessary to clarify the terminology.

Table 1. *Nomenclature*

Parameter	Notation	Measure unit
Wheelbase	A	[mm]
Wheel track	E	[mm]
Inner tier turning angle	v_i	[°]
Outer tier turning angle	v_e	[°]
Turning radius	R	[mm]

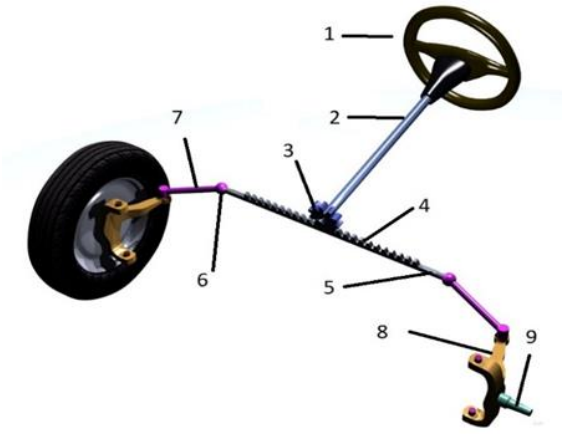

Fig. 1. *Steering system components: 1-steering wheel, 2-steering column, 3-pinion, 4-rack, 5-transverse bar, 6-rod end, 7-tie rod, 8-steering lever, 9-spindle* [2]

THE ANNALS OF "DUNAREA DE JOS" UNIVERSITY OF GALATI
FASCICLE IX. METALLURGY AND MATERIALS SCIENCE
N°. 4 - 2021, ISSN 2668-4748; e-ISSN 2668-4756
Article DOI: https://doi.org/10.35219/mms.2021.4.14

This paper aims to describe the logical steps that must be considered in designing an effective steering system for a passenger car. A steering system is effective if the paths of the wheels are concentric, in other words, the turn centre is placed on the extended line of the back axle. For achieving such concentric trajectories, the inner wheel must be steered more than the outer wheel. In Figure 2 is presented the ideal turn or Ackermann principle.

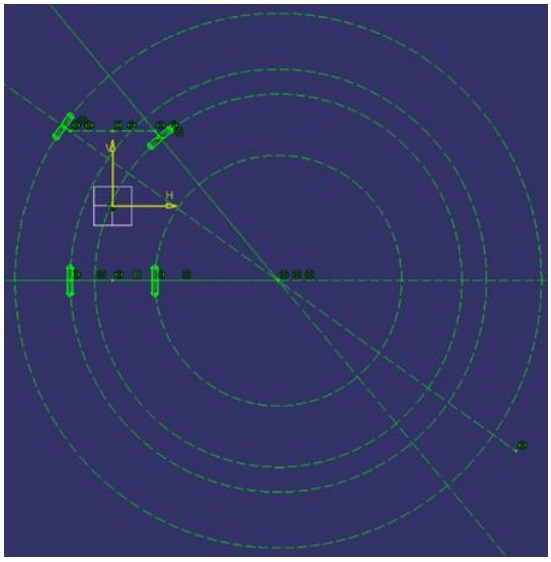

Fig. 2. *Ideal 360 turn/ Ackermann turn*

It is very important to know that such an ideal turn is a consequence of the steering geometry and steering kinematics [3]. Based on Figure 2, the next equation can be deduced, an equation which defines the ideal dependency between the two turning angles of the front wheels.

Theoretically, the ideal turn is based on a very simple equation. In real life, the trajectories of the wheels depend on such a complex system called steering system, and not only. Plotting this first equation, it will result the next chart.

$$v_e = \operatorname{acot}\left(\frac{E}{A} + \cot(v_i)\right) \qquad (1)$$

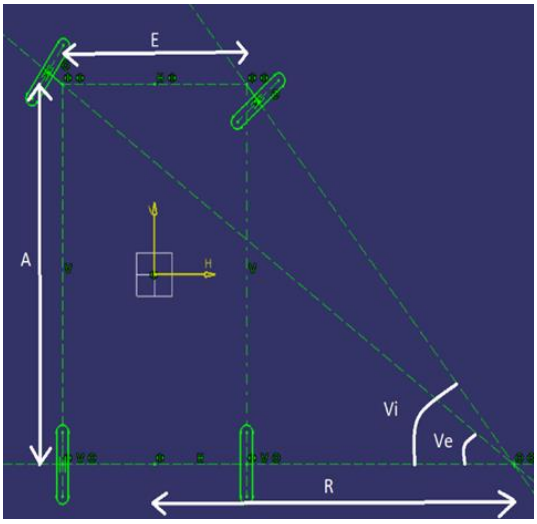

Fig. 3. *Ideal turn angles*

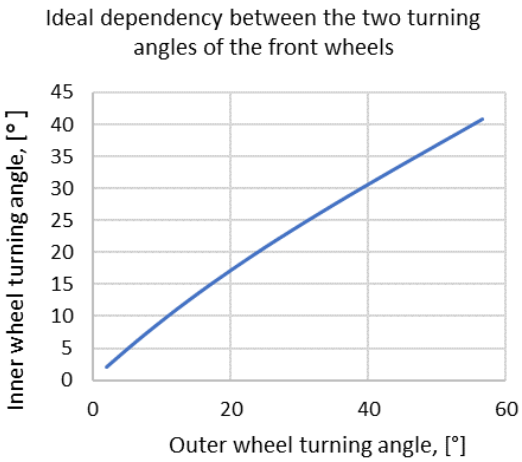

The blue line becomes our objective at this stage and, for achieving such an ideal curve, a kinematic algorithm is needed.

2. Kinematic algorithm

Every calculus algorithm has an input and an output.

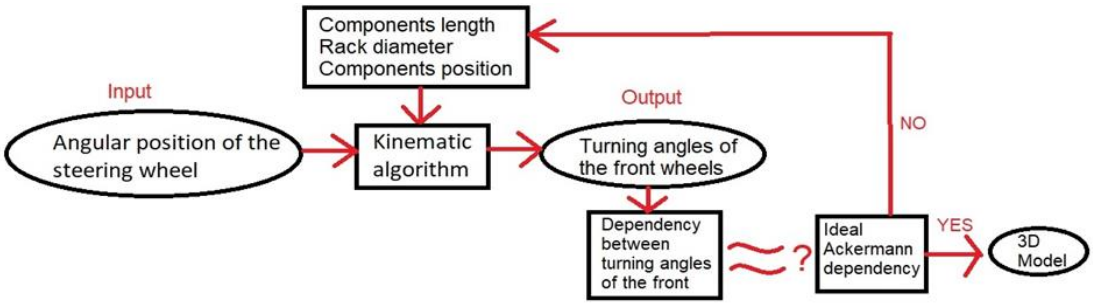

Fig. 4. *Kinematic algorithm overview*

THE ANNALS OF "DUNAREA DE JOS" UNIVERSITY OF GALATI
FASCICLE IX. METALLURGY AND MATERIALS SCIENCE
N°. 4 - 2021, ISSN 2668-4748; e-ISSN 2668-4756
Article DOI: https://doi.org/10.35219/mms.2021.4.14

2.1. Ackermann's angles

The theory proposes that the possibility of achieving Ackermann geometry is greater if the intersection point of the extension of steering arms is placed in the middle of the rear axle [5].

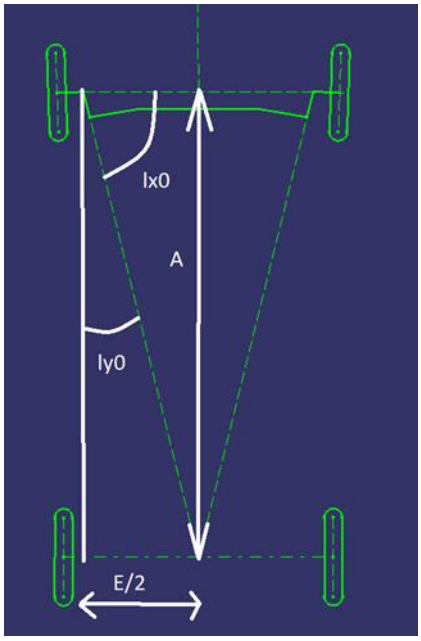

Fig. 5. *Ackermann angles*

Verry important for the following calculations are the two angles from Figure 5.

$$l_{y0} = \arctan\left(\frac{\frac{E}{2}}{A}\right) \; ; l_{x0} = 90° - l_{y0} \qquad (2)$$

2.2. Length of the tie rod

As in the figure 1, in figure 6 we see the following components: l-steering arm, b-tie rod, t-transverse bar, B and C- rod ends and A- steering axis.

$$x_A = \frac{E}{2};\; y_A = 0;\; x_C = \frac{t}{2} \qquad (3)$$

$$x_B = x_A - l\sin(l_{y0}) \qquad (4)$$

$$b = \sqrt{(x_C - x_B)^2 + (y_C - y_B)^2} \qquad (5)$$

For finding out the length of the tie rod, the first two unknown parameters, t and y_C, have been introduced. Till now, we analysed the steering linkage only in neutral position, in other words, the car is not turning. The car is steering only if the rack is moving in the rack and pinion box. Now, the third unknown parameter is introduced.

$$x = \pi \cdot d_p \cdot \frac{\varphi_v}{360^0} \qquad (6)$$

In equation 6: x - transverse bar displacement in x direction, the only direction the rack is moved by the driver via steering wheel; d_p - pinion diameter, the third unknown parameter, and φ_v - our input parameter, the angular position of the steering wheel. For passenger cars, the steering wheel makes 1.5 turns. This means that our input vector is [-540°, +540°].

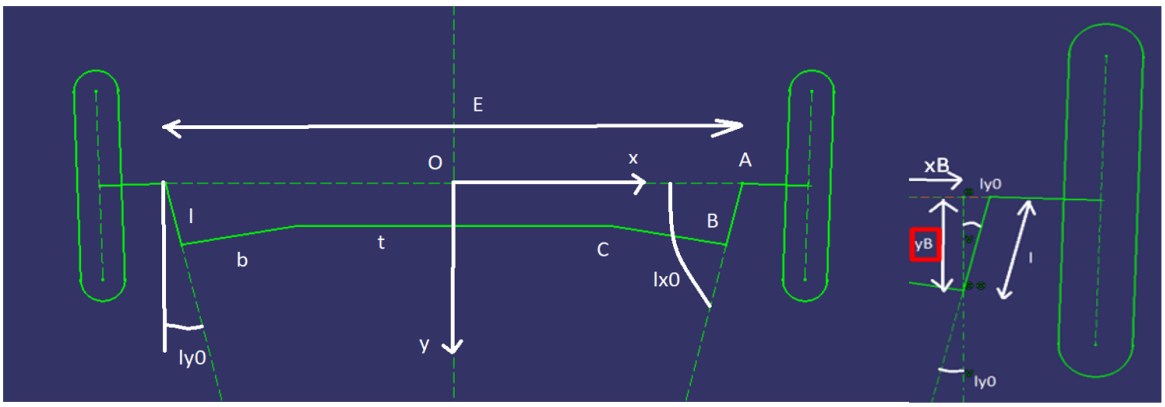

Fig. 6. *Length of the tie rod*

THE ANNALS OF "DUNAREA DE JOS" UNIVERSITY OF GALATI
FASCICLE IX. METALLURGY AND MATERIALS SCIENCE
N°. 4 - 2021, ISSN 2668-4748; e-ISSN 2668-4756
Article DOI: https://doi.org/10.35219/mms.2021.4.14

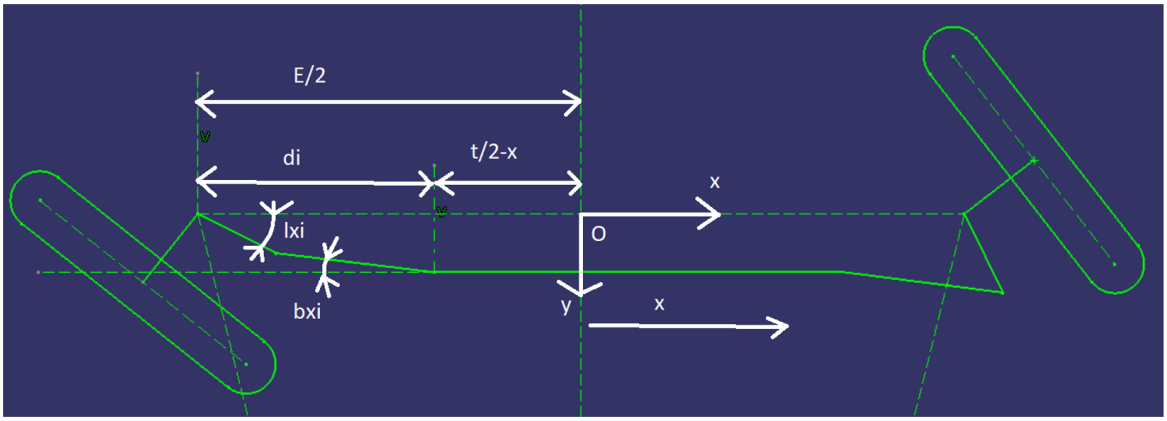

Fig. 7. *Top view of the steering linkage for finding the turn angle of the inner wheel*

2.3. Turn angle of the inner wheel

$$d_i = \frac{E}{2} - \frac{t}{2} + x \tag{7}$$

$$b \cdot \cos(b_{xi}) = d_i - l \cdot \cos(l_{xi}) \tag{8}$$

$$b \cdot \sin(b_{xi}) = y_C - l \cdot \sin(l_{xi}) \tag{9}$$

$$b^2 = d_i^2 + {y_C}^2 + l^2 \\ -2 \cdot d_i \cdot l \cdot cos(l_{xi}) \tag{10}$$

$$-2 \cdot y_C \cdot l \cdot sin(l_{xi}) \\ 2 \cdot d_i \cdot l \cdot cos(l_{xi}) \\ +2 \cdot y_C \cdot l \cdot sin(l_{xi}) \tag{11}$$

$$+b^2 - d_i^2 - {y_C}^2 - l^2 = 0 \\ P \cdot cos(l_{xi}) + Q \cdot sin(l_{xi}) + R = 0 \tag{12}$$

$$P = 2 \cdot d_i \cdot l \; ; \; Q = 2 \cdot y_C \cdot l \; ; \\ R = b^2 - d_i^2 - {y_C}^2 - l^2 \tag{13}$$

$$sin(l_{xi}) = \frac{2 \cdot tan\,(\frac{l_{xi}}{2})}{1 + tan\,(\frac{l_{xi}}{2})^2} \tag{14}$$

$$cos(l_{xi}) = \frac{1 - tan\,(\frac{l_{xi}}{2})}{1 + tan\,(\frac{l_{xi}}{2})^2} \tag{15}$$

$$sin(l_{xi}) = \frac{2 \cdot z}{1 + z^2} \tag{16}$$

$$cos(l_{xi}) = \frac{1 - z}{1 + z^2} \tag{17}$$

$$P \cdot \frac{1 - z}{1 + z^2} + Q \cdot \frac{2 \cdot z}{1 + z^2} + R = 0 \tag{18}$$

$$(R - P)z^2 + 2Qz + P + R = 0 \tag{19}$$

$$a = (R - P) \; ; \; b = 2Q; \; c = P + R \tag{20}$$

$$\Delta = b^2 - 4ac \tag{21}$$

$$z = \frac{-b - \sqrt{\Delta}}{2a} \tag{22}$$

$$z = tan\left(\frac{l_{xi}}{2}\right) \tag{23}$$

$$l_{xi} = 2 \cdot arctan\,(z) \tag{24}$$

$$\beta_i = l_{x0} - l_{xi} \tag{25}$$

In these equations we used for the first time "l", so we introduced our last unknown parameter. "β_i" is the angular variation of the inner wheel. There still is a toe angle, the angle that each tire makes with the longitudinal plane of the vehicle. For most passenger cars, the front tires are not only for steering, but also for traction. Because of this, even if the angular position of the steering wheel is "0", the front tires will be very little steered, that angle being called toe-out angle. Therefore, also this small angle must be considered for the final value [4].

$$v_i = \beta_i - \gamma_0 \tag{26}$$

THE ANNALS OF "DUNAREA DE JOS" UNIVERSITY OF GALATI
FASCICLE IX. METALLURGY AND MATERIALS SCIENCE
Nº. 4 - 2021, ISSN 2668-4748; e-ISSN 2668-4756
Article DOI: https://doi.org/10.35219/mms.2021.4.14

2.4. Turn angle of the outer wheel

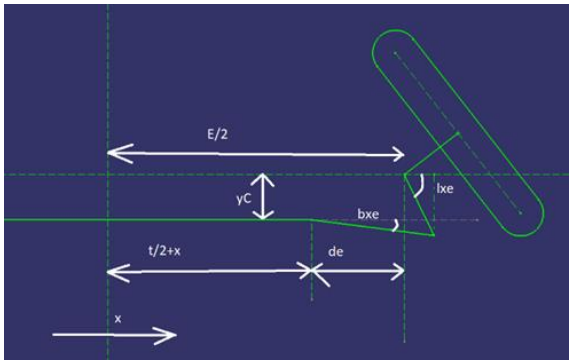

Fig. 8. *Top view of write half steering linkage*

The calculation method is almost identical with only a few differences.

$$d_e = \frac{E}{2} - \frac{t}{2} - x \tag{27}$$

$$b \cdot cos(b_{xe}) = d_e + l \cdot cos(l_{xe}) \tag{28}$$

$$b \cdot sin(b_{xe}) = l \cdot sin(l_{xe}) - y_C \tag{29}$$

$$b^2 = d_e^2 + {y_C}^2 + l^2$$
$$2 \cdot d_e \cdot l \cdot \cos(l_{xe}) \tag{30}$$

$$-2 \cdot y_C \cdot l \cdot \sin(l_{xe})$$
$$2 \cdot \mathrm{d}_e \cdot l \cdot \cos(l_{xe})$$
$$-2 \cdot y_C \cdot l \cdot \sin(l_{xe}) \tag{31}$$

$$-b^2 + d_e^2 + {y_C}^2 + l^2 = 0$$
$$P \cdot \cos(l_{xe}) + Q \cdot \sin(l_{xe}) + \mathrm{R} = 0 \tag{32}$$

$$P = 2 \cdot d_e \cdot l \; ; \; Q = -2 \cdot y_C \cdot l \; ;$$
$$\mathrm{R} = -b^2 + d_e^2 + {y_C}^2 + l^2 \tag{33}$$

From this point, equations (14)-(24) are the same, but this time we are trying to find the outer wheel turning angle, "l_{xe}", not "l_{xi}". As we found out "l_{xe}", based on Figure 9 we can deduce the angular variation of the outer wheel.

$$\beta_e = (180 - l_{xe}) - l_{x0} \tag{34}$$

$$v_e = \beta_e + \gamma_0 \tag{35}$$

In equation (52), as in (26), the γ_0 is a toe out angle.

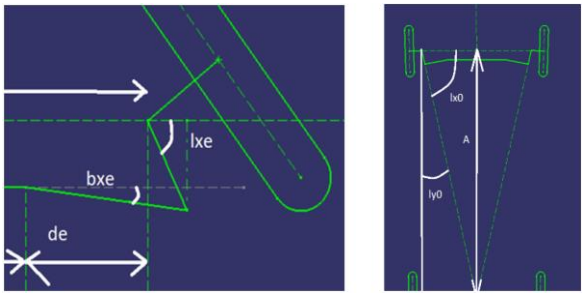

Fig. 9. *Turning angle of the write wheel*

3. Results

We see that there is no chance for an ideal rack and pinion steering system. Mathematically, it is impossible to obtain a 'blue curve' for every angular position of the steering wheel for a rack-and-pinion steering system. If we cannot obtain a "blue curve" for all steering wheel positions, then we can try to obtain it for large turning angles at least, where the speed of the vehicle is very low, and the car cannot take advantage of the slip angle.

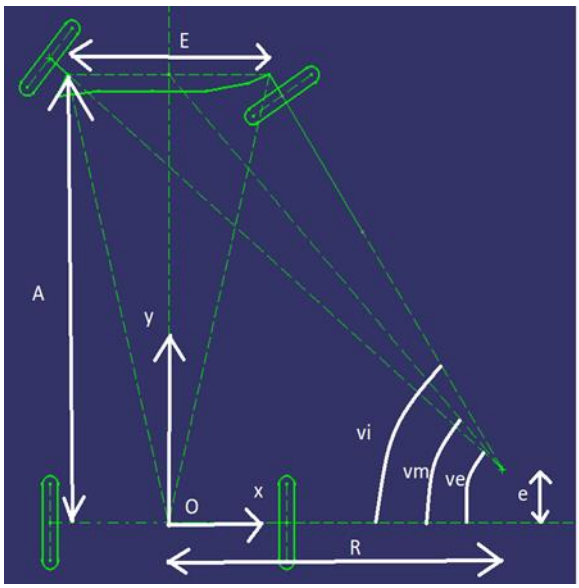

Fig. 10. *Ackermann error*

$$R = \frac{E}{2} \cdot \frac{tan(v_e) + \tan(v_i)}{\tan(v_i) - \tan(v_e)} \tag{36}$$

$$e = A - \left(R - \frac{E}{2}\right) tan(v_i) \tag{37}$$

As we can see, the relative error between our results and Ackermann principle is less than 5% for very tight curves. Moreover, the fact that in the less tight curve domain, the error is very high is normal.

THE ANNALS OF "DUNAREA DE JOS" UNIVERSITY OF GALATI
FASCICLE IX. METALLURGY AND MATERIALS SCIENCE
Nº. 4 - 2021, ISSN 2668-4748; e-ISSN 2668-4756
Article DOI: https://doi.org/10.35219/mms.2021.4.14

In this domain, the car is running almost straight with a higher speed, which increases the slip angle. Slip angle will reduce this high error. The values of slip angle are very unpredictable because they are based on many complex aspects regarding vehicle dynamics. In this paper an Ackermann curve in low speeds domain (extreme angular steering wheel positions) is desired to be obtained.

$$\varepsilon = \frac{|v_{ideal} - v_{real}|}{v_{ideal}} \cdot 100$$

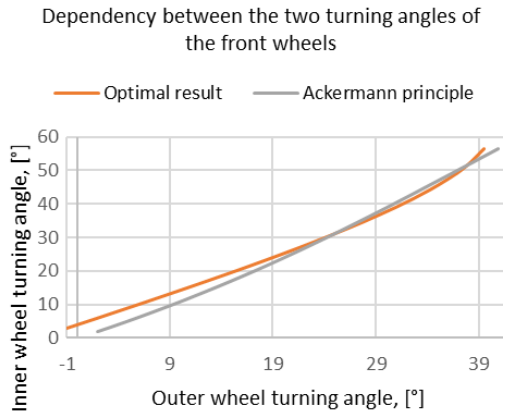

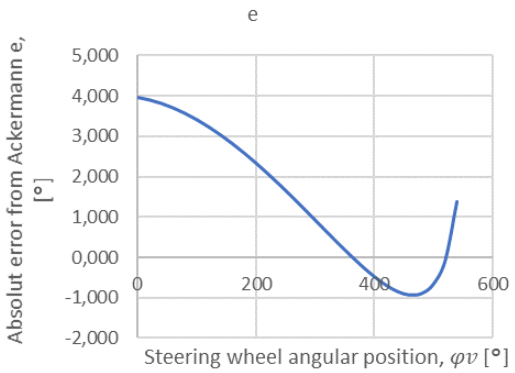

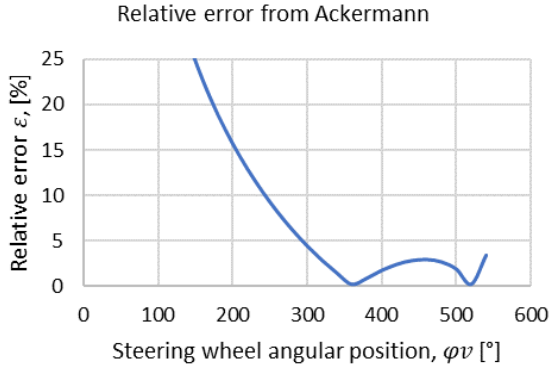

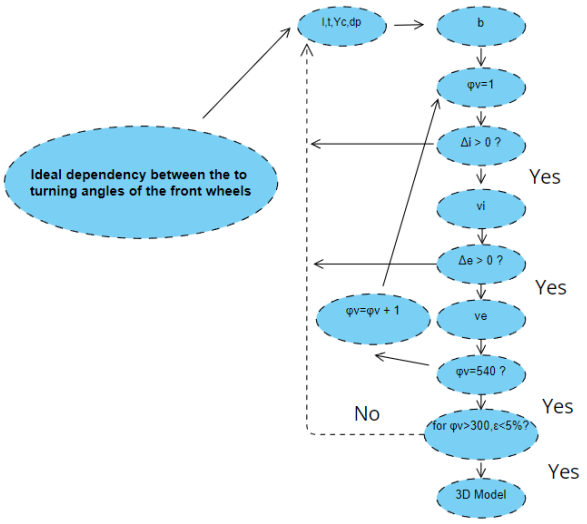

Fig. 11. *Kinematic algorithm*

After a lot of iterations these are the winning values which define the steering linkage geometry:

Table 2. *Winning values*

Notation	Measure unit	Value
l	[mm]	150
t	[mm]	700
y_C	[mm]	100
d_p	[mm]	22

The only known from the beginning parameters were:

Table 3. *Known dimensions*

Parameter	Notation	Measure unit	Value
Wheelbase	A	[mm]	2650
Wheel track	E	[mm]	1530

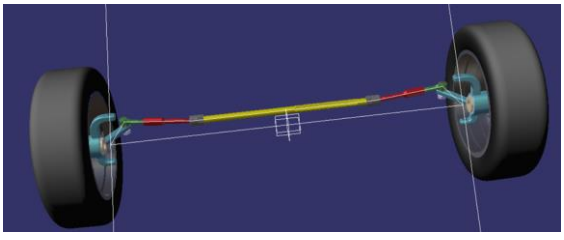

Fig. 12. *Steering linkage CAD*

THE ANNALS OF "DUNAREA DE JOS" UNIVERSITY OF GALATI
FASCICLE IX. METALLURGY AND MATERIALS SCIENCE
Nº. 4 - 2021, ISSN 2668-4748; e-ISSN 2668-4756
Article DOI: https://doi.org/10.35219/mms.2021.4.14

4. CAD and CAE

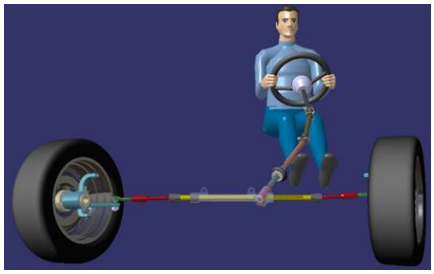

Fig. 13. *Steering system CAD*

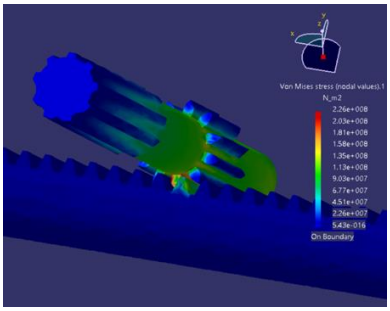

Fig. 14. *Finite Element Analyse for rack and pinion*

Table 4. *Materials*

Component	Material
Rack and Pinion	42CrMo4
Tie rod	High strength steel
Rod end	PH13-8Mo
Steering knuckle	Al 7057-T6
Steering column	Carbon fiber

5. Conclusions

This paper presents a possible approach to the design and optimization of a such a complex system as a steering system. The project started with a very solid objective, an algorithm calculus has been created based on 2D sketches, the dimensions of the steering linkage were continuously changed based on the algorithm. If 2D model helped the kinematic improvement of the system, later, a CAD model has been created for running kinematic simulations and finite element analyses. It is also well to know that even if Ackermann is the most used name in steering system design, there were another 2 men, Darwin and Lnakensperger, who invented a steering linkage geometry used in horse-drawn carriages for improving the stability, a geometry which is also used today in our cars steering system. We also saw that it is very hard to keep all four wheels on concentric paths with a mechanical steering system. Also, to be noticed that a toe out angle is often used for a better steerability.

References

[1]. King-Hele D., *Erasmus Darwin's Improved Design for Steering Carriages-And Cars*, Notes and Records of the Royal Society of London, 56 (1), p. 41–62. http://www.jstor.org/stable/532121, 2002.
[2]. ***, https://axleaddict.com/.
[3]. Harrer M., Pfeffer P., *Steering Handbook*, Springer, 2017.
[4]. Untaru M., Cîmpian V., Ionescu E., Seitz N., Soare I., Automobile, București, 1975.
[5]. Frățilă G., *Calculul și construcția automobilelor*, București.

THE ANNALS OF "DUNAREA DE JOS" UNIVERSITY OF GALATI
FASCICLE IX. METALLURGY AND MATERIALS SCIENCE
Nº. 4 - 2021, ISSN 2668-4748; e-ISSN 2668-4756
Article DOI: https://doi.org/10.35219/mms.2021.4.15

CFD MODELING AND SIMULATION OF AN INDUSTRIAL HALL

Florin-Bogdan MARIN, Mihaela MARIN
"Dunarea de Jos" University of Galati, Romania
e-mail: flmarin@ugal.ro, mihaela.marin@ugal.ro

ABSTRACT

The subject of this research is the use of artificial vision techniques to optimize the placement of hot air sources depending on the location of certain equipment in industrial halls operating at low temperatures. Low temperature industrial halls require optimization of the location of hot air sources to achieve low consumption and efficient heating, taking into account the fact that workplace safety standards require the halls are high and at a certain area of windows (to ensure a hall for this reason, it is necessary to optimize the location and hot air sources flow to ensure the heating of these halls.

KEYWORDS: CFD, modeling, simulation, industrial hall

1. Introduction

Computational fluid dynamics (CFD) is a part of the mechanics of having fluids different numerical methods and computational algorithms used by computers for determining the various problems related to the flow of fluids in various fields [1-22]. Programs often used in industry that are based on C.F.D. are: Ansys, OpenFoam, XFlow, Star-CCM +, Flow-3D, FloWorks, Autodesk Simulation CFD, Solidworks CFD Simulation. The mentioned programs present various calculation methods, each having their advantages and disadvantages, the main factors affecting the data obtained are based on discretization and calculation methods integrated in programs.

CFD modeling is based on the principles of fluid mechanics, to solve problems that involve fluid flows numerical methods and algorithms approach are used. The basic idea in the finite element method is to find the solution to a complicated problem by replacing it with a simpler one. The finite element method has emerged as a consequence of the need to calculate complex strength structures for which analytical calculation methods are not operable. The main idea is that a structure is divided into several parts called "finite elements" for each of them can be applied the calculation theories corresponding to the scheme adopted (bar theory, plate or solid). Dividing the whole into smaller parts, an operation that bears the well-known name of "discretization" will have the effect of obtaining simple shapes for the finite elements' components of the structure.

In order to perform a CFD simulation, four important steps are required: 1 - C.F.D. domain analysis/fluid in which the virtual model will be introduced, 2 - discretization of the fluid domain by various methods to determine the pressure gradient at different calculation points, 3 - setting flow conditions, fluid parameters, turbulence patterns, and another conditions to be able to start the aerodynamic calculation, 4 - aerodynamic analysis of the result is performed, as well as a change of the physical conditions previously used in case of the virtual model. The main programs based on dynamic fluid calculation use the same calculation methods and algorithms.

Low temperature industrial halls require hot air optimization location of sources to achieve low consumption and efficient heating, taking into account the fact that workplace safety standards require high halls and at a certain area of windows. For this reason, it results that the windows have a relatively poor insulation, it is necessary to optimize the location and hot air flow to ensure the halls heating. Using several CFD simulations, which allow to calculate with a very good accuracy the way heat, air currents circulate in the air, we want to train a neural network that will allow intelligent control of the heating system by estimating the optimal positioning of air sources. This optimization is necessary because some tools with considerable volume in the hall are fixed but other components of the industrial flow, such as temporary processing machines or trucks (which can park for hours or days) can influence the heating of the industrial hall operating at low temperatures [23-28]. The neural

THE ANNALS OF "DUNAREA DE JOS" UNIVERSITY OF GALATI
FASCICLE IX. METALLURGY AND MATERIALS SCIENCE
Nº. 4 - 2021, ISSN 2668-4748; e-ISSN 2668-4756
Article DOI: https://doi.org/10.35219/mms.2021.4.15

network manages to estimate the location of the heat source quite well. Further developments should also include parameters such as the distance to objects with high volume and the variability of these volumes.

2. Experimental procedure

The aim of this research is the use of artificial vision techniques in order to optimize the placement heat sources considering: i) the location of equipment in industrial halls operating at low temperatures, ii) relative high height of industrial hall, iii) considerable percent of glass because of safety standards concerning explosion and fire. Consequently, low temperature industrial halls require optimization of the location of hot air sources to achieve low consumption and efficient heating. For this reason, it is necessary to optimize the location and hot air sources flow to ensure the heating of these halls. The simulations on an industrial la a hall was executed. The simulations consider a heating system and a cold air flow of from outside.

The purpose of this paper is to determines if the location, as well as the heating system power allow the heating of the hall in extremes temperature conditions. The industrial hall is considered to be made of steel without any additional thermal insulation. The simulations with the following initial conditions were done: outdoor temperature: -10 degrees, radiator temperature: 80 degrees, inlet flow and outlet flow: 0.3 m^3/s.

3. Results and discussions

As seen in Fig. 1 and Fig. 2 often happens in real case scenarios when high volume in the hall such as products or trucks change the way the air is circulating in the hall. Following the experiments performed using the Open Foam program, the trajectories of the air currents have the trajectories presented in Fig. 3 and Fig. 4. It is observed that there is a movement of the air currents from the heat source to the ceiling, where the air mass is colder. There is also a disordered and non-optimized motion in 3D space.

As seen in Fig. 5 and Fig. 6 in case of unoptimized placement of heating source in respect to the other objects, the heating distribution is not efficient. There is a difference of even 10 degrees between different areas of the industrial hall. A neural network is trained using 30 simulations in order to determine optimal placement of heating for an industrial hall.

The neural network needs to output 2D coordinates of heating source taking into account the volumes in the hall, both temporary and permanent. The trained network architecture consisted of 10 hidden layers. The results show good temperature estimation, as the network was able to predict with a precision of 91%.

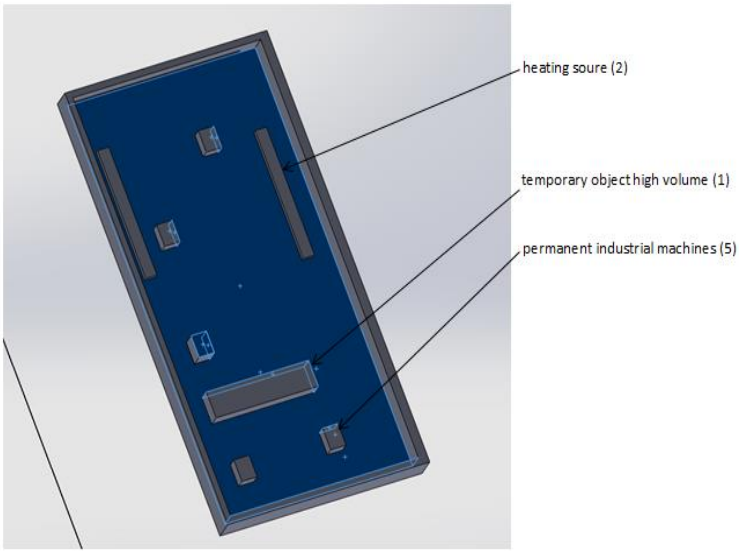

Fig. 1. *Scenario of placement*

THE ANNALS OF "DUNAREA DE JOS" UNIVERSITY OF GALATI
FASCICLE IX. METALLURGY AND MATERIALS SCIENCE
Nº. 4 - 2021, ISSN 2668-4748; e-ISSN 2668-4756
Article DOI: https://doi.org/10.35219/mms.2021.4.15

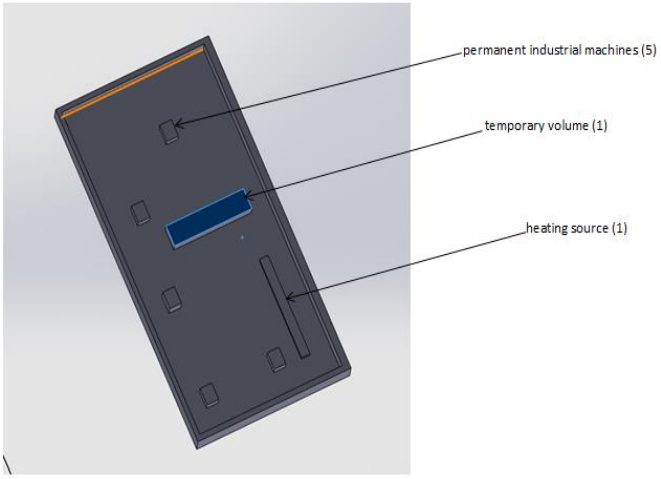

Fig. 2. *One of the scenarios of placement*

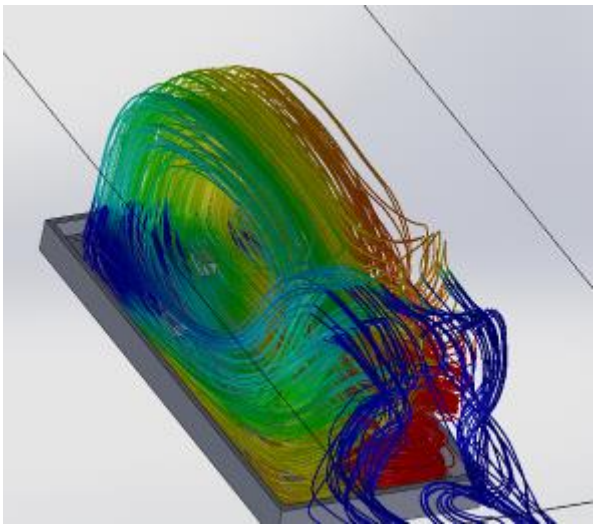

Fig. 3. *Air circulation*

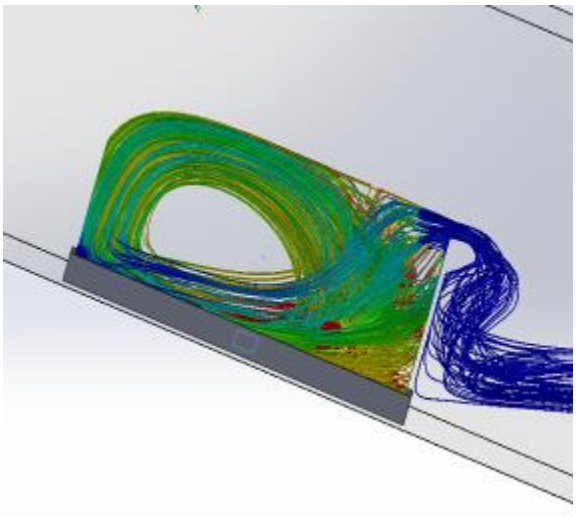

Fig. 4. *Air circulation*

THE ANNALS OF "DUNAREA DE JOS" UNIVERSITY OF GALATI
FASCICLE IX. METALLURGY AND MATERIALS SCIENCE
Nº. 4 - 2021, ISSN 2668-4748; e-ISSN 2668-4756
Article DOI: https://doi.org/10.35219/mms.2021.4.15

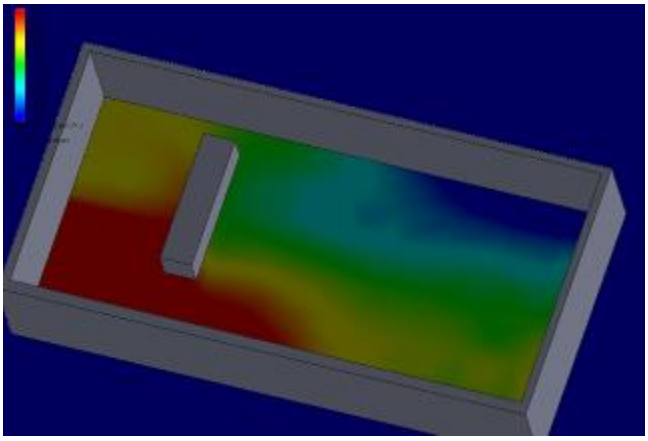

Fig. 5. *Heating variation of the fluid (air) in a horizontal plane placed at 2.5 meter above ceiling*

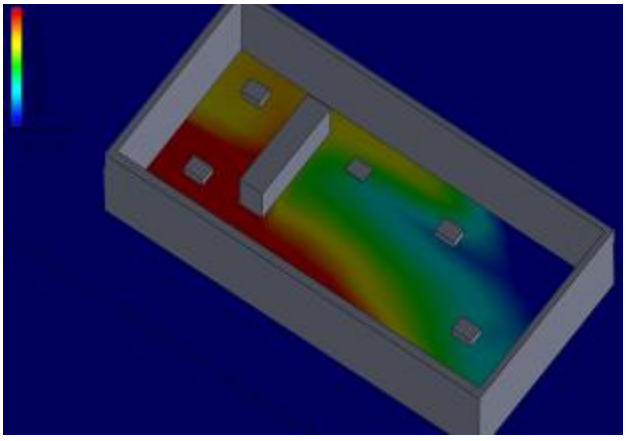

Fig. 6. *Heating variation of the fluid (air) in a horizontal plane placed at 0.5 meter above ceiling*

4. Conclusions

The neural network manages to estimate the location of the heat source quite well. Further developments should also include parameters such as the distance to objects with high volume and the variability of these volumes.

The neuronal network will allow a better approximation in case of training a larger number of samples.

References

[1]. Tanasic N., Jankes G., Skistad H., *CFD analysis and airflow measurements to approach large industrial halls energy efficiency: A case study of a cardboard mill hall*, Energy and Buildings, vol. 43, issue 6, p. 1200-1206, 2011.

[2]. Fujii K., *Progress and future prospects of CFD in aerospace-Wind tunnel and beyond*, Progress in Aerospace Sciences, vol. 41, issue 6, p. 455-470, ISSN 0376-0421, 2005.

[3]. Xia H., Tucker P. G., Dawes W. N., *Level sets for CFD in aerospace engineering*, Progress in Aerospace Sciences, vol. 46, issue 7, p. 274-283, ISSN 0376-0421, 2010.

[4]. Wang C., Li F., Ding Z., Zhang L., *Numerical Simulation of Hypersonic Flow Around an Aerospace Plane by Parallel RANS based CFD*, Procedia Engineering, vol. 61, p. 23-27, ISSN 1877-7058, 2013.

[5]. Danca P., Bode F., Nastase I., Meslem A., *On the Possibility of CFD Modeling of the Indoor Environment in a Vehicle*, Energy Procedia, vol. 112, p. 656-663, 2017.

[6]. Gosman A. D., *Developments in CFD for industrial and environmental applications in wind engineering*, Journal of Wind Engineering and Industrial Aerodynamics, vol. 81, Issues 1-3, p. 21-39, ISSN 0167-6105, 1999.

[7]. Kohler H., Liebmann V., Golla C., Frohlich J., Rudiger F., *Modeling and CFD-simulation of cleaning process for adhesively detaching film-like soils with respect to industrial application*, Food and Bioproducts Processing, vol. 129, p. 157-167, ISSN 0960-3085, 2021.

[8]. Ghaffari M., Hoffmann A., Skjold T., Rolf K., Eckhoff K., Wingerden, *A brief review on the effect of particle size on the laminar burning velocity of flammable dust: Application in a CFD tool for industrial applications*, Journal of Loss Prevention in the Process Industries, vol. 62, 103929, ISSN 0950-4230, 2019.

[9]. Aksenov A. A., Kharchenko S. A., Konshin V. N., Pokhilko V. I., *FlowVision software: Numerical simulation of industrial CFD applications on parallel computer systems*, Parallel Computational Fluid Dynamics, p. 401-408, ISBN 9780444516121, 2003.

[10]. Pavan K. Sharma, *Modeling of fire with CFD for nuclear power plants (NPPs)*, Advances of Computational Fluid Dynamics in Nuclear Reactor Design and Safety Assessment, p. 663-727, 2019.

[11]. Berni F., Cicalese G., Borghi M., Fontanesi S., *Towards grid-independent 3D-CFD wall-function-based heat transfer*

models for complex industrial flows with focus on in-cylinder simulations, Applied Thermal Engineering, vol. 190, 116838, ISSN 1359-4311, 2021.

[12]. Tutar M., Ustun C., Campillo-Robles J. M., Fuente R., Cibrian S., Arzua I., Fernandez A., Lopez G., *Optimized CFD modelling and validation of radiation section of an industrial top-fired steam methane reforming furnace*, Computers & Chemical Engineering, vol. 155, 107504, ISSN 0098-1354, 2021.

[13]. Rizzi A., Jluckring J. M., *Historical development and use of CFD for separated flow simulations relevant to military aircraft*, Aerospace Science and Technology, vol. 117, 106940, ISSN 1270-9638, 2021.

[14]. Wang M., Wang Y., Tian W., Qiu S., Su G. H., *Recent progress of CFD applications in PWR thermal hydraulics study and future directions*, Annals of Nuclear Energy, vol. 150, 107836, ISSN 0306-4549, 2021.

[15]. Seshaiah T., Vasu B., Vijaya K., Reddy K., Bridjesh P., *Analysis on aircraft winglet at different angles by using CFD simulation*, Materials Today: Proceedings, ISSN 2214-7853, 2021.

[16]. Garcia-Ribeiro D., Flores-Mezarina J. A., Bravo-Mosquera P. D., Cerón-Muñoz H. D., *Parametric CFD analysis of the taper ratio effects of a winglet on the performance of a Horizontal Axis Wind Turbine*, Sustainable Energy Technologies and Assessments, vol. 47, 101489, ISSN 2213-1388, 2021.

[17]. Zhu X, Dai Y., Ma F., *CFD modelling and numerical simulation on windage power loss of aeronautic high-speed spiral bevel gears*, Simulation Modelling Practice and Theory, vol. 103, 102080, ISSN 1569-190X, 2020.

[18]. Zobaer T., Sutradhar A., *Modeling the effect of tumor compression on airflow dynamics in trachea using contact simulation and CFD analysis*, Computers in Biology and Medicine, vol. 135, 104574, ISSN 0010-4825, 2021.

[19]. Perinajov R., Juffermans J., Westenberg J. M., Roel L.F., Palen Pieter J. Boogaard, Hildo J. Lamb, Sas a Kenjeres, *Geometrically induced wall shear stress variability in CFD-MRI coupled simulations of blood flow in the thoracic aortas*, Computers in Biology and Medicine, vol. 133, 104385, ISSN 0010-4825, 2021.

[20]. Shoeibi S., Kargarsharifabad H., Rahbar N., Ahmadi G., Reza M. S., *Performance evaluation of a solar still using hybrid nanofluid glass cooling-CFD simulation and environmental analysis*, Sustainable Energy Technologies and Assessments, vol. 49, 101728, ISSN 2213-1388, 2022.

[21]. Norton T., Sun D., *Computational fluid dynamics (CFD) – an effective and efficient design and analysis tool for the food industry: A review*, Trends in Food Science & Technology, vol. 17, Issue 11, p. 600-620, 2006.

[22]. Wutz J., Waterkotte B., Heitmann K., Wucherpfennig T., *Computational fluid dynamics (CFD) as a tool for industrial UF/DF tank optimization*, Biochemical Engineering Journal, vol. 160, 107617, ISSN 1369-703X, 2020.

[23]. Silvestri L., *CFD modeling in Industry 4.0: New perspectives for smart factories*, Procedia Computer Science, vol. 180, p. 381-387, ISSN 1877-0509, 2021.

[24]. Lim J., Ooka R., *A CFD-Based Optimization of Building Configuration for Urban Ventilation Potential*, Energies, 14, 1447, 2021.

[25]. Souza C., Kurka P., Lins R., Araujo J., *Performance comparison of non-adaptive and adaptive optimization algorithms for artificial neural network training applied to damage diagnosis in civil structures*, Applied Soft Computing, vol. 104, 107254, ISSN 1568-4946, 2021.

[26]. Volker D., Lindner M., Weigold M., *Design Method for Building Automation Control Programs to Enable the Energetic Optimization of Industrial Supply Systems*, Procedia CIRP, vol. 104, p. 229-234, ISSN 2212-8271, 2021.

[27]. Si B., Wang J., Yao X., Shi X., Jin X., Zhou X., *Multi-objective optimization design of a complex building based on an artificial neural network and performance evaluation of algorithms*, Advanced Engineering Informatics, vol. 40, p. 93-109, ISSN 1474-0346, 2019.

[28]. Iijima F., Ikeda S., Nagai T., *Automated computational design method for energy systems in buildings using capacity and operation optimization*, Applied Energy, vol. 306, Part A, 117973, ISSN 0306-2619, 2022.

MANUSCRISELE, CĂRŢILE ŞI REVISTELE PENTRU SCHIMB, PRECUM ŞI ORICE CORESPONDENŢE SE VOR TRIMITE PE ADRESA:

MANUSCRIPTS, REVIEWS AND BOOKS FOR EXCHANGE COOPERATION, AS WELL AS ANY CORRESPONDANCE WILL BE MAILED TO:

LES MANUSCRIPTS, LES REVUES ET LES LIVRES POUR L'ECHANGE, TOUT AUSSI QUE LA CORRESPONDANCE SERONT ENVOYES A L'ADRESSE:

MANUSCKRIPTEN, ZIETSCHRITFTEN UND BUCHER FUR AUSTAUCH SOWIE DIE KORRESPONDENZ SID AN FOLGENDE ANSCHRIFT ZU SEDEN:

After the latest evaluation of the journals by the National Center for Science Policy and Scientometrics (**CENAPOSS**), in recognition of its quality and impact at national level, the journal will be included in the B^+ category, 215 code (http://cncsis.gov.ro/userfiles/file/CENAPOSS/Bplus_2011.pdf).

The journal is already indexed in:
DOAJ: https://doaj.org/
SCIPIO-RO: http://www.scipio.ro/web/182206
EBSCO: http://www.ebscohost.com/titleLists/a9h-journals.pdf
Google Academic: https://scholar.google.ro
Index Copernicus: https://journals.indexcopernicus.com
Crossref: https://search.crossref.org/

The papers published in this journal can be viewed on the website: http://www.gup.ugal.ro/ugaljournals/index.php/mms

Name and Address of Publisher:
Contact person: Prof. Dr. Eng. Elena MEREUȚĂ
Galati University Press - GUP
47 Domneasca St., 800008 - Galati, Romania
Phone: +40 336 130139
Fax: +40 236 461353
Email: gup@ugal.ro

Name and Address of Editor:
Ș. L. Dr. Eng. Marius BODOR
"Dunarea de Jos" University of Galati, Faculty of Engineering
111 Domneasca St., 800201 - Galati, Romania
Phone: +40 336 130208
Phone/Fax: +40 336 130283
Email: marius.bodor@ugal.ro

AFFILIATED WITH:

- THE ROMANIAN SOCIETY FOR METALLURGY
- THE ROMANIAN SOCIETY FOR CHEMISTRY
- THE ROMANIAN SOCIETY FOR BIOMATERIALS
- THE ROMANIAN TECHNICAL FOUNDRY SOCIETY
- THE MATERIALS INFORMATION SOCIETY (ASM INTERNATIONAL)

Edited under the care of the FACULTY OF ENGINEERING

Annual subscription (4 issues per year)

Fascicle DOI: https://doi.org/10.35219/mms

Volume DOI: https://doi.org/10.35219/mms.2021.4

Editing date: 15.12.2021
Number of issues: 200
Printed by Galati University Press (accredited by CNCSIS)
47 Domneasca Street, 800008, Galati, Romania